Dynamic description of the circadian clock entrainment in cyanobacteria by a phase oscillator model

Christoph Weiss-Schaber

UNIVERSITE DE GRENOBLE

THESE
Pour obtenir le grade de
DOCTEUR DE L'UDG
Spécialité : Physique pour les Sciences du Vivant
préparée au Laboratoire de Spectrométrie Physique
dans le cadre de l'Ecole Doctorale de Physique
par

Christoph WEISS-SCHABER
Soutenance le 25 juin 2010

Dynamic description of the circadian clock entrainment in cyanobacteria by a phase oscillator model

Description de la dynamique de l'horloge circadienne des cyanobactéries sous entraînement par un modèle d'oscillateur de phase

---

Directrice de thèse :
Irina MIHALCESCU

JURY

Hans GEISELMANN	President
M. François-Yves BOUGET	Rapporteur
M. Didier CHATENEY	Rapporteur
Irina MIHALCESCU	Examinateur
Till ROENNEBERG	Examinateur

Abstract

English abstract

Cyanobacteria are the simplest known organism with a circadian clock. This clock produces stable rhythms with a period close to 24h and can be entrained to exactly 24h by external time cues like illumination or temperature cycles.

In this work we show that this biological clock behaves like a phase oscillator. Furthermore its behaviour under the influence of an external entrainment can be discribed by the simple Adler model. For this we performed experiments on populations and used either illumination or temperature cycles to entrain the circadian clock to different phases. We detail the experiment set-up that allows to monitor the circadian clock of the bacteria continuously over 2 weeks, show how to unmask additional perturbation of the bioluminescence reporter and quantify the coupling strength between the clock and the external extrainment. Fitting the model to the experimental data we show that it indeed reproduces very well the observed behaviour.

Via simulations we infer into the effects of a distribution of initial phases inside the populations, as well as the effect of possible noise on the phase or a distribution of proper frequencies. We also propose a new concept for single cell devices to infer further the effect of noise on this biological clock. These devices are designed for long term (>20 generations) observation of individual bacteria inside a population.

Abstract en français

Les cyanobactéries sont les organismes les plus simples connus possédant une horloge circadienne. Cette horloge produit des rythmes stables, dont la période est proche à 24 heures et peut être entraînée à exactement 24h par des signaux externes, comme des cycles d'éclairage ou de température.

Dans ce travail, nous montrons que cette horloge biologique se comporte

comme un oscillateur de phase. De plus, sous influence d'un entraînement externe, son comportement peut être simplement décrit par le modèle d'Adler. Pour le montrer, nous avons réalisé des expériences sur des populations, en utilisant des cycles d'éclairage ou de température qui entraînent l'horloge circadienne à des phases différentes. Nous détaillons le montage expérimental qui permet de surveiller en permanence l'horloge circadienne de la cyanobactérie; et ce pendant plusieurs semaines consécutives. Nous montrons comment démasquer des perturbations supplémentaires du rapporteur de bioluminescence et nous quantifions la force de couplage entre l'horloge et l'entraînement externe. Par ajustement numérique des données expérimentales nous montrons que le modèle utilisé reproduit très bien le comportement observé.

Via des simulations, nous cherchons les effets d'une distribution de phases initiales à l'intérieur de la population, ainsi que l'effet d'un bruit éventuel sur la phase ou d'une distribution des fréquences propres. Nous proposons également un nouveau concept pour les dispositifs à cellule unique pour observer plus en détail les effets du bruit sur cette horloge biologique. Ces dispositifs sont conçus pour des expériences à long terme (> 20 générations) d'observation de bactéries individuelles à l'intérieur d'une population.

Thank You!!

After my PhD work at SPECTRO in Grenoble, I know pretty well that the result is due to the efforts of many people besides myself. Without their help and support I would not have been able to finish.

First of all I would like to thank my supervisor Irina Mihalcescu, who accepted me in her research group and introduced my to the field of chronobiology.

A big thanks you also to the members of my jury: François-Yves Bouget and Didier Chatenay that kindly accepted to act as reporters of the manuscript and Hans Geiselmann and Till Roenneberg as part of the jury.

I would also like to thank Patrice for uncounted times he helped me solving experimental problems and many hours spend on programming issues, Jessie for her patience and kindness that helped me to overcome the pleasures of french bureaucracy, David for his advice how to fix my notoriously broken bikes, Marc and Marijke for proofreading the final version of the manuscript and very helpful comments about it. Also all the other PhD students of the lab regardless the floor they are located in ;-). An especially big "thank you" to Malika and Edith, my predecessor and successor, in particular for Edith's kindness, which is second to none.

The work on the single cell devices would not have been possible without the preliminary efforts of Jack Merrin and Laurent Montes and without the help of Thierry Fournier, who let me use his facilities at Nanofab, and Christoph Lemonias, a technician over there, who patiently explained and showed me the procedures necessary for the creation of the molds.

Finally, thanks to all the other people of the lab for shared coffees, apéros, chocolate and nitrogen ice creams.

Contents

Part I

INTRODUCTION

English introduction

How do we measure time? What is time and how do we feel it? We all know that our perception of time is relative, not in terms of the special theory of relativity, but in terms of personal sensation. Time spent during the day while being awake is perceived completely different from during the night while asleep. We cannot trust our own time perception, yet our body is able to keep a precise timing throughout the day in both cases. When travelling quickly through the timezones we can be faced to another feature of our internal clock: adaptation to the new time zone, the so called jet-lag.

One of the first evidence for independent time keeping in biology was reported by Jean-Jaques de Mairan in 1729. He noted that a mimosa plant keeps the opening rythm of its leaves even under constant darkness. This proved that the plant had an internal biological clock. From its period of time which is roughly one day long, these systems were later given the name of circadian clocks (from latin *circa-* roughly, and *-dies* day) or circadian oscillators. This type of oscillators were found in many organisms. The so far simplest known organisms possessing a circadian clock are the cyanobacteria. These bacteria show a remarquable stability of their circadian clock towards stochastic noise. It has previously been demonstrated that this is a capacity of each individual bacterium and does not depend on group synchronisation ([5, 6]). In this work we investigate the influence external periodic perturbation can have on the circadian clock of cyanobacteria.

We begin this work by a general introduction to circadian oscillators in general and the special case of the cyanobacteria in particular. We then approach the subject from a theoretical point of view and introduce the notion of self-sustained oscillators and their reaction to external perturbation.

In the second part we detail the experimental set-up and the techniques required to follow the circadian oscillation of a population via a bioluminescence reporter for several days and present the device used to create 12 independent illumination perturbation conditions in parallel. We also characterise the measured bioluminescence signal in function of the applied illumination. We then

proceed to analyse the measured signal and set it into relation of the theoretical description.

We then proceed by a qualitative and quantitative description of our results and consider the effect of noise on the circadian clock under influence of periodic perturbations. We also propose a new experimental set-up allowing to reproduce the experiments done on populations with individual cells.

Introduction en français

Comment mesurons-nous le temps? Qu'est-ce que le temps et comment le percevons-nous? Nous savons tous que la perception du temps est relative, non pas en termes de théorie de la relativité, mais en termes de sensation personnelle. Le temps que nous passons réveillés pendant la journée est perçu de manière complètement différente de celui que nous passons à dormir. Nous ne pouvons pas faire confiance en notre propre perception du temps. Malgré cela notre corps est tout à fait capable de garder son rythme quotidien dans les deux cas. Quand nous voyageons à travers des zones temporelles, nous sommes confrontés à une autre propriété de notre horloge interne : l'adaptation à une nouvelle zone temporelle, c'est le décalage horaire (jet-lag).

L'une des premières manifestations des rythmes biologiques indépendants a été observée et rapportée par Jean-Jaques de Mairan en 1729. Il avait noté un rythme persistant d'ouverture des feuilles de mimosa sous obscurité constante, prouvant ainsi l'existence d'une horloge biologique en ces plantes. On donnera plus tard à ces longueurs de périodes d'environ un jour le nom d'horloges circadiennes (du latin *circa-* environ et *-dies* jour) ou d'oscillateur circadien. Ce type d'oscillateur a été trouvé dans nombreux organismes. Les organismes les plus simples connus possédant une horloge circadienne sont les cyanobactéries. Ces bactéries montrent une stabilité remarquable de leur oscillateur circadien envers du bruit stochastique. Il a été montré auparavant que ceci est une caractéristique de chaque cellule unique et n'est pas dû à une synchronisation à l'intérieur d'une population ([5, 6]). Dans cette thèse nous nous intéressons à l'influence qu'une perturbation périodique externe peut avoir sur l'horloge circadienne de la cyanobactérie.

Nous commençons ce travail par une introduction des oscillateurs circadiens en général, et du cas particulier chez la cyanobactérie. Ensuite, nous aborderons le sujet sous un angle théorique où nous introduisons aussi la notion d'un oscillateur auto-entretenu et sa réaction face à des pertubations externes.

Dans la deuxième partie nous détaillerons le dispositif expérimental et les tech-

niques nécessaires, pour pouvoir suivre les oscillations in vivo pendant plusieurs jours à travers un rapporteur de bioluminescence. Nous présenterons également l'appareil utilisé pour créer 12 conditions d'entraînement par lumière en parallèle. Nous caractérisons aussi la bioluminescence en fonction de l'intensité d'éclairage appliquée. Ensuite nous nous pencherons sur le signal mesuré et le mettons en relation avec la description théorique.

Nous terminerons par une description quantitative et qualitative des résultats expérimentaux et considérons l'effet d'un bruit stochastique sur l'horloge circadienne sous entraînement. Nous développerons également un nouveau dispositif expérimental qui ouvre la voie vers des expériences d'entraînement avec des cellules uniques.

Chapter 1

Biology

1.1 Biological oscillators

Earth is an environment where periodic changes are very frequent. The period length of these fluctuation ranges from historic to sub-daily. Examples for events oscillating at a historic timescale are the alternation in the earth magnetic field and the ice ages. The timescale of these events is so long that biological systems, having generation times orders of magnitudes shorter, adapt to them (or not) by evolutionary pressure. On an already much shorter timescale we find the seasonal changes as well as the biologically most important variation, the day/night rhythm given by the earth rotation. A major habitat shaping periodic event with a period shorter than one day are the tides occurring approximately all 12 h 25 min ([17]).

Besides these periodical events occur with rather fixed frequency, there are also various non-periodic fluctuations. The changing weather conditions include non predictable variations in illumination, temperature and humidity, which require adaptation of living organisms. Now while adaptation is possible, predicting at least the periodic events is better. To achieve this, organisms have developed several strategies, most of them built around a central clock with a period length of about 24 h. This central pacemaker then rhythms the day and can entrain secondary oscillators with longer period times. Since their discovery in 1729 by the French astronomer Jean Jacques d'Ortus de Mairan who observed that the daily rhythm in leaf movement in Mimosa pudica ([33, 58]) persisted even in constant darkness numerous examples of circadian clocks have been found in all higher organisms. It was also shown that, by accelerating the circadian clock, it is possible to accelerate annual oscillators, for example in deers, which made them grow and loose their antlers earlier then under normal day length conditions

([49]).

1.2 Circadian Rhythms

A circadian rhythm is defined by three properties: a) the rhythm persists under constant conditions, so called free run, b) the rhythm shows little variation of the cycle length over a 10 °C range of temperature and c) it can be entrained to exactly 24 h by external rhythms.

- Free run. When left in constant conditions biological organisms that have a circadian clock continue their usual daily pattern with a period length close to 24 h. This criteria is used to distinguish between clock driven rhythms and responses to external cues.

- Temperature compensation. To fulfill its role as timekeeping mechanism the period length needs to be independent from environmental mean temperature. As this is generally not the case for biochemical reactions, this also allows to identify circadian rhythms from other rhythms that may express a 24 h period at a certain temperature.

- Entrainability by external cues, called zeitgebers. A *zeitgeber*, which means "timegiver" in German from the words *zeit* for "time" and *geben* for "to give" can be any exogenous signal that synchronizes an organism's endogenous clock. The circadian clock can be entrained to other periods by external periodic events, for example to exactly 24 h by the day/night cycle. It can also be entrained to another phase, as it happens when we experience jet-lag after travelling by plane over many timezones.

Examples for circadian control can be found in many species ranging from unicellular organisms like cyanobacteria ([27]), the algae to plants, insects ([12]), fish ([54]), reptiles and mammalians ([48]). They organize the every day life by triggering behavioural rhythms, like the sleep cycle or the food intake. Other examples for circadian clock-driven cycles are variations in body temperature for mammals and the expression of certain proteins at a specific moment during the day. Some travelling species also use the circadian clock in combination with sun position to keep track of travelling route. It has been shown, that these species orient themselves differently towards the sun in function of the day time ([34]).

We live in a global society where people situated in different time zones interact and work with each other. Also shiftwork becomes more and more frequent.

Understanding the role of the circadian clock becomes thus more and more important ([23]). To study them in more detail several model organisms have been selected. The cyanobacteria we use in this study is one of them.

1.3 Cyanobacteria

The oldest evidence for the existence of cyanobacteria is around 3.5 billion years old. This makes them one of the oldest, if not the oldest, life form still present on earth. They form the largest group of phototrophic prokaryotes and were a key player in enriching the atmosphere with oxygen. They adapted to almost any environment where they had access to light and water, which is their primary reductant during oxygenetic photosynthesis ([9]). Besides chlorophyll a and b, most strains also bear phycobilisomes with photosynthetic accessory pigments that allow them to use a broader light spectrum. This gives cyanobacteria their blue-green colour, hence their name "blue-green algae", although they are no algae. Actually, not all cyanobacteria are blue-green in colour. Their colour depends on the environment a certain strain has adapted to. We study the cyanobacterium Synechococcus elongatus PCC 7942 (fig. 1.1) a 6 µm x 2 µm rod shaped unicellular bacterium. Besides their importance for the oxygen supply on earth, they also play an important role in the nitrogen cycle of the biosphere by fixing nitrogen N_2 into ammonia NH_3. The process of nitrogen fixation is oxygen-sensitive and thus incompatible with photosynthesis, where oxygen is produced as a by-product ([8]). Cyanobacteria have come up with different strategies to separate these two processes. In many filamentous strains some cells specialize on nitrogen fixation. These cells degrade their photosystem II proteins and develop a thicker cell wall to separate the nitrogen fixation spatial from the oxygen produced in neighbouring cells. Another strategy is to temporally separate both processes by performing photosynthesis during the day and nitrogen fixation during the night, when pho-

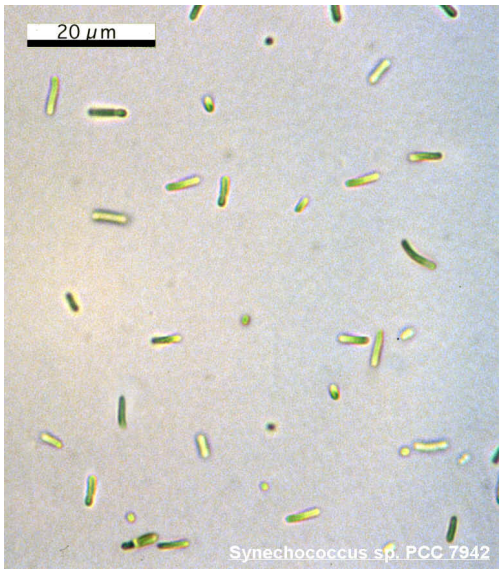

Figure 1.1: Cyanobacteria (Synechococcus elongatus PCC 7942) viewed under a microscope. ([1])

tosynthesis is not possible. In order to use this organization to its full potential, a good timekeeping system is needed. Shortly after the discovery of temporal separation in unicellular cyanobacteria under constant illumination ([41]) it was shown that the rhythms of cell division and nitrogen fixation were temperature compensated, entrainable and showed a 24 h free running period ([38]).

This was the first discovery of circadian rhythm in a prokaryote. The amount of genetic tools available to cyanobacteriologists at that time triggered a concentrated effort that turned cyanobacteria into the prokaryotic model organism for circadian research. Furthermore it was shown that all promoters are under circadian control, even foreign promoters that were cloned into the genome showed this circadian oscillations ([21]). By introducing a bacterial luciferase gene set (*luxAB*) fused to native promoters into the genome, it was possible to produce bioluminescent reporter strains ([27]). Monitoring the photon emission from these bacteria allows to follow their circadian clock in vivo.

1.3.1 Stability of the circadian clock

Before the discovery of their circadian rhythms it was widely accepted that a circadian clock would not exist in organisms with a reproduction time shorter than one day. This points into the direction of another astounding ability of the cyanobacteria: the clock remains stable even when cells divide faster than the circadian period ([29]). Further experiments that followed the circadian clock in single bacteria during several cell divisions ([35]) have indeed confirmed that the daughter cells inherit their phase and proper frequency ω_0 from their mother cell and continue to oscillate in phase with each other. In order to be able to follow the circadian clock in single cells, a bioluminescent reporter was used under the control of the strongest promoter in this strain ([18]). The strain also produced its own aldehyde substrate. Figure 1.2 (a,b) shows an example of a cell, called here F, growing, dividing and showing circadian oscillations at the same time. During the experiment the cells have several cycles of division. See for example Fig 1.2c, showing individual cell size growth, followed by divisions over the experiment and the resulting micro-colony in an exponentially growth regime (Fig 1.2d shows the total size of the micro-colony growing exponentially).

The density of bioluminescence (defined as the total bioluminescence emitted by a cell divided by its size in pixels) will oscillate with a circadian period (here 25.4 hours). Astoundingly all the descendants from an initial cell will oscillate synchronously (Fig 1.2e). The amplitude of oscillation fluctuates from cell to cell and over the time, but the temporal precision of the oscillator is impressive. A

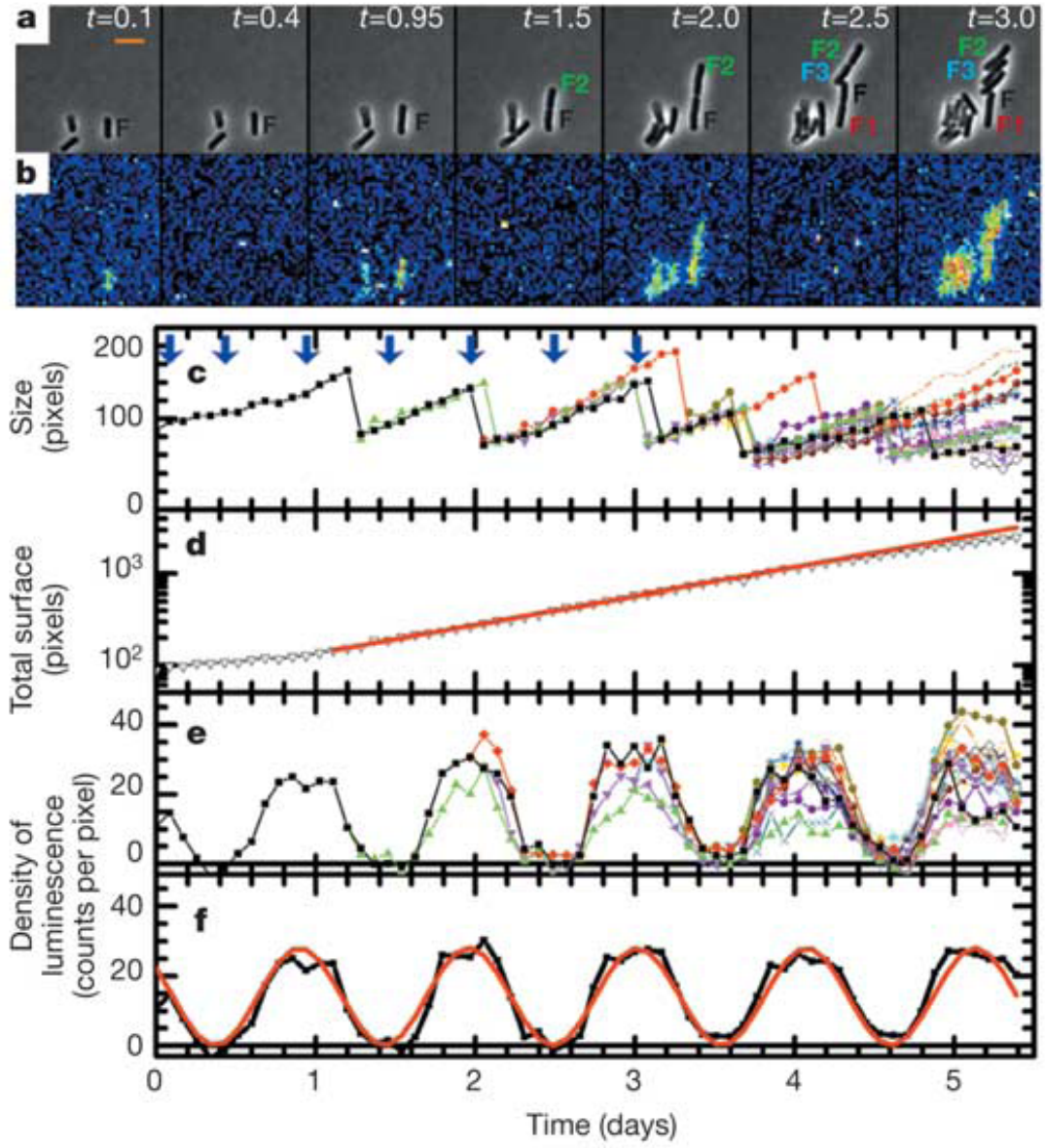

Figure 1.2: Circadian oscillation of bioluminescence in individual bacteria. (a) Phase-contrast images showing cell F and its progeny at different times t (given in days, a 24 h period of time) from the beginning of the measurement. (b) Corresponding pictures in bioluminescence. Pixels in the bioluminescence images were binned 3×3 (pseudo-colour, where red is high signal intensity and blue is low signal intensity). Scale bar, $5\,\mu m$. (c) Surface in pixels covered by cell F and all its progeny in the phase-contrast images. The arrows point to the time where the snapshots in a and b were taken. (d) The total number of pixels occupied by F and its all progeny in a logarithmic scale. The red line is the corresponding exponential growth fit. (e) Density of bioluminescence for the same cell and all its progeny versus time. (f) The average density of bioluminescence versus time (black line) and its fit (red line) with: $\langle d(t) \rangle = A + B\cos(\omega_0 + \varphi_0)$ ([35]).

rough measure of the amplitude and temporal noise of the oscillator has been done by taking the simplest model of stochastic processes for these oscillators with a stationary gaussian process for the amplitude and a Wiener process for the oscillator phase. This gives for the amplitude a noise 25% from the mean and a coherence time of 166 ± 100 days within a 95% confidence interval. A noise level of gene expression of 0.25 is not unusual, stochastic effects in gene expression fluctuations, such as molecular noise, can be at the origin of these fluctuations. What is surprising is the small level of temporal fluctuations. One has to keep in mind the experimental value of this apparent diffusion constant $D = 0.012\,\mathrm{day}^{-1}$.

As one possible explanation of the temporal stability is the inter-clock coupling, the authors inquired the possible coupling between neighbouring cells. Indeed cells with different initial phases were let grow in microcolonies which soon merged. After a couple of days of direct interaction, each detected cell kept its own phase. This result gave strong hints toward an internally built stability, excluding a strong interaction between individual clocks.

However, a faint interaction between clocks could not be excluded by these experiments, as an evaluation of the upper bound of the coupling constant was larger than the measured temporal precision. Next paragraph will show how exactly this has been solved.

1.3.2 Stability without mutual coupling

To evaluate a possible very faint intercellular interaction, the cells with different initial phases were hold in interaction for a longer time (a couple of weeks). As microscopically it becomes impossible to follow single cells over more than 5-6 cycles of division, due to evident crowding constraints, a different strategy has been taken. Two populations of cells, with different initial phases were mixed: the measurement consists of following the possible phase change of a minority population in the presence of another, 20 times larger majority, ([5], [6]). The majority cells were wild-type and had no reporter, while the minority cells had a chromosomal transcriptional reporter: a bioluminescent reporter following the promoter activity of the main clock protein KaiC ([18]). Both strains have therefore a circadian clock ticking in the same way, but only the minority circadian clock has been monitored.

The strains were entrained in the same way, frozen, and then thawed at different time. If freezing, the bacteria stops the clock, thawing them will restart it. In this way a similar width of the initial distribution of phase inside a population of clocks was insured, only the average would be shifted, depending on the thawing

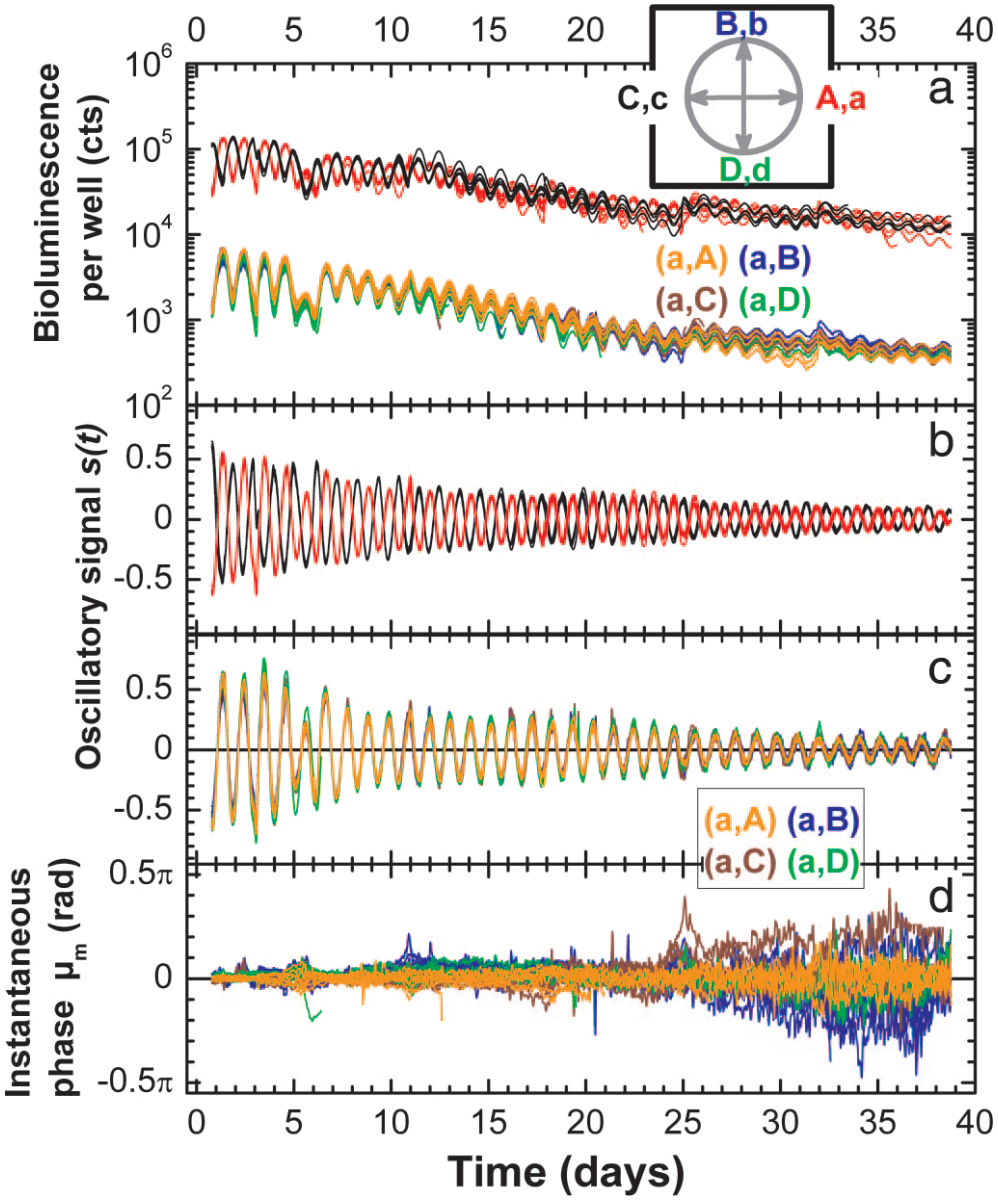

Figure 1.3: The mean phase of a minority population of bioluminescent cyanobacteria (phase a) is unaffected by the presence of a majority population with different phases (4 conditions: phases A, B, C and D). Controls of pure bioluminescent conditions (red, black) show the same behaviour as the minority populations. (a) The raw bioluminescence signal. (b) The circadian oscillation of the two control conditions. They maintain the phase opposition of their phases during the whole experiment. (c) The circadian oscillation of the minority population. Their phase appears unchanged by the presence of a different phase majority. (d) The instantaneous phase of the minority population. ([5]).

time. This created strains with 90° phase shifts between them. Sixteen different experimental conditions were created by mixing each of the four phases (0°, 90°, 180° and 270°) of the majority populations denoted here respectively (A, B, C, D) with each of the four phases (0°, 90°, 180° and 270°) of the minority population denoted here respectively (a, b, c, d). See for illustration the Insert of Figure 1.3a.

Figure 1.3a shows an example of two independent opposite phase populations of cells (A, C) which keep their difference of phase all along the almost 40 days of experiment. Also when one minority population is mixed with 4 different majority populations, there is no apparent influence on the minority phase by the presence of the majority of a different phase. By directly looking at the oscillatory signal (Fig. 1.3b, c) (see also ch. 6.3), the two previous patterns are enhanced: i) the independent wells keep their difference of phase, confirming that one population of cells keeps over long time its average phase ii) a minority population indifferently of the phase of the majority present will imperturbably keep its own pace. An even more detailed analysis by extracting the instantaneous phase of the minority population in all mixtures (Fig 1.3d) shows the same: there is very little or no difference between the evolution of phase of a minority population mixed with same average phase majority, here (a, A), and the evolution of any other mixture (a,B), (a,C), (a,D).

This experimental work is associated to a theoretical one, which shows that when two populations with widely different abundances are mixed, the time evolution of the mean phase of the minority population allows the coupling constant (ε) between bacteria to be measured directly. For that, the population of circadian oscillator has been considered as having the same proper frequency (ω_0) but different initial phases and each one submitted to stochastic noise in a generic Wiener process, defined by the diffusion constant D. However the circadian oscillator was strongly simplified to a phase oscillator (ch. 2.2.4). Experimentally, from the previous experimental data it had been established within a 95% confidence interval that $|\varepsilon| < 0.0015$ day^{-1}.

A second conclusion from this theoretical work is, that the outcome of a population of noisy, identical, free-running oscillators depends on how the noise D is related to the coupling constant ε. If $\varepsilon > D$, the coupling is stronger and the phases can be driven toward a distribution of limited width. In contrast, if $\varepsilon < D$, the noise is stronger and the phases will ultimately be uniformly distributed. It appears that for the circadian oscillator in cyanobacteria the upper limit for the coupling constant 0.0015 day^{-1} is much smaller than the previously measured ap-

parent diffusion constant in the single cell experiment D=0.012 day^{-1}. Therefore the strong single cell stability of the circadian clock in cyanobacteria is not due to an intercellular coupling, but originates from the internal wiring of the genetic and metabolic network.

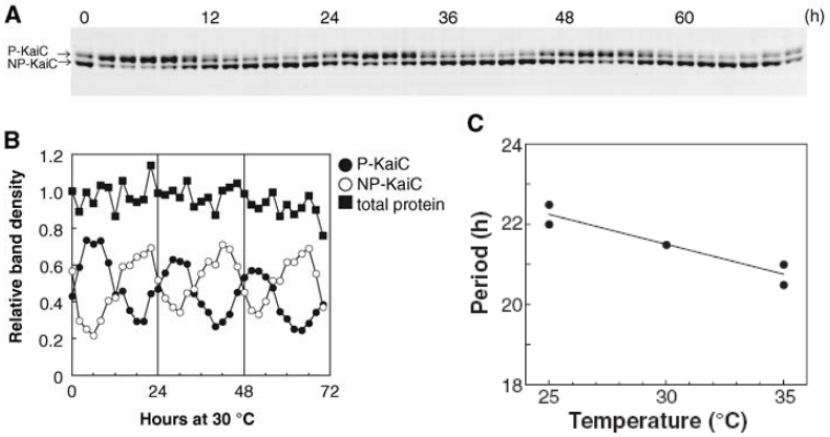

Figure 1.4: (A) Phosphorylation oscillations of KaiC in vitro. (B) Ratio of phosphorylated P-KaiC (black dots), unphosphorylated NP-KaiC (white dots) and total KaiC number (black squares). (C) Temperature dependency of the Kai oscillator period. The period length changes only very little over a range of 10 ℃. ([42])

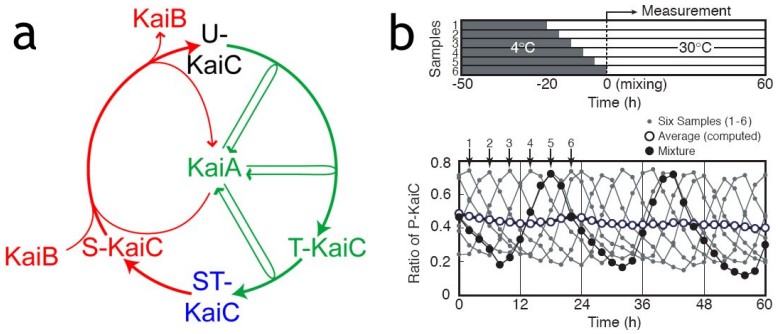

Figure 1.5: (a) The KaiC phosphorylation cycle (from [11]). During a circadian cycle (represented by a circle), the phosphorylation states of KaiC proceed in an orderly manner. The relative timing of the peak for each phosphoform, based on published data ([44, 50]), is shown by its position on the circle. (b) *top:* Preparation of the Kai oscillator at 6 different phases: they were kept at 4 ℃ for more than 30 h which halts the oscillation and then put at 30 ℃ every 4 h. *bottom:* At t=0 equal amounts of the six samples were mixed. The graph shows the evolution of the mixture (black dots) as well as the evolution of the six samples (gray dots) and their arithmetic mean (open circles) ([19]).

1.3.3 Core oscillator

If stability is not achieved via external coupling inside the population it has to be an intrinsic ability of each bacterium and thus its clock. Three proteins are

at the base of the circadian clock, KaiA, KaiB and KaiC. They were identified in 1998 ([18]) and it has been later shown that these three proteins produce a stable in vitro rhythm in presence of ATP ([42]). This rhythm shows temperature compensation, a close to 24 h (Fig 1.4) period for the wildtype proteins and is entrainable by a temperature zeitgeber.

KaiC forms large hexamers that get periodically phosphorylated and dephosphorylated during the day, while KaiA and KaiB are present as dimers. KaiC possesses two different phosphorylation sites (serine 431, theorine 432) ([43, 59]) which enable it to take four phosphorylation forms (U-KaiC, unphosphorylated; T-KaiC, T432-phosphorylated; ST-KaiC, S431-phosphorylated; S-KaiC fully phosphorylated) (Fig. 1.5) ([42]). KaiA stimulates KaiC phosphorylation by repeated association with KaiC. Starting from unphosphorylated KaiC (U), the first step in the phosphorylation phase (shown in green) is phosphorylation at T432 (T), which is further phosphorylated at S431 to the fully phosphorylated form (ST). Only then starts the dephosphorylation phase (shown in red) where T432 gets dephosphorylates first, resulting in KaiC phosphorylated only at S431 (S). From there it returns to the initial state by dephosphorylation at S431 (U). KaiB preferentially binds to S-KaiC, which inactivates KaiA and allows KaiC to return to the unphosphorylated state. When mixing KaiC molecules at different phosphorylation levels at equal proportions, the mixture still shows a clear circadian rhythm (Fig. 1.5b) ([19]).

Around this core oscillator there are additional transcription/translation feedback loops that control the interaction with the rest of the cell activities and further stabilize the oscillation (Fig. 1.6).

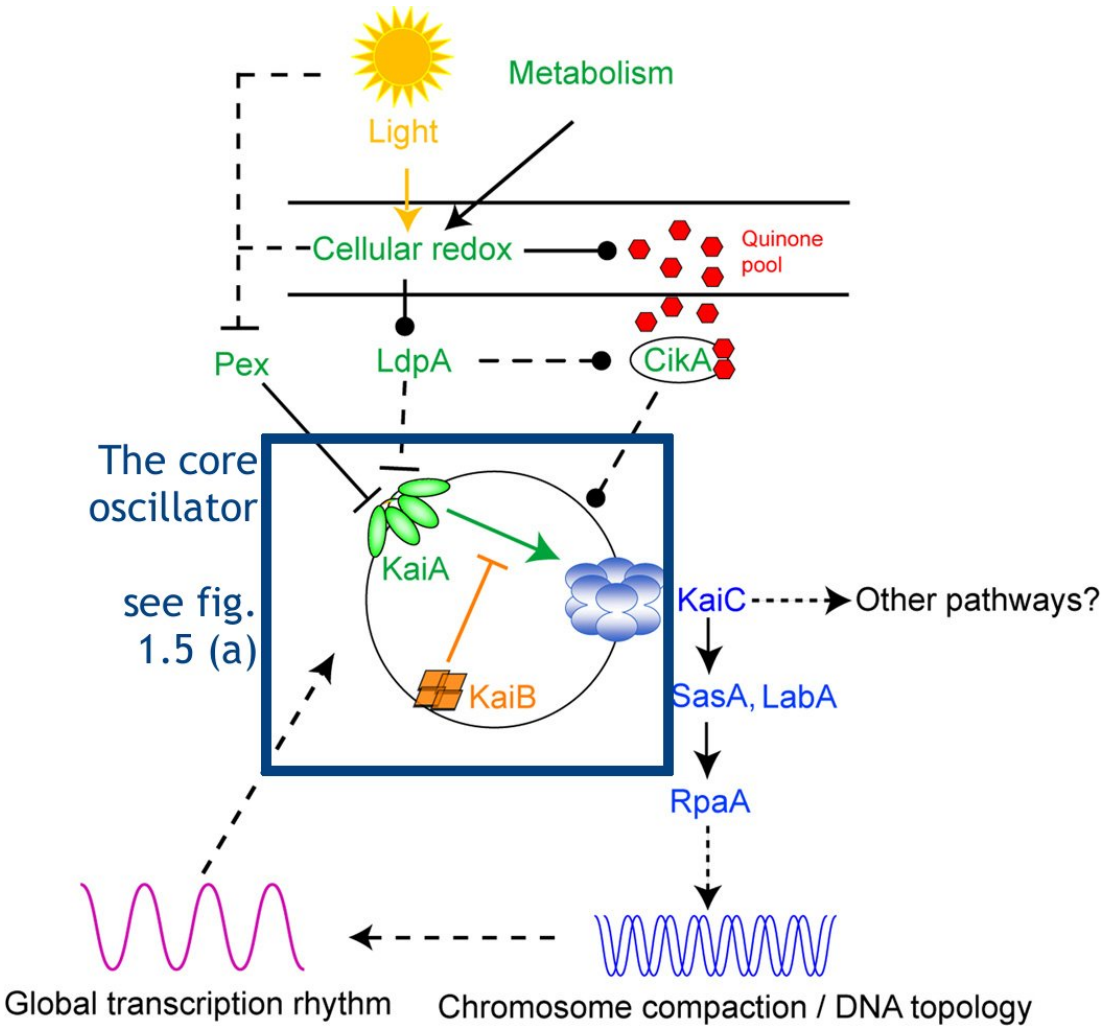

Figure 1.6: Input- and output pathways (from [11]). The core oscillator consists of KaiA, KaiB and KaiC, where KaiA favors KaiC phosphorylation and KaiB inhibits KaiA when KaiC reaches a certain phosphorylation level (see Fig). Input pathway: LdpA and CikA are sensitive to the cellular redox state, which is regulated by light and cell metabolism. LdpA also acts directly on CikA, but the mechanism is yet unknown. Pex is a transcriptional repressor of KaiA. This extends the circadian period. Output pathway: SasA interacts directly with KaiC and transfers timing information via SasA and LabA to RpaA. RpaA has a DNA binding site but its target remains to be identified ([53]). This possibly causes the rhythmic chromosome compaction that is involved in the global gene expression patterns present in cyanobacteria.

1.3.4 Input/Output pathways of the cyanobacterial circadian clock

Three proteins are known to play a role in the input pathways of the clock: Pex, LdpA and CikA. Pex has its activity peak during the night ([52]) and suppresses the transcription of KaiA which extends the circadian period ([30, 31]). Contrary to eukaryotic circadian systems, where at least one photoreceptor relays light information to the clock ([13, 15, 32]), no such pathway was found in cyanobacteria. Instead it seems that the clock senses the cellular redox state via LdpA and CikA ([20, 61]). LdpA is known to affect both KaiA and CikA, but the mechanism is yet unknown ([20]). CikA is also the key player for darkness detection. Without it, the bacteria do not get phase shifted by 5-h dark pulses, which can shift the clock phase of a wildtype bacterium up to 8h ([51]).

1.3.5 Entrainment of the circadian clock

1.3.5.1 In cyanobacteria

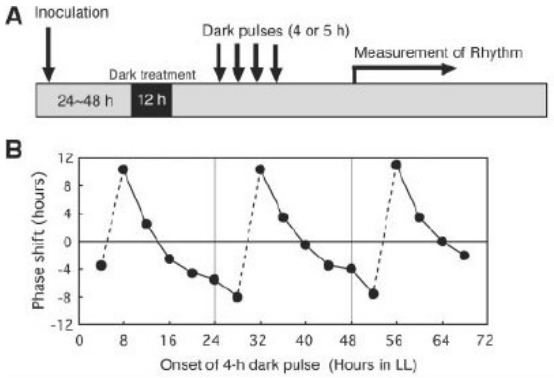

Figure 1.7: Phase shifting by dark pulses. (A) Standard protocol for phase shifting by dark pulses in continuous illumination (LL). The cyanobacteria were kept under LL condition for 1 or 2 days, then synchronised with a single 12-h dark pulse and kept in LL. At various times after the return to LL, samples were subjected to 4 h dark pulses. (B) Phase response curve for 4-h dark pulses. The phase shifts induced by the dark pulses are plotted against time after returning back LL. Positive values represent phase advance and negative values phase delay. ([26])

Depending on the moment in the circadian cycle, a dark pulse occurs; it can delay or advance the clock. Measuring the phase shift of dark pulse applied at various times to initially synchronized populations allows to plot the phase response curve (PRC) of the system (Fig. 1.7) ([26]). The circadian clocks of other organisms show similar behaviour towards light pulses ([47]).

1.3.5.2 In other organisms

The general setup with a core oscillator and a set of input and output pathways that relay timing information is also commonly found in other organisms, but these basic components can vary a lot depending on the species. This ranges from the core oscillator, made out of few proteins in the cyanobacteria, up to the suprachiasmatic nucleus (SCN). The SCN is a complex of approximately 20 000 neurons with more than one core oscillator. It is located in the hypothalamus and is the dominant circadian pacemaker in mammals ([7]). Inside each individual SCN neuron, the circadian rhythm is generated by a transcription-translation negative-feedback loop, where stability of this rather noisy process is achieved by intercellular coupling between the neurons. Also the neurons of the SCN are organized into different networks that peak at different moments of the day. They can roughly be categorized into two oscillators called the morning- and the evening-oscillator, after their respective peak time. It is hypothesized that this two-oscillator layout allows higher organisms to adapt themselves to variable day lengths during the year. It should be noted that for higher organisms most of the measurements are done on behavioural patterns, for example locomotor activity or food intake, but these rhythms may not only depend on the rhythms of the SCN ([36, 16]).

Contrary to the mammals with their central master pacemaker, the plants do not seem to possess this kind of core oscillator. The best studied organism here is Arabidopsis thaliana where a complex set of clock proteins produce rhythmic oscillations via autoregulatory feedback loops ([40]). Light entrainment is done with the help of the chryptochrom proteins CRY1 and CRY2. They have been shown to play major roles in plant photomorphogenesis, such as inhibition of stem elongation by blue light, stimulation of leaf expansion by blue light, and regulation of floral initiation by day length ([32]).

A wide variety of zeitgeber signals has been tested. The most common are light dark cycles of various period length and patterns ([55]), but also temperature cycles ([10]), food intake ([37]) and social interaction ([39]). They all have in common that they are capable of entraining the circadian oscillator, but due to the complexity of these systems and the common problems to directly measure the state of the circadian clock, it is difficult to extract the strength of the coupling for these systems. It was also shown that the shape of the signal has an effect on its capacity to entrain the circadian oscillator ([56]). In this study they report entrainment of rats with sinusoidal light signals with T=23h. As only 50% of the rats have been entrained, they conclude that this is close to the

lower limits of entrainment of this protocol. They also compare this result with a similar experiment, where they used rectangular light–dark (LD) cycles with maximum illumination, minimum illumination, and accumulated illumination per cycle identical to the sinusoidal light intensity entrainment. In the experiment with rectangular entrainment, none of the test subjects has been entrained, which suggests that gradually changing conditions might be a stronger zeitgeber signal ([56]), for the mammalian circadian clock.

In this study we will quantify the conditions and limits of the circadian clock entrainment in cyanobacteria by zeitgeber factors like illumination and temperature. As we show in the next chapter, we associate this entrainment to the simplest model describing the response of a self-sustained oscillator to periodic forcing: the phase oscillator. This model has been successfully applied to small periodic forcing in different fields like laser physics or Josephson junctions and appears sufficient to easily describe a complex system such as the circadian clock in cyanobacteria.

Chapter 2

Theoretical description of the oscillator

Generally speaking, the term oscillator represents any system with periodic variations over time. In this chapter we translate the requirements formulated for circadian oscillators and present the mathematical foundations and approximations we used to describe the experiments.

We begin by introducing the central terms of phase and amplitude on the example of a linear oscillator. Then we use them to describe self-sustained oscillators that use an energy supply to create an oscillation with a proper period, independent of fluctuations in the energy supply. We then explore how these oscillators can be coupled to other oscillating systems and present a minimal model that allows to describe the dynamics under these conditions. At the end of the chapter we look on the predictions made by this model.

2.1 Linear oscillator

The dynamics of these oscillators are described by a set of linear differential equations. In the easiest case there is only one single varying value, and we speak of a system with a single degree of freedom. Examples for systems like that are pendula and masses connected to springs. Two forces act on the mass, its attraction by earth gravity downwards and the power of the spring it is attached to upwards. In equilibrium, both forces cancel each other out and the mass does not move either up or down. If it gets displaced vertically, it will oscillate around the equilibrium position with constant amplitude and frequency (Fig 2.1a). The

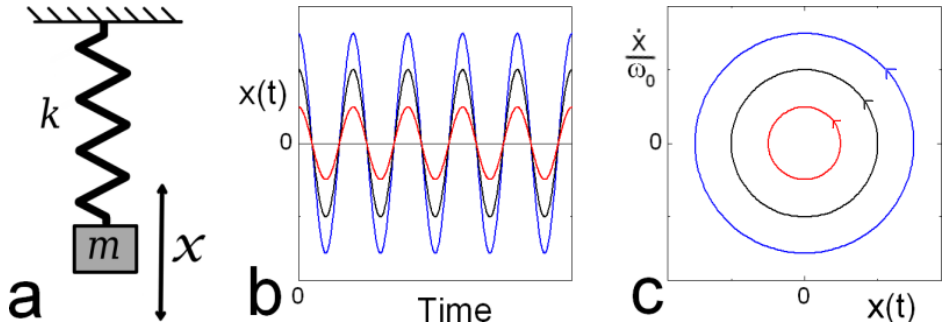

Figure 2.1: Linear oscillator without damping. (a) simple example for a linear oscillator without damping: a mass m connected to a spring with spring constant k. (b) its position x plotted vs. time (c) representation in the phase space.

position of the mass is a simple harmonic motion and is given by:

$$m \cdot \frac{\mathrm{d}^2 x}{\mathrm{d}t^2} + kx = 0.$$

This system is characterized by its amplitude A, its angular frequency $\omega_0 = \frac{2\pi}{T}$, and its phase ϕ_0, which determines the starting point on the oscillation. In our example $\omega_0 = \sqrt{\frac{k}{m}}$. A possible solution (Fig 2.1b) is written as:

$$x(t) = A \cdot \cos(\omega_0 t + \phi_0).$$

We can plot either its position x vs. time or its speed $\frac{dx}{dt}$ vs. x. The second is the representation in the phase space (Fig 2.1c). Here the oscillation is represented by a point that moves with the speed ω_0 on closed curves as the movement is periodic. Its polar coordinates are its instantaneous phase

$$\phi(t) = \omega_0 t + \phi_0 \tag{2.1}$$

and its instantaneous amplitude A or $A(t)$ in the case that the amplitude varies with time. In real oscillators friction, or damping, slows the motion of the system. This results in a slightly different frequency than the undamped case and an amplitude gradually decreasing to zero.

2.2 Self-sustained oscillator

This category of oscillators compensate the damping with the use of an energy supply which they use to maintain continuous oscillation. In general these oscillators can be classified in two categories: relaxation oscillators, in which a capaci-

tor is charged gradually and then discharged rapidly, and quasi-linear oscillators, which produce almost sinusoidal signals. Examples for relaxation oscillators are the periodic light bursts of fireflies, the heart beat ([57]) or a water reservoir with a siphon which empties the reservoir completely as soon as its threshold is reached. Examples for quasi-linear oscillators are metronomes or the vocal apparatus when it sings a single tune. In our experiments the oscillations recorded in freerun are very close to a sinusoidal function. The circadian rhythm is thus another example for a quasi linear oscillator.

2.2.1 Limit cycle as the description of self-sustained oscillator

A limit cycle is a closed trajectory in the phase space that acts as an attractor to other trajectories as time approaches infinity. In the case that all trajectories rejoin the limit cycle it is called a stable limit cycle. It implies that the system's instantaneous amplitude $A(t)$ is independent of the initial conditions once steady-state is reached as trajectories for various initial states converge to the limit cycle ([46]). Perturbations of the instantaneous phase on the other hand do not relax as any point on the limit cycle is equivalent. The system has no 'memory' where it was before (Fig 2.2). In general the oscillation of a system can be described by:

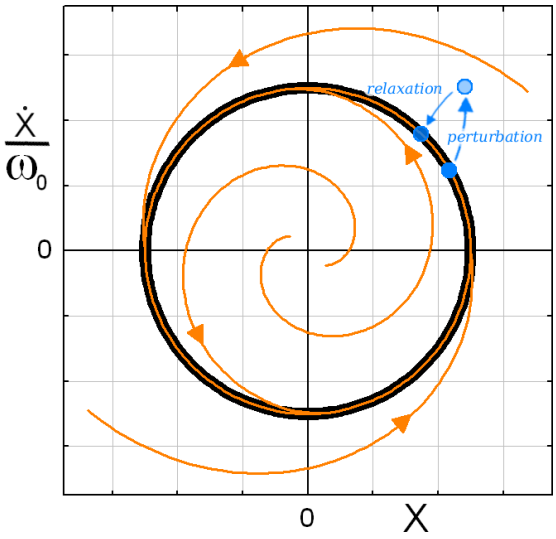

Figure 2.2: Stable limit cycle. Regardless where the oscillator motions begins it is attracted by the limit cycle. This also implies that the system relaxes back to the limit cycle after a perturbation.

$$\frac{\mathrm{d}\overrightarrow{x}}{\mathrm{d}t} = \overrightarrow{f\left(\overrightarrow{x}\right)} \qquad \overrightarrow{x} = (x_1, \ldots, x_M) \tag{2.2}$$

For a limit cycle oscillator one can define an equivalent phase $\phi\left(\overrightarrow{x}\right)$ which will rotate uniformily on the limit cycle:

$$\frac{\mathrm{d}\phi\left(\overrightarrow{x}\right)}{\mathrm{d}t} = \omega_0 \tag{2.3}$$

An example for a limit cycle oscillator is described by the Stuart-Landau

oscillator:

$$\frac{\mathrm{d}W}{\mathrm{d}t} = (1 + iC_0)\, W - (1 + iC_2)\, |W|^2\, W \tag{2.4}$$

Here W is a complex number. This can be rewritten in polar coordinates, with $W = Re^{i\theta}$. Then we get:

$$\dot{R} + i\dot{\theta}R = (1 + iC_0)\, R - (1 + iC_2)\, R^3$$

This leads to:

$$\begin{cases} \dot{R} &= R\,(1 - R^2) \\ \dot{\theta} &= C_0 - C_2 R^2 \end{cases}$$

The limit cycle here is the unit cycle with $R = 1$ on which θ rotates with the angular frequency $\dot{\theta} = C_0 - C_2 = \omega_0$. In case the initial amplitude is inequal 1 there is an additional phase shift due to the term C_2R^2. It is possible to find a parameter combination that rotates uniformly on the whole plane, here we can take

$$\begin{aligned} \dot{\theta} &= \underbrace{C_0 - C_2}_{\omega_0} + C_2\left(1 - R^2\right) \\ \Longrightarrow \dot{\theta} - \omega_0 &= C_2\left(1 - R^2\right) = C_2 \frac{\dot{R}}{R} = C_2(\dot{\ln R}) \\ \Longrightarrow (\theta - C_2 \dot{\ln} R) &= \omega_0 \end{aligned}$$

We can therefore define a variable ϕ in the whole plane so that

$$\phi(R,\, \theta) = \theta - C_2 \ln R\,.$$

One can easily check that ϕ rotates uniformly and thus it will be the phase description of the limit cycle:

$$\begin{aligned} \dot{\phi} &= \omega_0 \\ \Rightarrow \phi(R,\, \theta) &= \theta - C_2 \ln R = \omega_0 t + \phi_0 \end{aligned} \tag{2.5}$$

2.2.2 Small periodic perturbations

Repeated perturbations from the outside can entrain the oscillator and couple it to the source of the perturbations. Depending on the strength of the entrainment force, it can change or completely override the proper phase, period and amplitude of the oscillator. The source of this perturbation can either be a mutual

influence between two or more oscillators or as an external driving force that itself is not influenced by the oscillator. A striking display for mutual coupling can be observed when putting two or more metronomes with similar period times on a common support, mounted on some wheels, and let them run. After some periods, all oscillators are synchronized to the common mean phase and show the same period length. Videos of this can be easily found on Youtube.com ([2]). An example for synchronization of a large number of oscillators to a common driving force is the radio clock system, where a central very precise clock periodically corrects other clocks of lesser precision.

For small perturbations equation 2.2 can be rewritten to:

$$\frac{\mathrm{d}\overrightarrow{x}}{\mathrm{d}t} = \overrightarrow{f\left(\overrightarrow{x}\right)} + \varepsilon\overrightarrow{p}\left(\overrightarrow{x},\, t\right) \tag{2.6}$$

The periodic perturbation or entrainment force $\varepsilon\overrightarrow{p}(\overrightarrow{x},\, t) = \varepsilon\overrightarrow{p}(\overrightarrow{x},\, t + T_e)$ has it own period T_e and thus also its own proper frequency ω_e, which in general is not equal to the proper frequency of the oscillator ω_0.

The eq. 2.6 becomes for the oscillator phase:

$$\frac{\mathrm{d}\phi(\overrightarrow{x})}{\mathrm{d}t} = \omega_0 + \varepsilon Q\left(\phi,\, t\right) \tag{2.7}$$

with

$$Q\left(\phi,\, t\right) = \sum_k \frac{\partial\phi}{\partial x_k} \cdot p_k\left(\overrightarrow{x},\, t\right).$$

Since the perturbation term of eq. 2.7 is small (proportional to ε), and the deviations of $\overrightarrow{x}$ from the limit cycle $\overrightarrow{x_0}$ are small as well, we can neglect higher order terms and in first approximation:

$$Q\left(\phi,\, t\right) = \sum_k \frac{\partial\phi\left(\overrightarrow{x_0}(\phi)\right)}{\partial x_k} \cdot p_k\left(\overrightarrow{x_0}(\phi),\, t\right).$$

2.2.3 An example: The Stuart-Landau oscillator

Let's apply this to the Stuart-Landau oscillator. For that we consider a one-dimensional periodic perturbation along x: $\varepsilon\cos\left(\omega t\right)$. When adding this periodical perturbation to the x-component of the oscillator described by eq. 2.4 we

obtain[1]:

$$\dot{x} = x - C_0 y - \left(x^2 + y^2\right)(x - C_2 y) + \varepsilon \cos(\omega t)$$

Expressing this in polar coordinates we get:

$$\begin{aligned} \phi &= \theta - C_2 \ln R = \arctan\left(\frac{y}{x}\right) - C_2 \ln\left(\sqrt{x^2 + y^2}\right) \\ \phi &= \arctan\left(\frac{y}{x}\right) - \frac{C_2}{2} \ln\left(x^2 + y^2\right) \end{aligned}$$

with $R = \sqrt{x^2 + y^2}$ and $\theta = \arctan\left(\frac{y}{x}\right)$.

When applying this to the Stuart-Landau oscillator, this leads to a rewritten expression for the phase (eq. 2.5):

$$\begin{aligned} \frac{d\phi}{dt} &= \omega_0 + \varepsilon(\overrightarrow{\nabla_x \phi}) \cdot \overrightarrow{p}\left(\overrightarrow{x}, t\right) \\ &= \omega_0 + \frac{\varepsilon}{R}\left(-\left(\sin\theta + C_2 \cos\theta\right), \cos\theta - C_2 \sin\theta\right) \begin{pmatrix} \cos(\omega t) \\ 0 \end{pmatrix} \\ &= \omega_0 + \frac{\varepsilon}{R} \cos(\omega t) \cdot (\sin\theta + C_2 \cos\theta) \end{aligned}$$

For small perturbations the system remains close to the limit cycle, so $R \simeq 1$ and $\theta \simeq \phi$.

$$\Longrightarrow \frac{d\phi}{dt} = \omega_0 - \varepsilon \underbrace{\cos(\omega t) \cdot (\sin\phi + C_2 \cos\phi)}_{Q(\phi, t)} \tag{2.8}$$

where $Q(\phi, t)$ is periodic in ϕ and in t.

When looking at the phase of the Stuart-Landau oscillator under influence of a weak periodic perturbation (eq. 2.8) and apply the variable change $\psi = \phi - \omega_e t$ to it we get:

$$\frac{d\psi}{dt} = -\nu - \varepsilon \cos(\omega t) \cdot [\sin(\psi + \omega_e t) + C_2 \cos(\psi + \omega_e t)] \tag{2.9}$$

For small coupling constants ε and comparable detuning $\nu = \omega_e - \omega_0$ the evolution of $\frac{d\psi}{dt}$ is small as well. During the course of a single period ψ will hardly change.

[1] The Stuart-Landau oscillator in cartesian coordinates $W = Re^{i\theta} = x + iy$:

$$\begin{aligned} (\dot{x} + i\dot{y}) &= (1 + iC_0)(x + iy) - (1 + iC_2)\left(x^2 + y^2\right)(x + iy) \\ \dot{x} &= x - C_0 y - \left(x^2 + y^2\right)(x - C_2 y) \\ \dot{y} &= C_0 x + y - \left(x^2 + y^2\right)(C_2 x + y) \end{aligned}$$

Instead we can take the average over a period of $\frac{2\pi}{\omega}$:

$$\Gamma(\psi) = \frac{1}{2}(\sin\psi + C_2\cos\psi)$$

Using it in eq. 2.9 we get:

$$\frac{d\psi}{dt} = -\nu - \frac{\varepsilon}{2}(\sin\psi + C_2\cos\psi)$$

With the expression $\sin\psi + C_2\cos\psi = \sqrt{1+C_2^2}\sin(\psi + \arctan C_2)$ this can be rewritten to:

$$\frac{d\psi}{dt} = -\nu - \frac{\varepsilon\sqrt{1+C_2^2}}{2}\sin(\psi + \arctan C_2)$$

So, for a small sinusoidal perturbation in x that has similar proper frequency as the oscillator itself $\omega_0 \simeq \omega_e$ we obtain a result very similar to the Adler equation (eq. 2.11):

$$\frac{d\psi}{dt} = -\nu - \varepsilon_{app}\sin(\psi + \phi_0) \tag{2.10}$$

With $\phi_0 = \arctan C_2$ and $\varepsilon_{app} = \frac{\varepsilon\sqrt{1+C_2^2}}{2}$ as the apparent coupling constant.

2.2.4 Phase oscillator

When a phase oscillator is under the influence of a weak driving force, this entire system possesses a new stable limit cycle which is close to the one of the unperturbed oscillator. Evidence for an external entrainment accumulates in the instantaneous phase and the proper frequency ω_0, while the amplitude remains basically unchanged. Our primary source of information is thus the evolution of the phase of the oscillator.

The phase oscillator model was used to describe synchronisation effects between interacting oscillators in electronics, chemistry and biology. Examples are laser coupling, Josephson-junction arrays, chemical oscillators like Belousov-Zhabotinsky reaction systems ([4]) or the mutual coupling of fireflies ([45]). It is also a commonly used approximation in Neurosciences ([14]). For example it can be used to describe the neuron complexes generating the rhythms for the respiratory system ([22]).

2.3 Adler equation

The simplest equation describing the dynamics of a phase oscillator under entrainment is often called the Adler equation after Robert Adler ([3]). In case of a weak coupling force we can keep only the first term of the Fourier approximation of $Q(\phi, t)$. We thus assume that the coupling force resembles simply a sinus, eq. 2.7 then becomes the Adler equation:

$$\frac{\mathrm{d}\phi}{\mathrm{d}t} = \omega_0 - \varepsilon \sin(\phi - \theta). \tag{2.11}$$

where $\theta = \theta_{e_0} + \omega_e t$ stands for the entrainment force.

As this approach is valid only for weak entrainment forces, it may take several oscillations before the oscillator is fully entrained. It is thus useful to observe only the variation or evolution of the phase introduced by the entrainment. For that purpose we use a rotating frame, turning at the same frequency as the entrainment force. The phase in this reference frame is given by $\psi = \phi - \omega_e t$. If an oscillator is successfully entrained, it has the same frequency as the entrainment force. This means that its phase will reach a stationary value in the rotating frame. The detuning is given by the gradient of a freerun plot $\nu = \omega_e - \omega_0$.

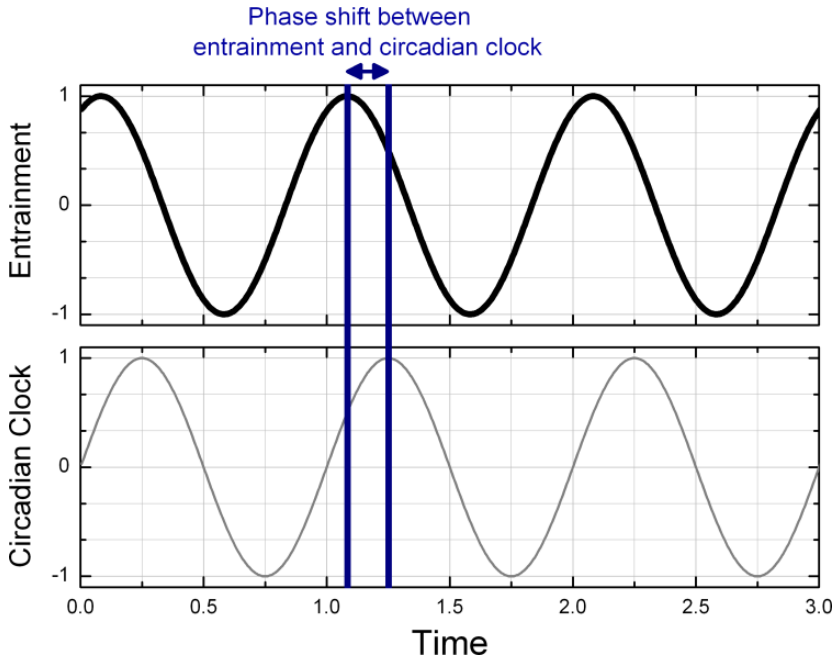

Figure 2.3: Stable phase shift between the entrainment and the entrained oscillator as described by eq. 2.12.

The Adler equation becomes then:

$$\frac{\mathrm{d}\psi}{\mathrm{d}t} = -\nu - \varepsilon \sin(\psi)$$

In case the oscillator gets entrained, its period will be locked to the period of the entrainment force, and in a rotating frame turning with the same angular frequency, its phase variation will become zero

$$\frac{\mathrm{d}\psi}{\mathrm{d}t} = 0$$

This allows to easily show that an entrained oscillator generally will not have exactly the same phase at the entrainment force, but will lag behind by a certain stable phase shift (fig. 2.3).

$$\psi\Big|_{t\to\infty} = -\arcsin\left(\frac{\nu}{\varepsilon}\right) \tag{2.12}$$

When looking for the analytical solution of the Adler equation we need to distinguish between 3 cases depending on the values of ε and ν:

$$\tan\left(\frac{\psi(t)-\psi_0}{2}\right) = \begin{cases} \frac{\tanh\left(\Omega\cdot\frac{t}{2}\right)\cdot[\varepsilon\sin(\Delta\theta)+\nu]}{\Omega+\tanh\left(\Omega\cdot\frac{t}{2}\right)\cdot\varepsilon\cos(\Delta\theta)}\,,\ \Omega=\sqrt{\varepsilon^2-\nu^2} & \forall\varepsilon>\nu \\ \frac{[\sin(\Delta\theta)-1]\cdot\varepsilon t}{2+\varepsilon t\cdot\cos(\Delta\theta)} & \varepsilon=\nu \\ \frac{\tan\left(\Omega_b\cdot\frac{t}{2}\right)\cdot[\varepsilon\sin(\Delta\theta)+\nu]}{\Omega_b+\tan\left(\Omega_b\cdot\frac{t}{2}\right)\cdot\varepsilon\cos(\Delta\theta)}\,,\ \Omega_b=\sqrt{\nu^2-\varepsilon^2} & \forall\varepsilon<\nu \end{cases} \tag{2.13}$$

with $\Delta\theta = \theta_{e_0} - \psi_0$.

2.3.1 Entrainment by an external force: Phase locking

When a phase oscillator is under influence of an entrainment force (the zeitgeber for circadian clock), this coupling force has to overcome the attractive force of the stable limit cycle. In general, the proper period of the oscillator ω_0 is different from the one of the entrainment. When we imagine the oscillator and the entrainment oscillator in the phase space, the coupling force can be seen a spring with a spring constant ε (fig. 2.4).

2.3.1.1 Phase locking

If this coupling is stronger than the attraction from the limit cycle, it will be able to successfully entrain the oscillator. In this case the period of the coupled oscilla-

tor

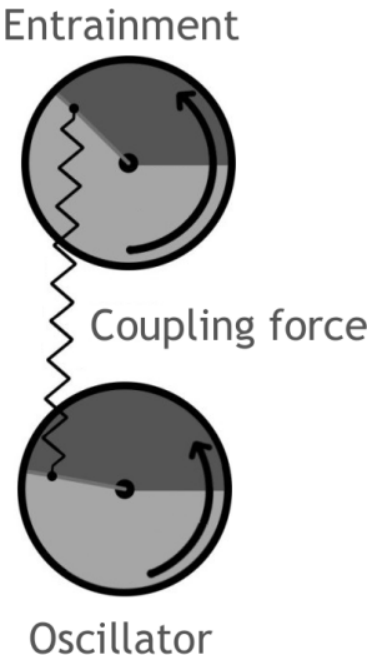

Figure 2.4: Schematic image of the relation between entrainment force and the oscillator. Both rotate with their own proper frequency, but the oscillator is coupled to the entrainment via the coupling force represented by a spring.

will be the same as the period of the entrainment, this is called frequency locking. The larger the detuning is, the larger the coupling needs to be in order to entrain the oscillator to overcome this difference. Depending on the strength of the coupling force, the entrained oscillator and the entrainment force show a stable phase shift:

$$\psi|_{t\to\infty} = -\arcsin\left(\frac{\nu}{\varepsilon}\right) \tag{2.14}$$

This behaviour is shown in figure 2.5(a). Both parts of the graph show the same oscillator (proper frequency ω_0, drawn in orange) under influence of a periodic perturbation (proper frequency ω_e, drawn in black) of initially opposite phase. On top, we plot the actual oscillation pattern, and below the representation in the rotating frame of the entrainment force. Under influence of this entrainment the oscillator executes a gradual phase change until it reaches a new stable phase with a stable phase shift (blue). The time interval needed to adjust to the new phase is proportional to $\frac{\nu}{\varepsilon}$, the bigger ε becomes compared to ν the quicker phase an frequency locking will be achieved.

2.3.1.2 Pseudo-entrainment

In case the entrainment force cannot overcome the detuning, we observe pseudo-entrainment. The entrainment force is still able to influence the oscillator, but moments when both are in phase will alternate with ones when both desynchronize. The entrained oscillator will develop a more complex movement with two different period times, as the entrainment force will alternate between accelerating and slowing down the oscillator. The phase starts to oscillate around the beat frequency, which is given by:

$$\Omega_b = -\sqrt{\nu^2 - \varepsilon^2}$$

This behaviour can be seen in figure 2.5(b). The set-up is the same as before (ch. 2.3.1.1, 2.5(a)) only with a coupling force ε too weak to overcome the detuning ν. The oscillator alternately gets accelerated and slowed down by the external force. This leads to the tumbling behaviour of the phase around the beat frequency Ω_b (blue).

2.4 Can the in vivo circadian clock in cyanobacteria be described by a phase oscillator model?

The phase oscillator model is a simple, yet powerful mathematical model that was used to describe oscillation phenomena in completely different scientific fields. Moreover the Adler model is another drastic simplified model to describe the coupling of a phase oscillator to an external force. This simplification comes with certain conditions that needs to be matched to apply.

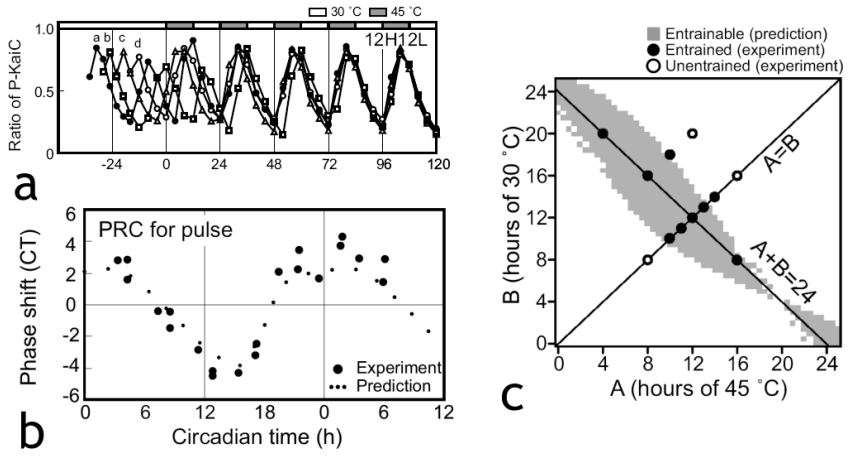

Figure 2.6: (a) Four mixtures were incubated at 30℃ for 34 hours (a, closed circle), 28 hours (b, open square), 22 hours (c, open triangle), and 16 hours (d, open circle), and then subjected to 45℃/30℃ cycles of 12H12L (12 hours 45℃ and 12 hours 30℃) (b) the phase response curve (PRC) for a 4h temperature pulse at 45° C, calculated by combining the PRCs for simple up and down temperature steps. (c) Prediction and experimental verification for temperature cycles. ([60])

In cyanobacteria the circadian core oscillator that is built with the three Kai proteins and ATP is temperature compensated. Its period length at 30° C is 23.4h, while at 45° C it is 23.3h (fig. 2.6a). Recent studies showed that this in vitro circadian clock can be entrained by temperature steps between 30° and 45° C and back. As the period length is almost the same at both temperatures, this cannot

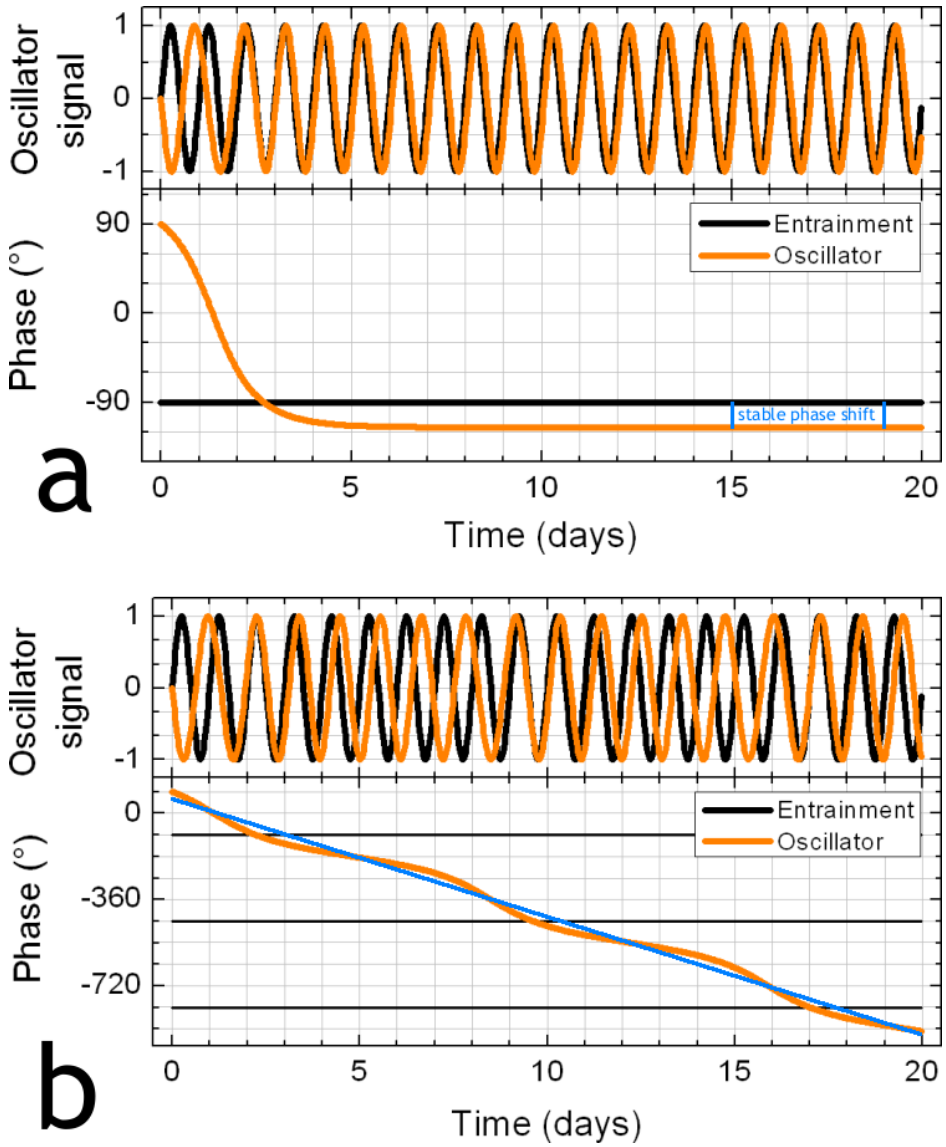

Figure 2.5: (a) behaviour of a coupled oscillator. top: The oscillations from both the entrainment (black) and the entrained oscillator (orange). They start at opposite phases until the oscillator joins the driving force and reaches phase and frequency locking with a stable phase shift (blue). bottom: The phase of these two oscillators represented in the reference frame of the entrainment force rotating at ω_e. Frequency locking is reached as soon as the oscillator phase becomes horizontal. (b) behaviour of an influenced oscillator. top: The oscillations periodically synchronize and desynchronize without reaching phase and frequency locking. bottom: Same set-up in a ω_e-rotating frame. The phase oscillates around the beat frequency Ω_b (blue). The three black lines represent the same entrainment phase as they are separated by 360° from each other.

be explained by period length variations. Instead the authors examined the phase shift induced by temperature steps (both up and down) at various moments during the circadian cycle and measured the phase response to it. The predicted phase shifts based upon the phase response curves (PRCs) were experimentally verified for 4-h pulses at 45° C (fig. 2.6b) and for repeated temperature cycles of various lengths (fig. 2.6c). This showed that the entrainment of the core oscillator can be described using phase shifts rather than period length changes. This confirmed results on previous temperature entrainment experiments done with *Drosophila pseudoobscura [62]*.

Based on previous work that showed the remarkable stability of single cell oscillations (ch. 1.3.1), and that this stability is in fact an inherent property of each individual bacterium (ch. 1.3.2), we want to elucidate the possibility to describe the in vivo circadian clock of a population of cyanobacteria by a phase oscillator model. To test this we set up an experiment that allows to entrain the bacteria with different coupling forces either by illumination or temperature and compare the phase dynamics to the Adler model. Besides verification of the phase oscillator model, we also want to inquire if the entrainment experiments can uncover the origin of the noise that acts on the whole circadian system.

Part II

EXPERIMENTAL SET-UP

English introduction

In this part we present the necessary techniques and the experimental set-up to follow the circadian clock of cyanobacteria in vivo.

We begin with the description of the cell culture and the necessary techniques to grow the bacteria before and during the experiment. To follow the circadian clock we use a bioluminescent strain, we describe how the bioluminescence is produced inside the bacteria and how this can be used to obtain information about the circadian clock. To parallelise the experiments we follow the oscillating signal from the bioluminescence reporter, using a pair of automatised photomultipliers for 192 independent populations simultaneously. At the end of the first chapter we introduce the entrainment devices that allow us to apply 12 different illumination pattern simultaneously with an additional temperature control.

In the next chapter we study the behaviour of the experiment and the reaction of the bacteria to the refillment of media during the experiment. In particular we were interested in the response of the bioluminescence reporter to the applied light intensity. Using this information, we will then tackle the task of correcting the light dependent variations of the bacterial bioluminescence production to obtain a clearer circadian signal. We close this chapter by an investigation of possible cross-illumination by our entrainment device and the effect it has on the circadian clock.

Next we characterise the bioluminescence signal of a population and show how to extract the mean phase $\langle\varphi\rangle$ and the amplitude $A(t)$ of a population. We also introduce the order parameter ρ of the population that describes the level of synchronisation inside the population.

Finally we describe our process of data treatment. This is done in four major steps. First comes the compensation of bioluminescence jumps due to medium refills during the experiment. As next step we apply the previously discussed correction of the bioluminescence production in function of the applied illumination signal. From this corrected signal we extract the circadian oscillatory signal and from it the instantaneous mean phase and the instantaneous amplitude. Finally

we describe the criteria by which we clean the experimental data to keep only the significant information about the circadian oscillation.

Introduction en français

Dans cette partie nous présentons les techniques nécessaires et le montage expérimental pour pouvoir suivre l'horloge circadienne des cyanobactéries in vivo.

Nous commençons par une description de la culture cellulaire et des techniques nécessaires pour faire pousser les bactéries avant et pendant l'expérience. Pour suivre l'horloge circadienne, nous utilisons une souche bioluminescente, décrivons comment la bioluminescence est produite à l'intérieur de la bactérie et comment elle peut être utilisée pour suivre l'oscillateur circadien. Pour des raisons de parallélisation nous suivons le signal oscillant de la bioluminescence avec une paire de photo-multiplicateurs automatisés pour 192 populations indépendantes simultanément. A la fin du premier chapitre nous présentons le dispositif expérimental qui nous permet d'appliquer 12 conditions d'illumination en parallèle avec un contrôle de température supplémentaire.

Dans le chapitre qui suit, nous étudierons le comportement des appareils et la réaction des bactéries lors du rajout de milieu de culture pendant l'expérience. En particulier, nous nous intéressons à la réponse du rapporteur de bioluminescence à l'intensité de la lumiere appliquée. A l'aide de ces informations, nous nous attacherons à corriger les variations de bioluminescence bactérienne dépendentes de l'illumination appliquée pour en obtenir un signal circadien plus clair. Nous terminons ce chapitre par une enquête d'éclairage transversal possible par notre dispositif de l'entraînement et l'effet qu'il peut avoir sur l'horloge circadienne.

Ensuite, nous caractérisons le signal de bioluminescence d'une population et nous montrons comment extraire la phase moyenne $\langle\varphi\rangle$ et l'amplitude $A(t)$ de la population. Nous introduisons également le paramètre d'ordre ρ de la population qui décrit le niveau de la synchronisation à l'intérieur de la population.

Enfin, nous décrivons notre processus de traitement des données. Cela se fait en quatre étapes principales : premièrement, la compensation des sauts de bioluminescence en fonction du rajout de milieu pendant l'expérience. Ensuite nous appliquons la correction de bioluminescence déjà discutée en fonction du signal d'illumination appliqué aux bactéries. A partir de ce signal corrigé nous

obtenons le signal circadien oscillatoire et de celui-ci la phase moyenne instantanée et l'amplitude instantanée. Enfin, nous décrivons les critères selon lesquels nous nettoyons les données expérimentales pour ne garder que les données significatives de l'oscillation circadienne.

Chapter 3

Experimental Set-Up

To observe the influence that a weak external force has on the circadian cycle, we need to follow it continuously during several cycles. By nature, a cycle of a circadian clock takes about one day, therefore we need an experimental set-up that allows us to keep the experiment running and the bacteria alive for several weeks while regularly taking data points. This necessitates a way to access the circadian clock *in vivo*, maintain the integrity of the population, reduce possible perturbations, and parallels data acquisition. To meet all of these requirements we use a genetically modified strain of cyanobacteria that emits light as a function of the circadian clock. During the experiment, the bacteria are kept in two 96 well plates, making it much easier to automatically read the bioluminescence signal from each well. In this way we perform 192 independent experiments at once, with a reading time interval of 40 minutes.

3.1 Cell culture

The bacteria can be grown either in liquid or solid BG11 (see App. A), the only difference being a gelling agent added for the solid media. BG11 contains all nutriments the bacteria need except CO_2 and O_2 which are furnished by ambiant air. For all our experiments, we grow the bacteria in liquid medium in sterile glass flasks (see Fig.: 3.1). Outside the experiment the bacteria are kept in an incubator specially designed for cell culture. The bacteria are grown under constant stirring at 30° C, 1250 ppm CO_2, and 1000 lux white light. The bacteria can be kept in total darkness (DD-condition from dark dark), constant illumination (LL-condition) or in periodically changing condition (LD-cycles for light-dark cycles). To entrain bacteria in the incubator, we automatically switch on and off the light every 12h. We use 12h of light at 1000 lux (day) followed

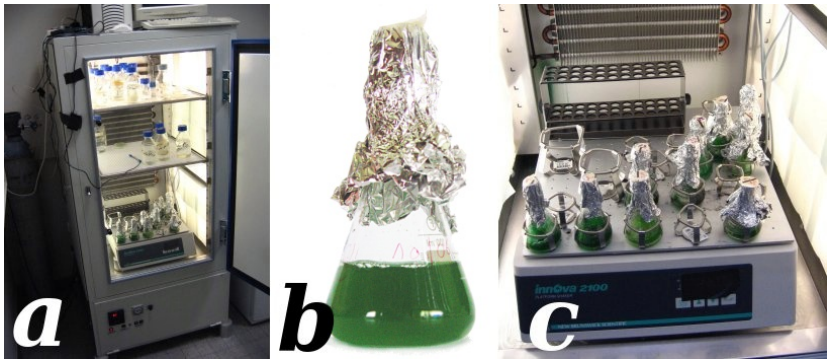

Figure 3.1: (a) Thermo- and CO_2-controlled Incubator for cell culture. (b) Sterilized glass flask with a culture of cyanobacteria in the incubator. (c) Shaker inside the incubator, constantly steering the flask to homogeneously furnish nutriments, illuminate and entrain all bacteria.

by 12h in total darkness (night) without any changes of temperature or CO_2 concentration.

3.1.1 Long term storage

For long time storage, it is possible to deep-freeze the bacteria. For that purpose it is necessary to add 15% glycerol to the media in order to reduce the formation of ice crystals inside the bacteria. The bacteria are kept into 2 ml screw top vials and put at -80° C. When needed, the bacteria are taken out of the freezer and diluted in approximately 20 times the media and put into the incubator to initiate exponential growing. Despite the glycerol, there is still a loss of bacteria in the population. The freezing process also halts the circadian clock which will continue its cycle after thawing.

3.1.2 Growing bacteria on microplates

Microplates consist of 96 wells ordered into 8 lines of 12 wells each. Each well is 1 cm deep and can contain up to 300 µl. We use white opaque microplates for our experiments which greatly reduce the diffusion of light from one well to another one and thus almost eliminate cross talk. This also imposes the necessity to illuminate the wells from above.

At the beginning of the experiment, we fill each well with 250 µl of homogeneously mixed bacteria solution (Fig. 3.2b left side). The bacteria will sediment to the ground of the well after some hours (Fig. 3.2b right side). During the experiment, we need to furnish the bacteria with the key components for their growing: light, CO_2 and O_2. But we also need to protect them from contam-

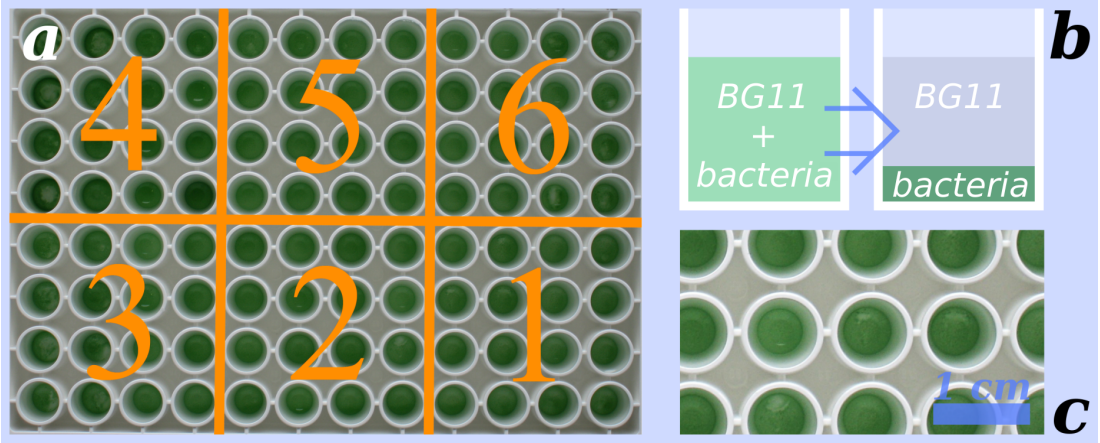

Figure 3.2: (a) 96 well opaque microplate organized into 6 clusters containing 16 wells each (b) sedimentation of the bacteria during the experiment (c) a zoom on single wells, the wells are separated from each others by opaque walls and space to minimize bioluminescence crosstalk

ination by the non sterile experimental set-up. For this we seal the top of the microplates with a transparent sterile film (TopSeal) and cut little openings with a sterile scalpel to let the air pass. This also prevents the liquid culture from being spilled out their well while manipulating the microplates and also limits media evaporation. There are gas permeable seals, but their permeability was not enough to keep the bacteria alive more than a few days. As a result we need to regularly furnish new media to counteract the evaporation during the experiment, normally every 5-7 days. For that purpose we transfer the microplates from the experiment to the sterile hood, remove the TopSeal and add the some drops of BG11 media to each well. This is done carefully drop by drop to minimize steering up the bacteria at the bottom of the well. Afterward we apply a new TopSeal, cut the openings about each well and put it back into the experiment. This whole procedure takes about 15 min per plate. By taking a plate out of the experiment right after it was read by the photomultiplier, it is possible to complete the whole procedure without having to stop the experiment. The addition of media still has the possibility to alter the measured signal. The way this is done and delt with is detailed in chapter 6.1.

3.1.3 Counting bacteria and initial density

Just before deploying the bacteria on the 96 well plates, we measure the optical density at 750 nm of the assay using a spectrometer (Shimadzu UV-1201) in absorption mode. This spectrometer directly measures the optical density ($\log\left(\frac{I_{incident}}{I_{transmitted}}\right)$). For OD lower than 0.5 the absorption varies linearly with

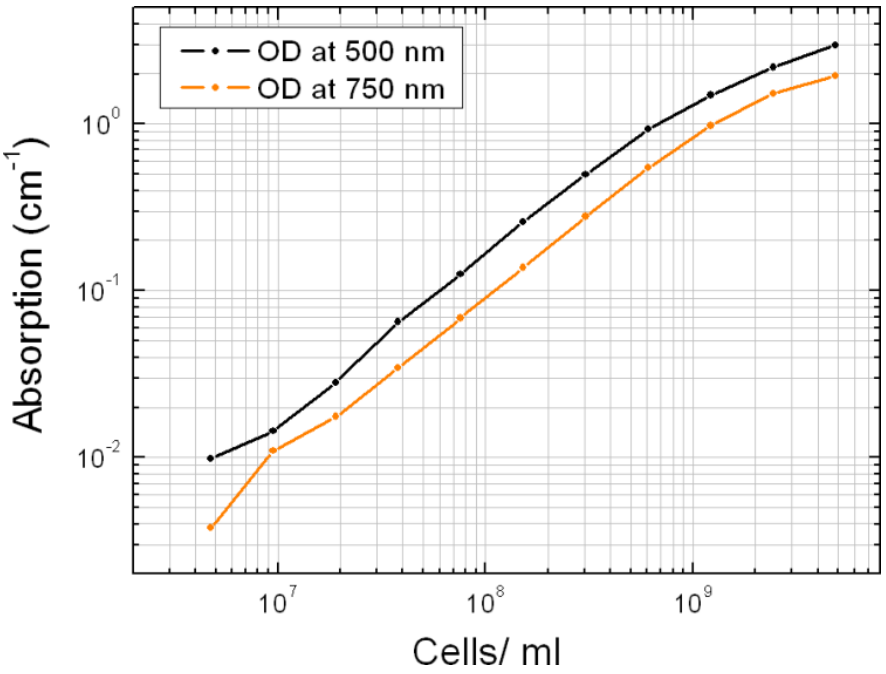

Figure 3.3: Absorption at 500 nm and 750 nm depending on the cellular density. (From [Amdaoud, M., rapport de stage de DEA, 2003])

the cellular density (Fig. 3.3). To control the cell concentration we measure the OD and adjust it to 0.1 by diluting the assay with BG11. This corresponds to$\approx 3 \cdot 10^7$ cells/well in a well containing 250 μl.

The OD of 0.1 was chosen because it marks the transition point between regimes of average light detected: a first strong exponentially growing regime and a second slightly decreasing regime. These regimes have their origin in the number of detected cells and the capacity of cyanobacteria to absorb photons (Fig. 5.2a) covering a spectral range form near UV to infrared. For low cell concentrations we detect the light emission of all bacteria. The amount of detected light grows with the number of cells (bulk detection) until the upper layers absorb all bioluminescence coming from the emitters below them (top detection). Even if the number of emitters continues to increase (visualized by an increasingly green colour of the wells), the number of detected photons will remain constant as only the bacteria close to the surface can be seen. This effect will be discussed in more details in section 5.2.

In our case an initial $OD_{750nm} = 0.1$ marks the transition to a "top detection" regime. The detected bioluminescence will be then independent of the absolute number of cells. The nutrient resources shared among increasingly numerous members will counteract the gain of the bioluminescence reaction/cell. The baseline bioluminescence of a well therefore decreases slowly in time (Fig. 6.2a).

3.2 Isolation box

To maintain the growing condition from the incubator during the length of the experiment we built an isolation box on top of the TopCount containing the stocking towers (Fig. 3.4). The box is connected to a CO_2 source and is equipped with a Peltier element for temperature regulation. During an experiment we constantly monitor both of this parameters. Typical values are 4000 ppm CO_2 and 30 °C ± 0.2 °C.

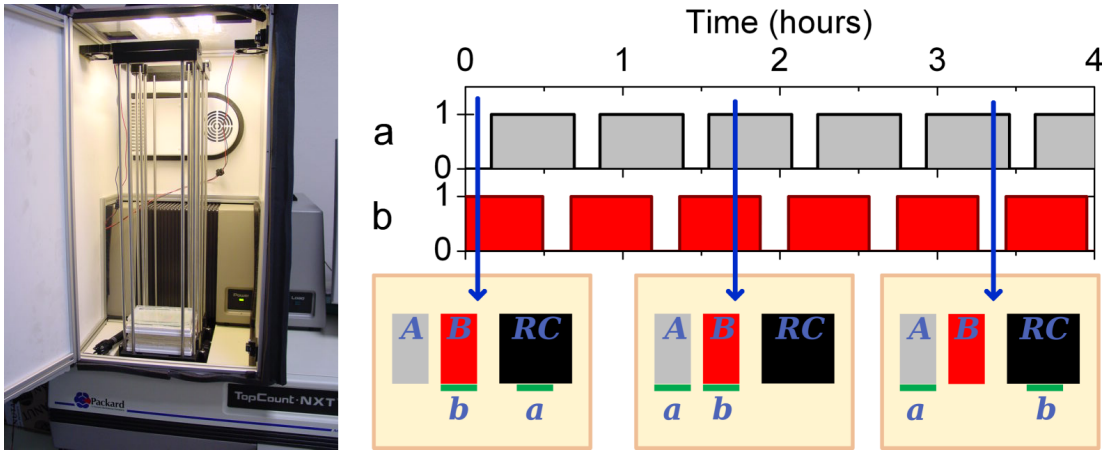

Figure 3.4: (left) Isolation box containing the microplates with the bacteria during the experiment. The box is thermoregulated and has a CO_2 supply. The box is mounted on the bioluminescence detector TopCount NXT. (right) Illumination pattern (top) due to the TopCount reading cycle (bottom) for each plate (a and b) in the case of constant illumination. During handling and data acquisition inside the reading chamber (RC) the plates are not illuminated. Entrainment by light is done only during the 'on' time on the stocking towers A and B. For detailed values see Appendix B.

3.3 Bioluminescence

Some organisms have developed the ability to emit light. The commonly best known example is the firefly that uses light pulses to attract possible mating partners. Other examples include jelly fish or the bacteria *Vibrio harveyi*.

Generally light emitted by higher organisms is used to transfer a message. Both "come here to have fun" and "come here so I can eat you" have in common that the light production is coupled to other processes and is part of a greater picture. For unicellular organisms like bacteria the use of bioluminescence is not as obvious. One hypothesis is, that in an atmosphere originally deprived of O_2 and where oxygen was toxic for organisms, the bioluminescence reaction might have been used to consume the internal free oxygen.

3.3.1 Reporter strain

By coupling the genes responsible for the light emission to other processes we can gain information about their activation and deactivation via the light emission. It can thus act as a reporter for other invisible activities inside the living cell. To decide when to produce a certain protein, living cells rely on activation sequences located right before the protein coding sequence. This activation sequences are called promoters. As the cell has no way to distinguish what lies behind a promoter, two or more proteins with the same promoter will be produced in parallel. As already mentioned in 1.3, all protein expression in cyanobacteria is controlled by the circadian clock. So for cyanobacteria any promoter would reveal information about the clock. Only the shape of the oscillation will depend on the promoter. To minimize other influences we will use the promoter of the master clock gene KaiC.

The bacteria strain we use here has such a reporter incorporated into its genome. This gives access to the *in vivo* clock simply by detecting the amount of light emitted by the bacteria.

3.3.2 Bacterial bioluminescence

Here we discuss in detail the components and reactions needed to give a bacterium the ability to "shine". Our bacteria use a part of the bioluminescence system of *Vibrio harveyi* to produce the bioluminescence. This system is built by two protein complexes LuxAB and LuxCDE. LuxAB is the light emitting protein while LuxCDE produces and recycles the required aldehyde (RCHO). The reaction itself has four steps as shown in Fig. 3.5 and requires the constant presence of reduced flavin mononucleotide ($FMNH_2$), O_2 and RCHO. It is important to keep in mind that when the incident light dampens, the photosynthesis reaction slows down or stops completely, and with it the available $FMNH_2$. This directly affects the bioluminescence signal, although the clock itself does not stop. This problem is discussed in more detail in 4.3, where we also present a method to estimate the amount of signal drop and to correct the measured signal.

For our experiments we use the strain AMC462 ([24]) with the gene insertions on two neutral sites of the bacterial chromosome: P_{kaiBC}*::luxAB* and P_{psbAI}*::luxCDE*. This means that LuxAB is under control of the KaiBC promoter (P_{kaiBC}) and LuxCDE under control of P_{psbAI}. P_{psbAI} is the strongest promoter present in cyanobacteria assuring the abundant presence of LuxCDE, respectively the aldehyde necessary for the bioluminescence reaction. Note that both P_{psbAI}

and P_{kaiBC} are class one promoters and therefore have the same phase of oscillation ([18]).

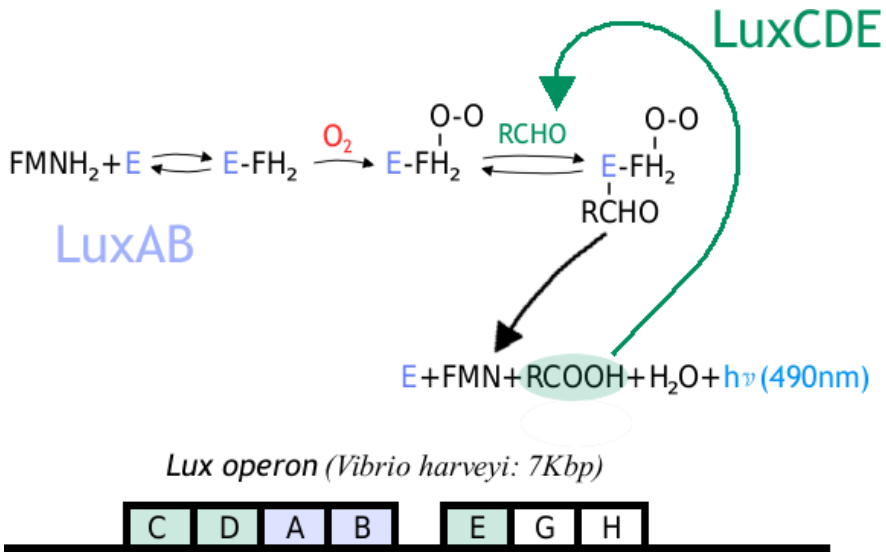

Figure 3.5: Biochemical reaction of the bioluminescence pathway from Vibrio harveyi. LuxAB emits light in presence of $FMNH_2$, O_2 and RCHO. O_2 is furnished by ambient air, while $FMNH_2$ and RCHO are produced and recycled by the bacterium itself. This is done by the LuxCDE protein complex for RCHO.

3.4 Data acquisition by robotic photon collector

The data collection is done by an automatic photon collector for 96 well microplates (Perkin Elmer TopCount NXT). This machine has 4 main components: 1) the reading chamber equipped with two photo-multipliers, 2) two micro plate stocking towers, 3) a robot for micro plate handling and 4) a computer that operates both the machine and storage of the acquired data.

3.4.1 TopCount reading sequence

Light plays several key parts in this experiment. On one hand it is *the* energy source for the bacteria and an easily controllable entrainment force. On the other hand, we detect the state of the bacteria circadian clock via light from the bioluminescent reporter. It is thus important to know when and for how long the bacteria are insolated and to assure that this does not interfere with the normal behaviour of the clock. The microplates with the bacteria spend 75% of their time during an experiment stacked directly under their LED microarray ensuring the illumination. The remaining 25% they are inside the reading chamber or moved

in or out of it. Here we look at each step in detail to explain how this pattern comes about (Fig. 3.4).

TopCount NXT is made for automatic analysis of large numbers of microplates. This is done by piling up all sample containing plates on tower A. After initiating the data acquisition, the robot will take the bottom plate from tower A, read its identity barcode and introduce it into the reading chamber. There it will pause for 3' while the natural fluorescence from the chlorophyll decreases before the photomultiplier will detect the light emission of each well. This takes 4' 45" per plate. After this, the robot takes the plate again and stocks in on tower B before introducing the next plate from tower A into the reading chamber. It continues to do so until there are no more plates on tower A or a plate bearing a stop code is detected. The lowest plate on tower A thus becomes the upper one on tower B. We call the whole sequence a reading cycle and TopCount allows to program a certain number of this cycles in advance or to loop infinitely. Before restarting the new cycle, the plates are retransferred to tower A, recreating the initial set up. Since we need to provide light for the bacteria from above, we can only use the first and last plate of a cycle to carry bacteria, as they are the only ones that stay on top of a tower most of time. We call them plate A and B, depending on the tower where they stay most of the time. We use two intermediate plates to stretch the cycle to ensure sufficient light exposure for the bacteria.

3.5 Entrainment devices

One of the main features of circadian clocks is their entrainability. This means they can adapt their proper period and phase to an external driving force called the entrainment force or simply entrainment. The ability to adapt has its limits, so we need to create rhythmic variations in the environmental parameters with a period close to the proper period of the circadian clock. Here we show how we create this type of variations, and how we use them to entrain the circadian clock to different rhythms. We used two different types of entrainment, first light entrainment and second temperature entrainment. Entrainment by light is by far the better choice as it is easier to control locally and offers better precision and reproducibility than entrainment by temperature. Therefore we did the great majority of our experiments using light entrainment. In this section we show the experimental devices and control software we made to entrain the bacteria.

3.5.1 In-situ illumination during experiment

Illumination control during the experiment is of great importance, as light is both the energy source for the bacteria and the easiest to control environmental parameter. This is done by two sets of white LED micro-arrays, containing 96 LEDs each. These micro-arrays have the same surface as the microplates and fit into the stocking towers of the TopCount. The whole system is constantly cooled by fans to protect the LED overheating to avoid permanent damage or premature aging. It has three main components: 1) the LED arrays with their electronic control cards, 2) the spacer plates ensuring correct alignment of micro-arrays and microplates and 3) flexible connectors to allow continuous movement during the experiment (Fig 3.6).

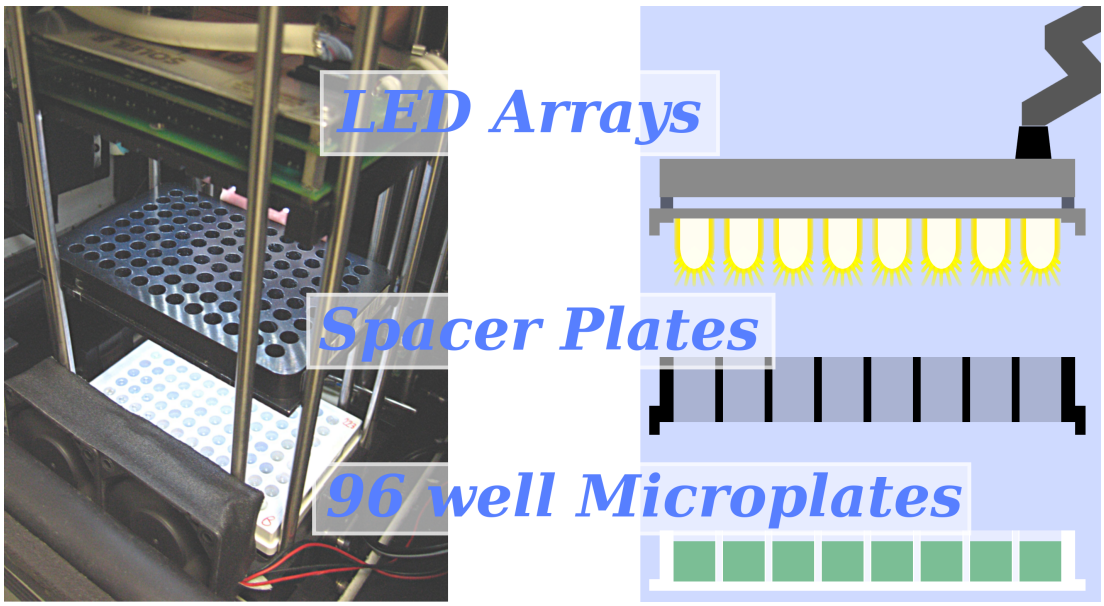

Figure 3.6: Experimental set-up used to illuminate the bacteria during the experiment. The fans used for cooling the LED during the experiment are shown on the left picture are not included in the schema. (bottom) 96 well microplates containing the bacteria. (middle) Spacer plates used for alignment and to shield each well from cross-illumination. (top) LED micro-array with one LED per well and flexible energy supply.

3.5.1.1 White LEDs used

The LEDs used are made by Marl Optosource. We use the clear white type with a peak wavelength around 475nm and a diameter of 5 mm. Their operating temperature ranges from -30°C to $+85$°C with a forward current of 20 mA. We operate them via a 14bit D/A controller (between 0 and 16383). Due to production tolerances, the light intensity and colour can vary individually. 16383 cps correspond to 3765 ± 120 lux. The LED in the illumination device show some

variability in colour. This variability is important enough to be visible by the human eye. We measured the spectra for different colours and verified that the bacteria show no significant behaviour in function of the incident light colour. (see Fig. 3.7).

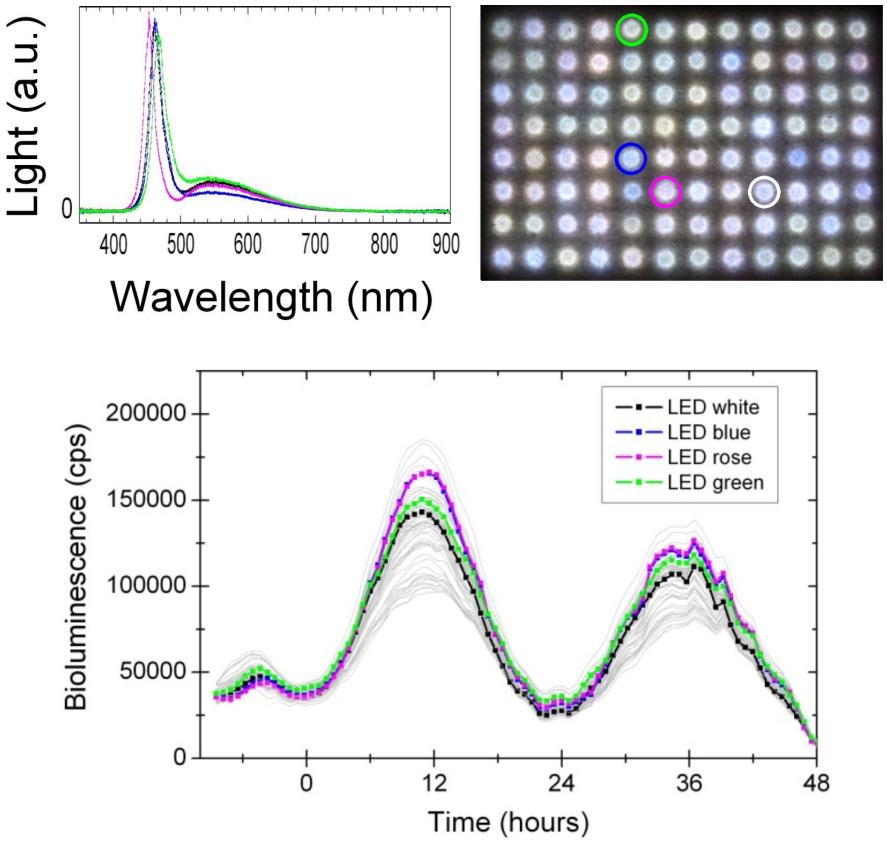

Figure 3.7: colour dependent spectra of the LED. (top left) Set of spectra measured on the illumination device for different colours. (top right) Photo of the one of the LED arrays showing the variability in LED colour. The LED used for the spectra are marked by coloured circles. (bottom) Bioluminescence signal in constant illumination at 500 lux. The wells illuminated by the LED used for the spectra are highlighted in their respective colour. In gray are all the lines belonging to the same clusters.

3.5.1.2 LED arrays

As we want each of the LED to illuminate exactly one well, their setup is adapted to the microplates we use to grow the bacteria during the experiment. We organized them in two arrays containing each 8 rows and 12 columns. The LED are operated in clusters analog to organisation we use on microplates (Fig. 3.2). Each LED of a cluster will get the same digital input signal, which it translates into illumination intensity.

3.5.1.3 LED calibration

The white LEDs in the arrays are not identical. Despite greatest effort to obtain them as homogeneous as possible (same manufacturer batch) there are still slight differences in colour and illumination level. To cope with this, the LEDs were individually adjusted and each cluster was calibrated individually. Calibration was done with two different light sensors (Fig. 3.8), a large sensor (Lutron LX-107) detecting the light of a whole cluster at once and a small sensor (LabTalk Light Sensor LS-BTA) used for the well illumination detecting the light of just one LED. Both sensors were put at the distance the bacteria have during the experiment. The LEDs are operated by feeding them a digital value in counts per second (cps) which they will translate in the same light intensity. The range goes from 0 till 16383 cps. We applied a series of different values and recorded the light in lux emitted by the different LED and clusters (Fig. 3.9a). This was done both with and without the spacer plates, in order to estimate how much light they absorb. The measured intensity was generally higher without spacer plates. The factor between those measurements varies between 2.7 for intensities above 1200 cps and 3.5 for low intensities. We approximated this curves obtained with the spacer plates on log scale (Fig. 3.9b) with a polynomial fit, both for cps vs. lux and lux vs. cps. This allows to set up our entrainment signal in lux and translate it into cps in function of the cluster. It also allows us to re-translate the cps values applied during the experiment back into lux. The exact parameters can be found in app. D.

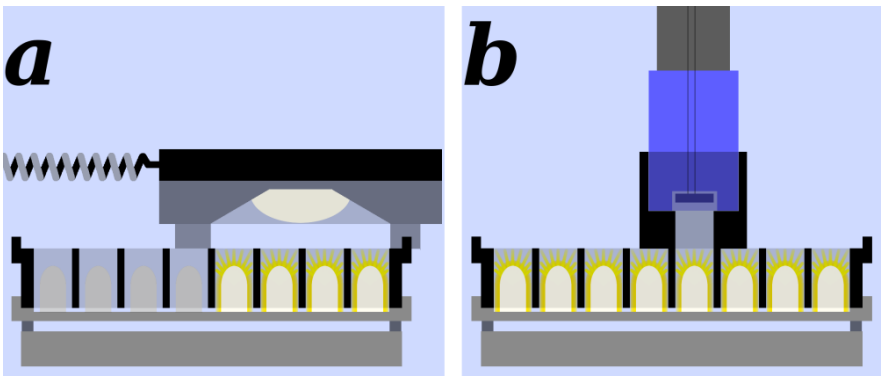

Figure 3.8: The LED calibration was done with two different sensors and always with the spacer plates. (a) A large sensor covering an entire cluster. All other clusters are switched off during the measurement. This measurement was repeated for all 12 clusters. (b) A small sensor with a custom top piece to fit it exactly over one single well. This measurement was repeated for all 192 LED.

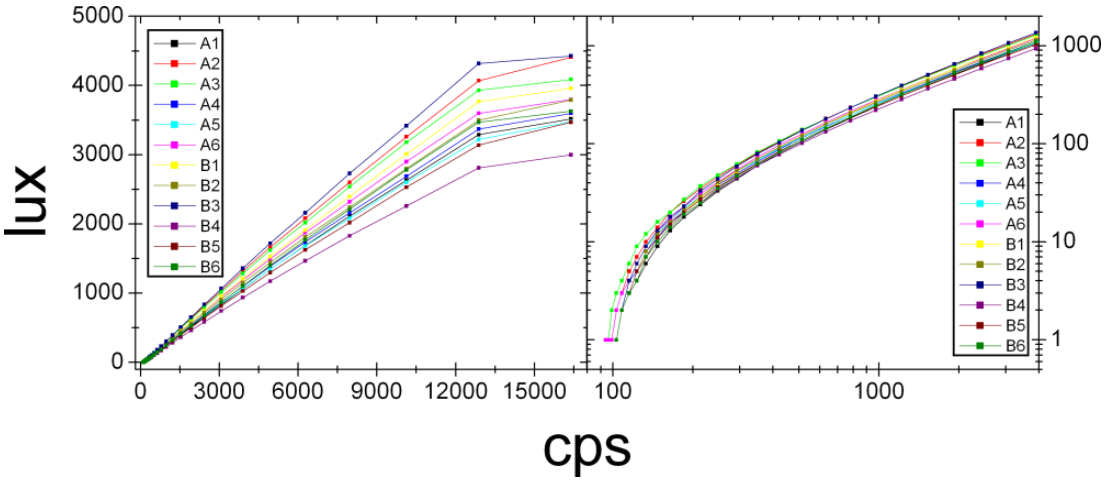

Figure 3.9: LED Calibration. Measurements for all 12 clusters with spacer plates. Linear scale showing the full range of the LED on the left and double logarithmic scale on the right focusing on the range between 0 lux and 1000 lux which we use to illuminate the bacteria during the experiment.

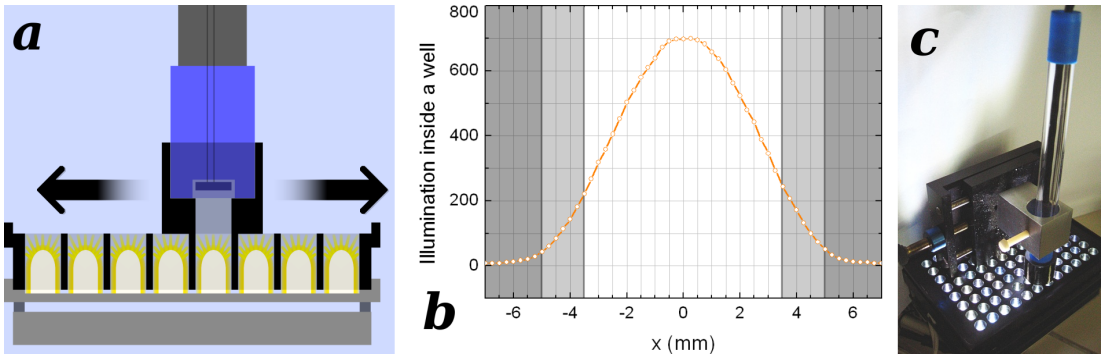

Figure 3.10: Distribution of illumination inside a single well. (a) Schema showing the principle of the measurement. The LED array is put upside down with the spacer plate above. The sensor with the top piece is then moved over a single well. (b) Illumination distribution inside a well. The white area marks the size of the well. In the light gray area the sensor gets partially illuminated and in the dark grey areas it detects only diffused light. (c) Photo of the setup.

LEDs are a point-like light source that do not illuminate a well homogeneously. To map the illumination pattern inside a well, we use the small sensor from 3.5.1.3 and fit it into a fixation. This fixation fits into the spacer plates and allows to move the sensor with a precision of 0.25 mm. Using this we measured the illumination pattern inside a well in different axis taking a data point every 0.25 mm. This measurement was repeated for several wells. We then adapted the LED calibration routine to the mean illumination (Fig.: 3.10).

3.5.1.4 Spacer plates

The spacer plates are made from anodized solid aluminium and have the same dimensions as the microplates. They fit on the microplates and the LED arrays to ensure their proper alignment during repeated cycles of the experiment. They feature 96 holes the size of a well through which each LED of the micro arrays will illuminate exactly one well. The spacer plates fulfill several critical tasks. They take care of the alignment of each LED directly above a well at a fixed distance during many load and unload processes. They protect each well from being illuminated by neighbouring LED and thus prevent cross talking. They also serve as stop plate for the TopCount cycle, after which a new cycle begins. This way they also protect the LED from being damaged by the TopCount robot as it will not grab any item behind a stop plate. And, last but not least, they provide sufficient weight on the microplates to eliminate grabbing errors of the TopCount robot.

3.5.1.5 Connector cables

Another important feature is the vertical mobility of the whole illumination device. During an experiment of 20 days the robot moves the microplates 6048 times. Each of these steps includes a vertical movement of the LED arrays, which is why flexible cables for energy supply and light control are important.

3.5.1.6 Comparison of different light sources used for photosynthesis

The photosynthesis process uses mainly the red and blue components of the visible spectrum. This also produces the characteristic green colour of plants as the green wavelengths get reflected. The spectral range of radiation used for photosynthesis is called the photosynthetically active radiation (PAR) and is the combination of the absorption functions of the different chromophors chlorophyll a, chlorophyll b and carotenoids. It can be plotted in function of the wavelength as $PAR(\lambda)$; using this function with the spectra of a lamp allows to calculate the amount of PAR energy it emits. To compare the effect different light sources have on the bacteria, it is important to normalize them by the amount of photosynthetically active photons via the PAR curve (Fig. 3.11). To do, that we first need to normalise all light sources by the total amount of photons $I_{Norm}(\lambda) = \frac{I(\lambda)}{N_{total}}$ with $N_{total} = \int_{\lambda} I(\lambda) d\lambda$. Then we use this normalized spectra to take into account the PAR function:

$$I_{PAR}(\lambda) = I_{Norm}(\lambda) \cdot PAR(\lambda)$$

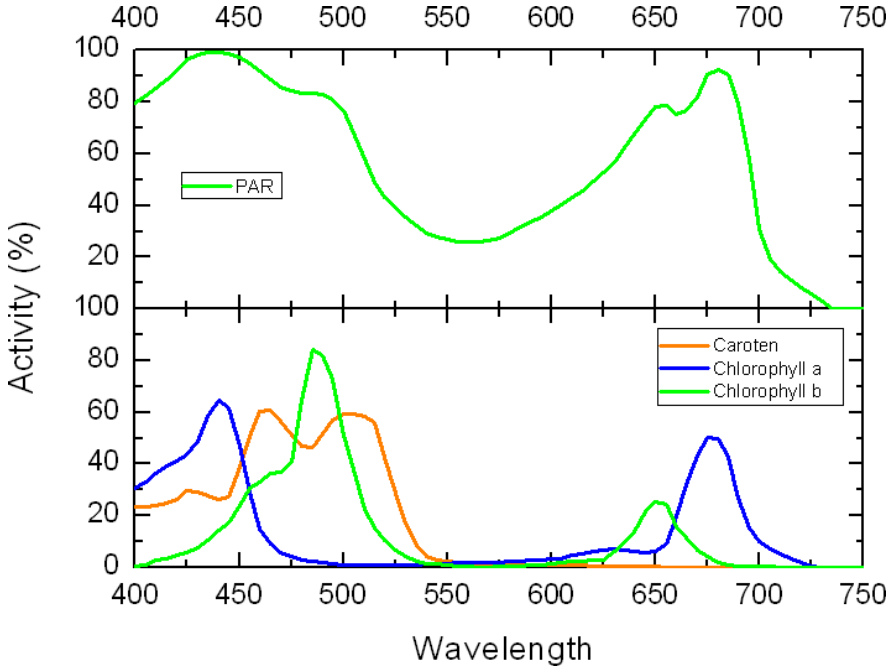

Figure 3.11: The PAR curve (photosynthetically active radiation) describes the spectra of light which plants can use for photosynthesis (upper graph, green). It is a combination of the absorption spectra of the three chromophors chlorophyll a, chlorophyll b and carotenoids (lower graph).

To estimate how our lux calibration will be detected by the bacteria, we calculate then the total number of photons, taking into account the luminosity function $V(\lambda)$ and the $PAR(\lambda)$ function

$$N_{lux} = \int_{\lambda} I(\lambda)V(\lambda)d\lambda$$
$$N_{PAR} = \int_{\lambda} I(\lambda)PAR(\lambda)d\lambda$$

and then divide $\frac{N_{PAR}}{N_{lux}}$. One can therefore notice that the white LED used are approximately twice effective for photosynthesis than white fluorescence lamps with the same lux value.

3.5.2 Entrainment by temperature variation

The other environmental parameter we use to entrain the bacteria is the temperature. Our set-up was built to maintain a constant temperature during the experiment. It consists of both passive (isolation) and active temperature control (by Peltier element) of the isolation box. It is done by varying the temperature

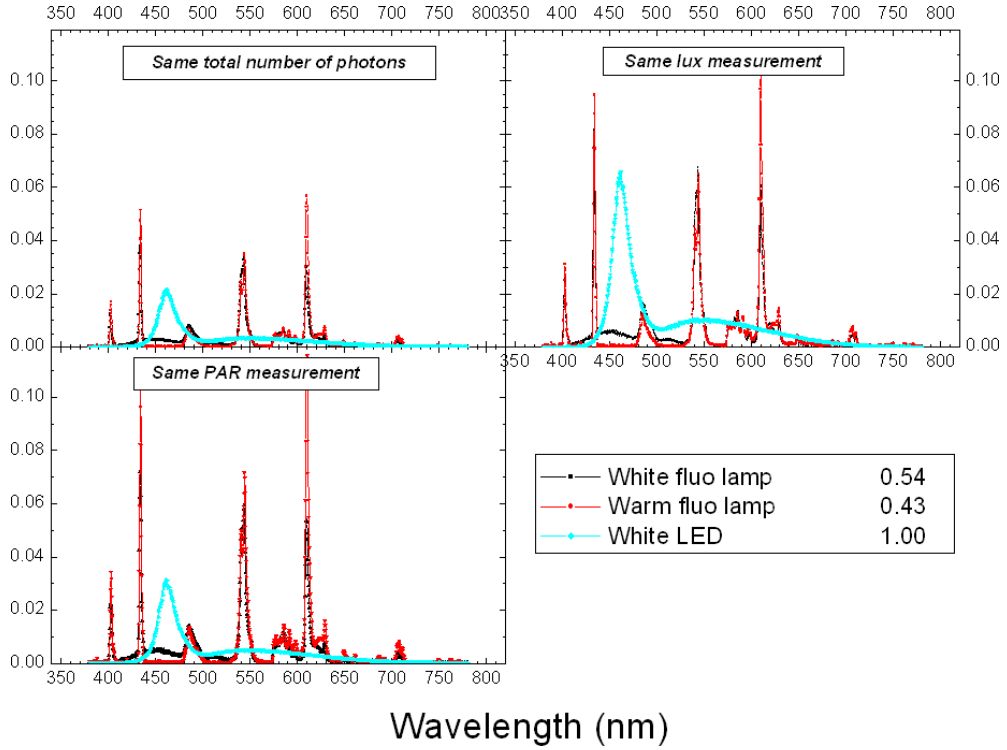

Figure 3.12: The spectra of different light sources. (top left) normalized to represent the same number of photons. (top right) Normalised spectra by taking into account the luminosity function used for lux measurements. (bottom left) Normalised spectra by taking into account the PAR function (Fig. 3.11). (bottom right) Comparison of $\frac{N_{PAR}}{N_{lux}}$ for different lamps.

of the whole box via regular changes of the Peltier set point. Note that temperature entrainment affects all the wells and not a single cluster, as does the light entrainment (Fig. 3.13).

The passive component of the temperature regulation is the isolated box in which the experiment takes place. This box is built on top of out detector. It has therefore a limited isolation at the bottom. The reading chamber has its own temperature regulation device, but nevertheless the fact that the bottom of the box has to allow plate manipulation is a limiting factor for the temperature range.

The active part of the temperature regulation is done by a Peltier element operated by a Sablesystems PELT-5 Temperature Controller. This controller has a temperature range of -5 to $+65$ °C, but due to the architecture of our set-up this is reduced to $+25$ to $+35$ °C and the temperature inside the box is sensitive to the room temperature. Therefore an air conditioned environment is still necessary to ensure good temperature control of the experiment.

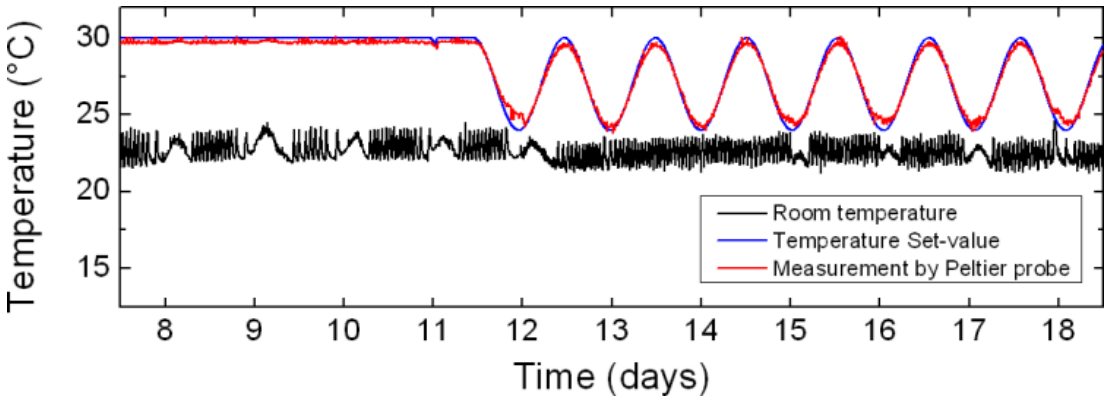

Figure 3.13: Temperature control of the isolation box. The set-value for the Peltier element is regularly updated by the control software. This allows to easily vary the set-value to either create constant or varying temperature conditions. While the set-value is easily changed, the size of the box and the power of the Peltier element do not allow quick and drastic temperature changes. The graph shows the temperature inside and outside of the isolation box for a constant temperature conditions and then a sinusoidal temperature oscillation from day 11.5 on. The coloured graphs represent the set-value (blue) and the measurement from the probe regulating the Peltier element (red). A third control probe measures the room temperature (black).

3.5.3 Software control of entrainment

We vary two different environmental parameters to entrain the bacteria, the illumination and the temperature. For our experiments it was necessary to control them independently while keeping good temporal correlation.

We achieved this by developing a software containing two independent parts (one for illumination, one for temperature control) connected only via a global timer and the experiment name. The interface is shown in figure 3.14. This allows us to adjust either illumination, temperature, or both of them. Both parts can be used either in constant mode to fix one of the parameters (light or temperature) or in input mode where the software is given an input file and processes it line by line. Switches between these modes can be scheduled any time. This allows for example to begin an experiment at constant temperature and illumination entrainment until each cluster is well entrained. After this is done, the light is switched to constant mode to check the entrainment and then start a temperature entrainment.

During the experiment, the software saves all effectively applied values of light and temperature and of course the time when it was done. Since our experiment takes up to several weeks and the interval between two data set points is of the order of several minutes, this data is written directly to the hard drive to avoid data loss in case of accidental power loss or computer crashes.

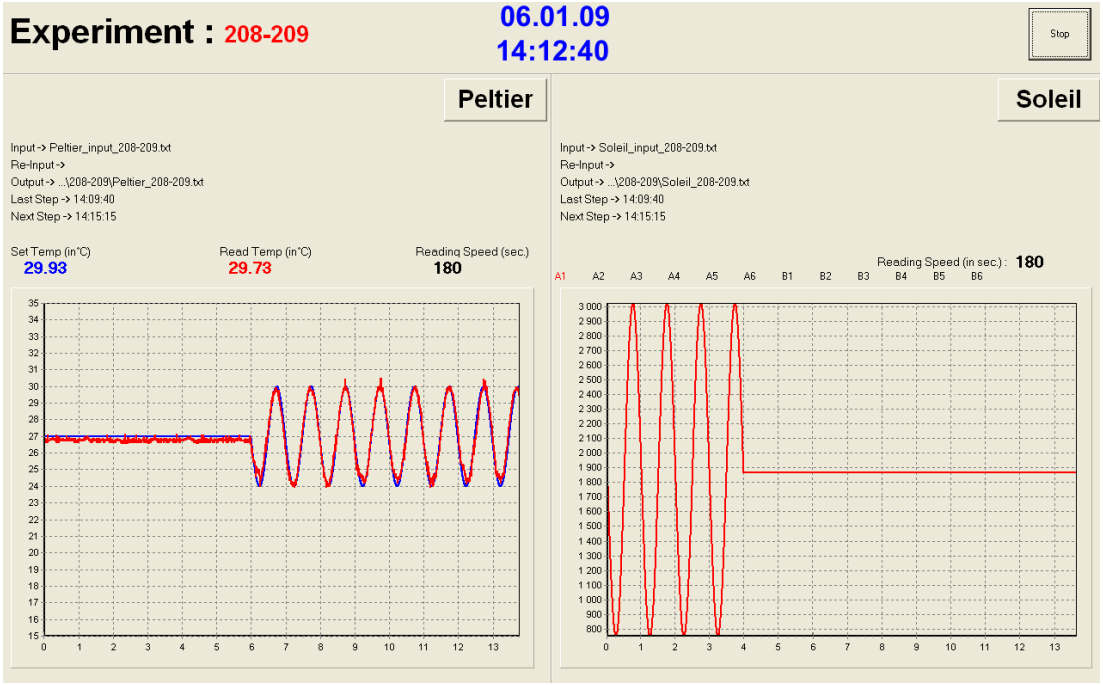

Figure 3.14: Interface of the control program. It allows the independent control of the temperature and the applied illumination of 12 LED clusters. Both can be set either to constant values or be operated with an input file. Changes between input modes, for example to switch from constant condition to an entrainment, can be scheduled in advance. In this example we applied 4 days of light entrainment, 2 days of constant conditions and finally 8 days of temperature entrainment. The experiment of this example is explained in chapter 7.3. (left) The control of the temperature during the experiment showing the current set temperature (blue) and the last measurement (red) as well as the evolution of both values during the experiment. (right) Illumination control ('Soleil' is the french word for sun). The graph panel allows to switch between the different illumination clusters to see their evolution during the experiment.

Chapter 4

Controls

In this chapter we detail the control experiments we did to learn how the bacteria reacted to different parameters of the experiment. As already mentioned in chapter 3.3.2, the illumination has a direct effect on the bioluminescence. Therefore we spent much effort to investigate how the bioluminescence level varies in function of illumination steps (Chapter 4.3) and how this can be characterised (Chapter 4.3.1). We used this information to separate the clock signal from the illumination dependent variations of the bioluminescence (Chapter 4.3.3).

Besides, we also verified that the microplates with the bacteria aligned well under the LED devices after each lecture (Chapter 4.1) and how strongly LED may cross-illuminate neighbouring wells (Chapter 4.4.1).

Last but not least, we investigated the effects the adding of fresh media has during the experiment, and if the pH of the media changes the observed phase (Chapter 4.2).

4.1 Plate alignment

To test the reliability of the alignment between microplates and LED arrays, we drilled holes into some of the wells and fixed a light sensor on a flexible cable to the back of the plate. We then used the TopCount robot to move this plate consecutively from one stocking tower to the other and back. In this way we tested the reproducibility of the alignment of both 'tower-spacer plate-LED array' ensembles. Independently from the well, we deduced that the variability was below 2%. This shows the high reproducibility of this system (see Fig. 4.1).

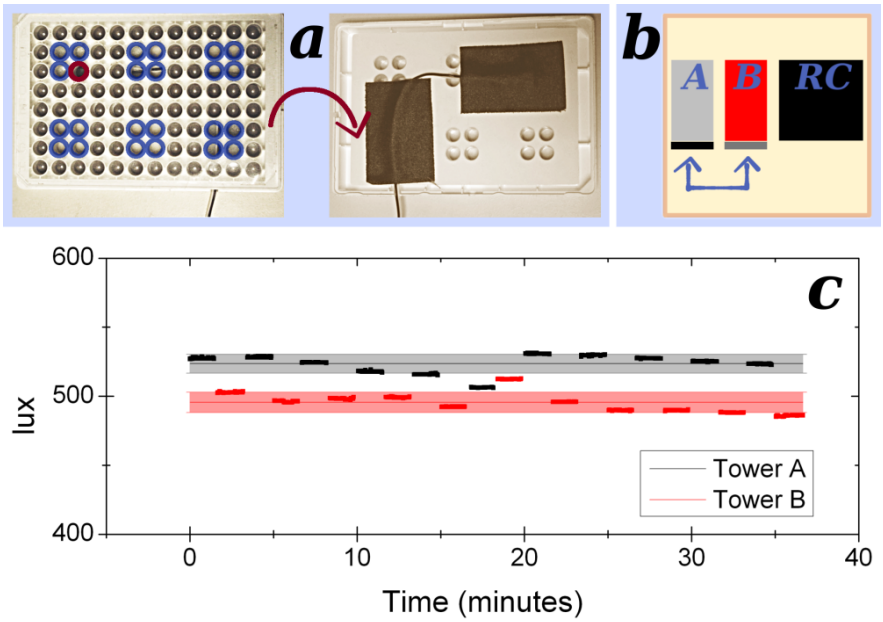

Figure 4.1: (a) Microplate with light sensor taped to the backside. left: Front side. Unmarked wells are filled with steel marbles to give some weight to the plate. Wells with a colour frame have been drilled through, the hole with the red frame has the sensor taped to its backside. right: Backside. The holes are clearly visible the sensor and its cable are fixed with duck tape to prevent it from moving while the microplate is grabbed and handled by the TopCount robot. (b) Movement of the microplate during the alignment test. The plate moves only from tower A to tower B and back. It does not enter the reading chamber as the trailing sensor cable would prevent the chambers door from closing. (c) Measurements during 10 cycles. Measurements under tower A in black and from tower B in red. The thin lines with lighter border represent the mean and its error area.

4.2 Adding media during experiment & pH effect

In order to survive, the bacteria need oxygen and CO_2 which is furnished by ambient air and CO_2 supply. This means we cannot seal the microplates airtight. After applying the TopSeal, we make a cut for every well to ensure the air exposure of the bacteria. This has the side effect that the liquid containing the bacteria evaporates slowly. To maintain a sufficient amount of liquid in each well we regularly add media BG11 (App A), about every 5 days, in order to keep the experiment running. This refill may perturb the bacteria, which is then seen on the bioluminescence signal, but can be corrected before phase and amplitude extraction (see 6.1). Additionally, keeping the experiment running for longer time by adding liquid more than once, the pH inside the wells can change.

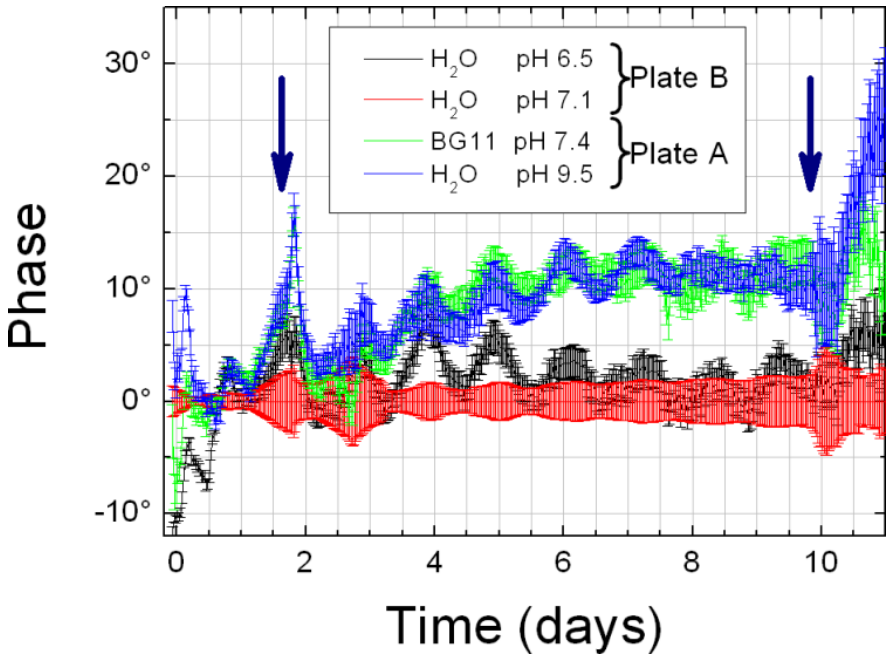

Figure 4.2: Effect the pH has on the extracted phase. Here are plotted 4 different clusters under LL conditions in the reference frame of the condition at pH 7.1. The wells initially filled with only 130 µl media with bacteria at OD 0.5 to simulate an old almost dried up well. After 2 days we filled them up using our standard protocol. For this used sterile water at pH 6.5, 7.1 and 9.5 and used BG11 at pH 7.4 as control on another cluster. 7 days later we added the same liquid to each cluster. The arrows mark the moments of adding liquid to the wells. All 4 clusters behave the same with a slight difference in freerun between the two plates.

In order to test a possible pH change we measured the pH for different wells after an experiment of 21 days, where media was added three times during the experiment all 5 days (no refill on day 20). The pH was measured with two different types of stripes. The values we obtained went from 8 till 10. The control measurement done on fresh BG11 confirmed a pH of 7.5.

To test whether it influences our results, we set up an experiment with 4 identical sets of conditions (LL, 0° shift, 90° shift where we add different liquids all 5 days: BG11 media at pH 7.4 and sterile water at pH 5.5, 7.1 and 9.5. To reproduce the condition of wells at the end of an experiment, we filled them with only 130 µl media with bacteria at OD 0.5. After 2 days we added liquid for the first time and a second time after 9 days (4.2). To better distinguish variations between the 4 conditions, the phases are plotted in the reference frame of the condition at pH 7.1. All clusters behave the same. The only small distinction coincides with the distribution on the plates, the black and the red conditions share a common plate (Plate B) as do the green and blue one (Plate A). The different behaviour can thus have its origin in inhomogenities inside the isolation

box rather than the pH value.

4.3 Response of the bioluminescence reporter to light

The bioluminescence reporter we use to follow the circadian clock transforms chemical energy into photons. The energy source for this process is reduced Flavin mononucleotide ($FMNH_2$) which will be transformed into *FMN*. It is also used in the respiration reactions taking place inside the cyanobacteria. In general, the additional consumption of *FMN* is no problem as the bacteria produce and recycle enough to sustain the bioluminescence, but in case of a light entrainment a bioluminescence peak can occur during an illumination minimum. The competition for $FMNH_2$ then becomes a non negligible factor when the cell is not able to produce enough $FMNH_2$, due to lack of incoming light. In that case we observe a slump in the bioluminescence signal that is not due to the circadian clock, but simply a lack of bioluminescence activity due to $FMNH_2$ shortage. This slump on the bioluminescence signal can alter the phase, and in the worst case can be detected as an additional cycle introducing 360 ° phase jumps. To separate the clock signal from slump, we measured the bioluminescence as a function of the incident light. We did this by monitoring the bioluminescence reaction of the bacteria to light steps from 500 lux LL to different LL value between 0 lux and 1100 lux.

4.3.1 Light to dark steps

In this set of experiments we applied a sudden change between two constant illumination intensities, the so called light step, and observed the dynamics of the bioluminescence (see Fig. 4.3: upper row). These experiments were performed without adding media or even opening the isolation box to avoid external perturbations as much as possible. This approach also limited the total duration of this experiments to about 7 days. But since we are interested in the short time effects, this is largely enough.

First we applied these steps to a population of entrained bacteria (see Fig.: 5.3). They were observed at 500 lux LL for one day before applying the step. Step range goes from 0 lux to 1000 lux. These experiments gave several results. First they showed that the bioluminescence oscillations continue for most illumination levels. Only the DD and the LL 10 lux do not oscillate. Wells with illumination

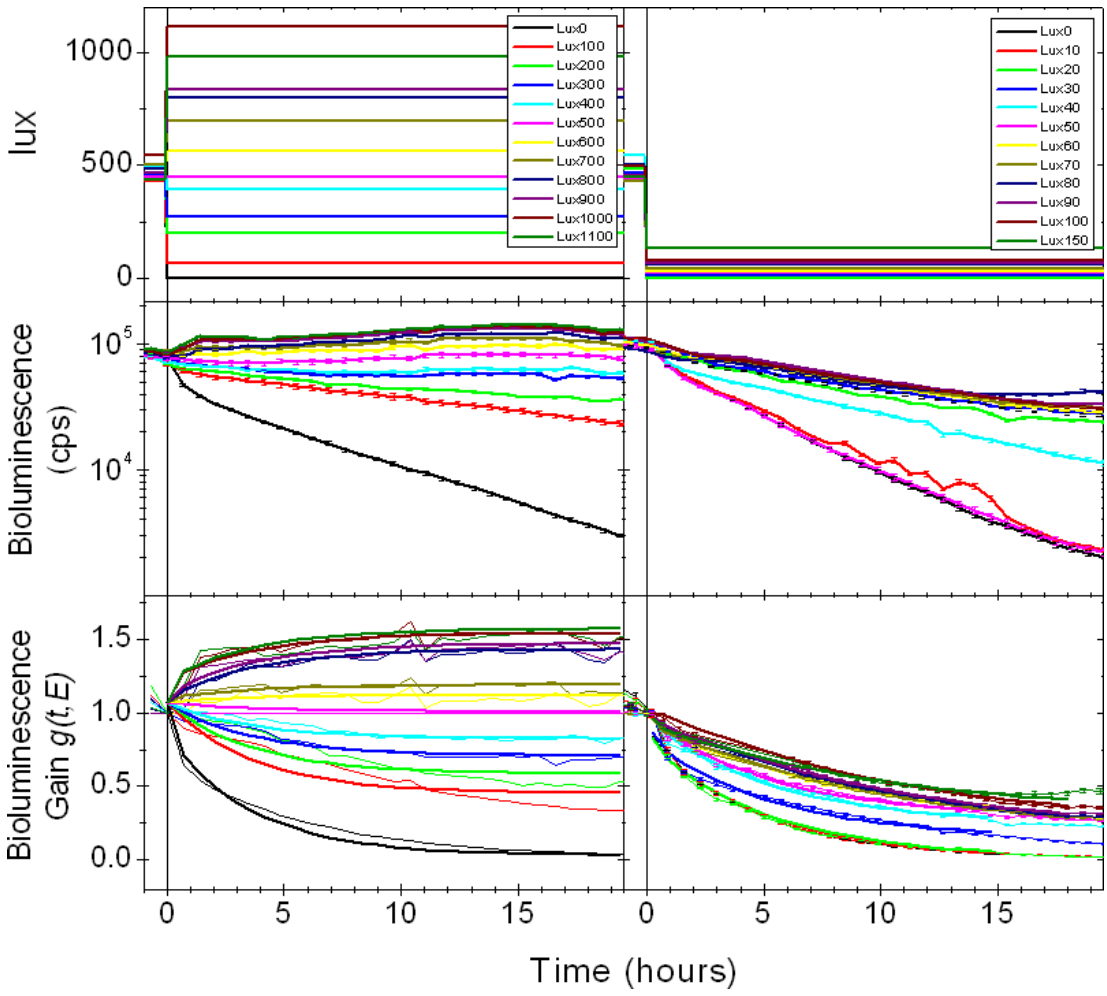

Figure 4.3: Experiments with light steps done to estimate the effect incident light has on the bioluminescence output. All clusters start from 500 lux before switching at $t = 0$. On the left an experiment with steps values ranging from 0 lux to 1100 lux with 100 lux stepwidth. On the right a second experiment exploring the lower regions between 0 lux and 100 lux with 10 lux stepwidth, plus a control at 150 lux. (first row) Applied light signal. (second row) Statistics of the raw bioluminescence of 16 wells inside a cluster on log scale. (third row) Same data as in the second row, but normalized for the starting point and the neutral step at 500 lux and with the fits.

below 500 lux show a gradually decreasing bioluminescence level depending on the illumination. Second, wells with LL 500 lux and above keep nearly the same amplitude and periodicity as before the step, indicating that the saturation of the bioluminescence is reached at approximately 500 lux.

In the next step we wanted to focus on the first effect and reduce as much as possible the effect of the circadian clock. So we set-up a very similar experiment just with unentrained populations to weaken the effect of oscillations from the circadian clock. After several days (>5 days) in the incubator at 500 lux LL the bacteria were put into microplates and illuminated for another 48 hours at 500 lux. This was done to observe at least one full oscillation in order to estimate the effect the circadian oscillations can have. From the raw data we made statistics on 16 wells per cluster (see Fig.4.3: middle row) and normalised them. To have a common point of departure, each cluster got then normalised using the measurement point at t=0 (the moment where the steps are applied) as reference. This way all 12 cluster begin in a common starting point at t=0. Next we normalize the graphs using the neutral step 500 Lux cluster as reference, which therefore is completely flat (see Fig.4.3: lower row). We will therefore define the reporter gain $g\,(E,\,t)$ which will be dependent of the illumination E:

$$g(E,t) = \frac{I_{Step}(E,t)}{I_{Step}(E,0)} \cdot \frac{I_{LL}(500\,\mathrm{lux},0)}{I_{LL}(500\,\mathrm{lux},t)}$$

To fit the resulting set of graphs, a single exponential decay was clearly insufficient. This is best seen in figure 4.5, where two decay regimes are easily distinguishable. First a quick decrease of bioluminescence, followed by a much slower one. To describe the bioluminescence response, we used a model containing two species with independent production and decay constants. These species do not correspond to different bacteria populations, but only to the two decay regimes observed.

$$\begin{aligned} \frac{dg_1(E,t)}{\mathrm{d}t} &= -\frac{g_1(E,t)}{\tau_1} + k_1(E) \\ \frac{dg_2(E,t)}{\mathrm{d}t} &= -\frac{g_2(E,t)}{\tau_2} + k_2(E) \end{aligned} \tag{4.1}$$

with $k_1(E)$, $k_2(E)$ as the production rate dependent of incident light E and τ_1, τ_2 the degradation times of each species independent of light. Solving the previous

equation for a step at $t = 0$ gives:

$$\begin{aligned} g_1(E,t) &= g_{1,0}e^{-\frac{t}{\tau_1}} + k_1(E)\,\tau_1(1-e^{-\frac{t}{\tau_1}}) \\ g_2(E,t) &= g_{2,0}e^{-\frac{t}{\tau_2}} + k_2(E)\,\tau_2(1-e^{-\frac{t}{\tau_2}}) \end{aligned} \tag{4.2}$$

where $g_{1,0}$ and $g_{2,0}$ are respectively the steady-state reporter gain of species 1 and 2 at $E = 500\,\text{lux}$. The total gain is the sum of both components $g(E,t) = g_1(E,t) + g_2(E,t)$. At $t = 0$ when the step occurs we obtain:

$$\begin{aligned} g(500\,\text{lux},0) = g_1(500\,\text{lux},0) + g_2(500\,\text{lux},0) &= g_{1,0} + g_{2,0} = 1 \\ &\Rightarrow\ g_{2,0} = 1 - g_{1,0} \end{aligned}$$

$$g(E,t) = g_{1,0}e^{-\frac{t}{\tau_1}} + k_1(E)\,\tau_1\left(1-e^{-\frac{t}{\tau_1}}\right) + (1-g_{1,0})\,e^{-\frac{t}{\tau_2}} + k_2(E)\,\tau_2\left(1-e^{-\frac{t}{\tau_2}}\right) \tag{4.3}$$

We next fitted each time dependent experimental gain curve (Fig. 4.3) following eq. 4.3 with independent fit parameters $k_1(E)$ and $k_2(E)$, but with common decay times τ_1 and τ_2 for all curves. This allowed us to evaluate τ_1 at 0.2 h and τ_2 at 5.2 h. The production rates for each species as function of illumination intensity are given in fig. 4.4. We phenomenologically fitted $k_2(E)$ by a simple Hill function (with convergence limit $V_{max} = 0.18 \pm 0.01$, illumination value of the half-height $\varsigma = 395.3 \pm 24.4$ and the Hill factor $n = 3.05 \pm 0.5$) and $k_1(E)$ by a two step Hill functions. Function for StepHill (Fig.: 4.4):

$$f_{StepHill}(x) = \left\{[(1-P)\cdot VT]\cdot\frac{x^{n_1}}{(\varsigma_1^{n_1}+x^{n_1})}\right\} + \left[(P\cdot VT)\cdot\frac{x^{n_2}}{(\varsigma_2^{n_2}+x^{n_2})}\right] \tag{4.4}$$

- $VT = 1.72 \pm 0.07$ is the total convergence limit of the combined Hill functions
- $P = 0.37 \pm 0.03$ is the percentage of VT of second step, in our case around 40%
- $\varsigma_1 = 19.1 \pm 2.2$, $\varsigma_2 = 825 \pm 11$ the x value where the respective Hill function reaches its half-height
- $n_1 = 2.15 \pm 0.51$, $n_2 = 45 \pm 27$ the different Hill factors

4.3.2 Transition to DD

To get additional data about the time scale of the decrease of bioluminescence signal in total darkness (DD), we set up a plate with only one 'cluster' of 16 wells

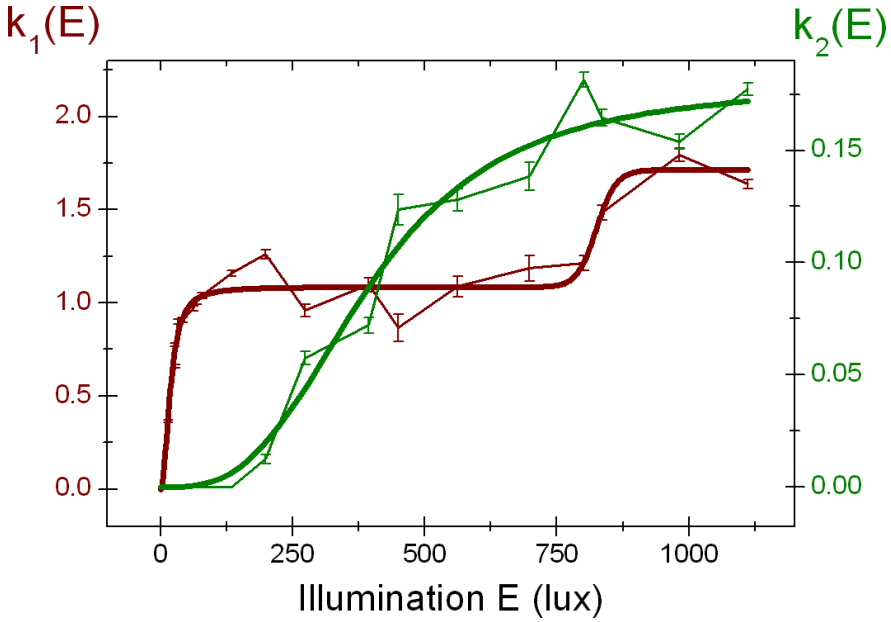

Figure 4.4: Plot and Hill-fits for $k_1(E)$ and $k_2(E)$. $k_2(E)$ in green does not show any activity until 200 lux and behaves then like a classic Hill function. $k_1(E)$ on the other hand is more complex. It starts much earlier and, adopts a plateau between 70 lux and 300 lux to then start a second rising. We fit this by combining two Hill functions where the final value of the first is also the starting value of the second Hill.

in the 1st and the 7th column of a 96-well lab plate. This way, each line is read by one of the two photo-multipliers in the TopCount. As soon as one reading cycle is completed, the next begins. This gives us the best time resolution possible with the TopCount, because the plate does not leave the reading chamber and each photomultiplier just reads a single line. Each reading cycle takes 1′7”, which is about 37 times faster than the 41′30” cycle time for illumination experiments (see Fig.: 4.5).

The data fits well using the two species model, but gives slightly different parameters (see Fig.: 4.6). This indicates, that there are differences in the setup, maybe because of the cross-illumination of the wells, or because the effective illumination of the DD clusters in the previous experiments was above 0 due to light shining on the plates during handling processes.

4.3.3 Bioluminescence correction for an arbitrary time dependent illumination

To correct the bioluminescence signal that we measure during the experiment, we use the light-bioluminescence dependency obtained in the step experiments and use the light signals applied during an experiment as input parameter. By

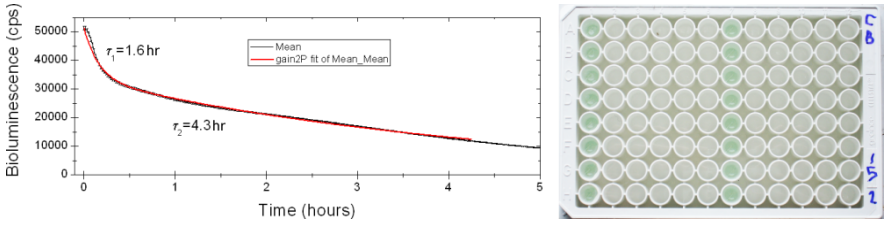

Figure 4.5: (left) Graph (black with error-bars) and fit (red) of the cyanblack plate. One data point every 67 sec, fit done with the same model as in the step experiments. (right) distribution of wells on the plate used for the transition to DD experiment. Only the first and the seventh column carry bacteria. A TopSeal protects the plate as in all other setups.

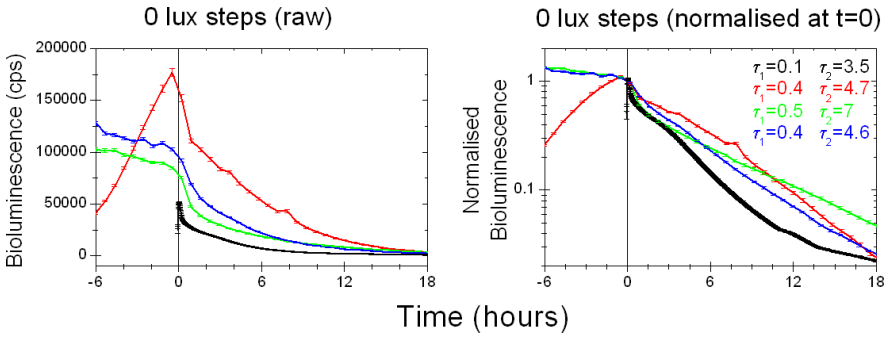

Figure 4.6: Two graphs showing the differences between the four DD conditions. On the left hand site the raw data, on the right hand site the raw data divided by its value at $t = 0$, the moment when the bacteria are put into DD. The three DD conditions from the step experiments show a higher bioluminescence than the cyan black experiment. This might be due to the short illumination the bacteria got during handling processes of the TopCount robot.

numerical integration of equations 4.1 done in Matlab 6.1 we reconstruct the variation of the bioluminescence gain due to the temporal variation of the incident light $E(t)$. By dividing the raw signal by this calculated gain we unmask the bioluminescence from variations independent of the incident light:

$$I_{corrected} = \frac{I_{raw}}{g\,(E,\,t)}$$

with $g\,(E,\,t) = g_1\,(E,\,t) + g_2\,(E,\,t)$ from equation 4.1. See figure 4.7 for the effects on the raw signal. The left side shows the data over a 14 days experiment length, while the right side shows 3 oscillations in more detail. The upper panel displays the applied illumination (red) and the bioluminescence gain calculated from it (green). The lower panel shows the raw bioluminescence measured during the experiment (black) and the corrected signal obtained by dividing the raw signal by the calculated gain. Proceeding that way we see that the decline of bioluminescence that coincided with the low illumination periods is corrected.

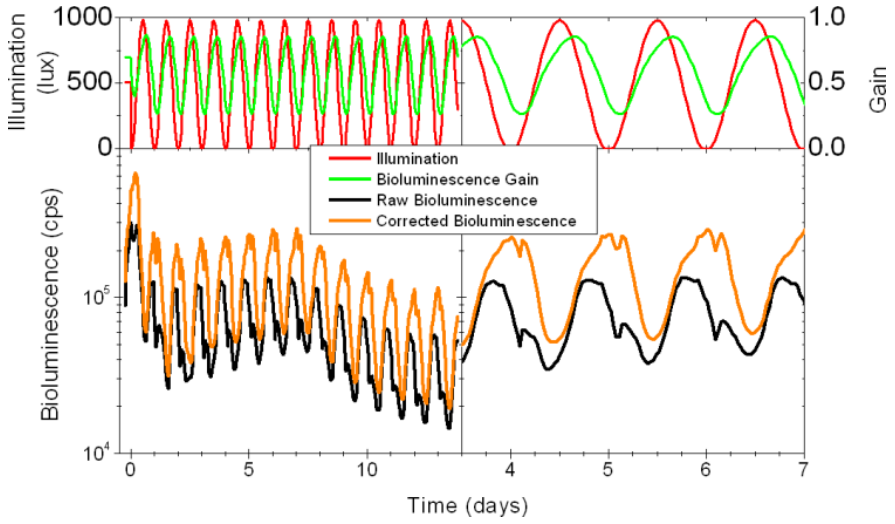

Figure 4.7: The raw oscillation before and after the unmasking of the reporter effect. Top: The illumination in red and the calculated reporter gain in green. It shows the amount of bioluminescence production and is normalized by $g_{1000lux}$=1. Dividing the raw bioluminescence signal (black) by the reporter gain (green) we obtain the unmasked bioluminescence signal (orange).

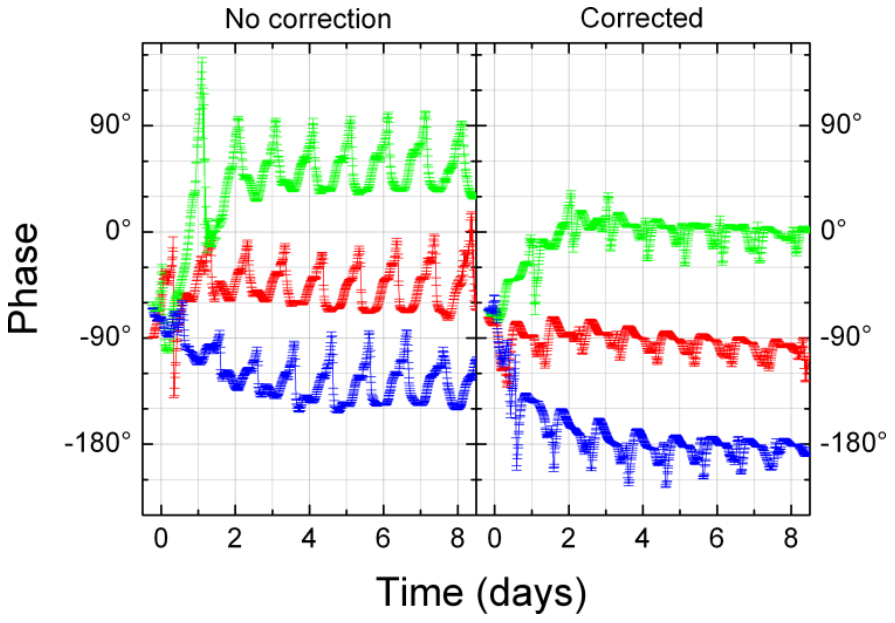

Figure 4.8: Effect of the bioluminescence correction on the phase. See figure 4.7 for the effect on the raw signal of this experiment. The phase of the corrected signal shows much less oscillation than the uncorrected. This allows to determine the phase of the oscillator with higher precision.

Although the obtained signal is closer to a sinusoidal than before it does not correct the bioluminescence bumps during complete darkness. In figure 4.8, a direct comparison of the same experiment with (right panel) and without (left panel) bioluminescence correction, we see that the phase extracted from the corrected signal shows a lower perturbation than the phase extracted from the raw signal. The overall variation we measure is unchanged, however the precision is increased due to the reduced fluctuations of the extracted phase. The stable phases at the end of the entrainment period are shifted. This happens due to the correction of the maxima as can be seen in fig. 4.7. The bioluminescence minima hardly move as they occur during high illumination periods for entrained phases. The reason for this lies in inherent phase shifts between the circadian clock and the bioluminescence production which will be discussed in more detail later (ch. 7.1).

4.4 Crosstalk effects

Under the term of crosstalk are considered two different phenomena. It may either refer to signal detection of a neighbouring well in case the photomultiplier is not well positioned, photon diffusion from one well into another or to cross-illumination from neighbouring LED.

To minimise photon diffusion during detection, we use opaque microplates where each well has its own independent walls. Alignment of micro plate and LED arrays is done by the spacer plates (see 3.5.1.4). As this alignment is highly reproducible (see 4.1) it remains to measure the amount to which a LED might cross-illuminate neighbouring wells.

4.4.1 Cross-illumination

To elucidate the possible effects due to cross-illumination from neighbouring LED, we set up an experiment where the whole plate would be kept in total darkness with only one or two clusters illuminated at 500 lux at any given moment. At the beginning we kept all clusters in the dark for about 30 hours to lower the bioluminescence output and hence reach better sensitivity. Figure 4.9 shows the raw bioluminescence signal measured from one 96 well micro plate. The wells are grouped by cluster and the background colour represents the exposure to illumination, with gray for total darkness and white for 500 lux light intensity. The inset shows the location of each well on the plate and the colours highlight the wells under possible cross-illumination from a neighbouring LED, while wells without such influence are marked in black.

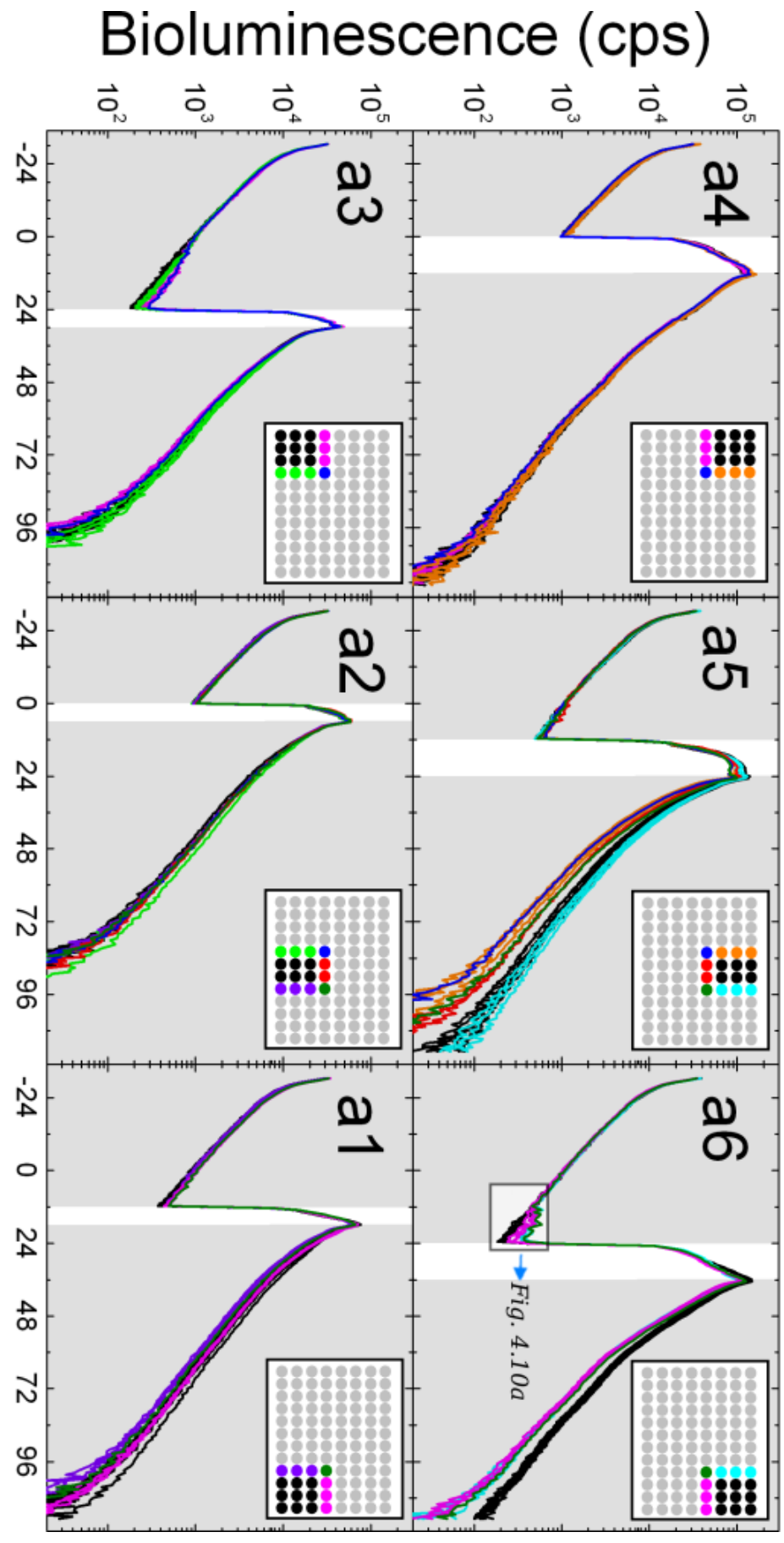

Figure 4.9: Cross-illumination effects on a 96 well microplate. The entire plate was kept in total darkness for 30 hours (gray areas at $t < 0$) before applying 500 lux light pulses (white areas) of different duration (6 hours and 12 hours) at different times (0 h, 12 h and 24 h). After the light pulse no direct illumination was applied to the wells. colours mark the wells under possible cross-illumination while wells without neighbouring clusters are in black. The insets shows the location on the micro plate of each group of wells. Two effects from cross-illumination are visible: a) a slight increase of bioluminescence and b) differences in the decay time for wells that got cross-illuminated for 12 hours before direct illumination.

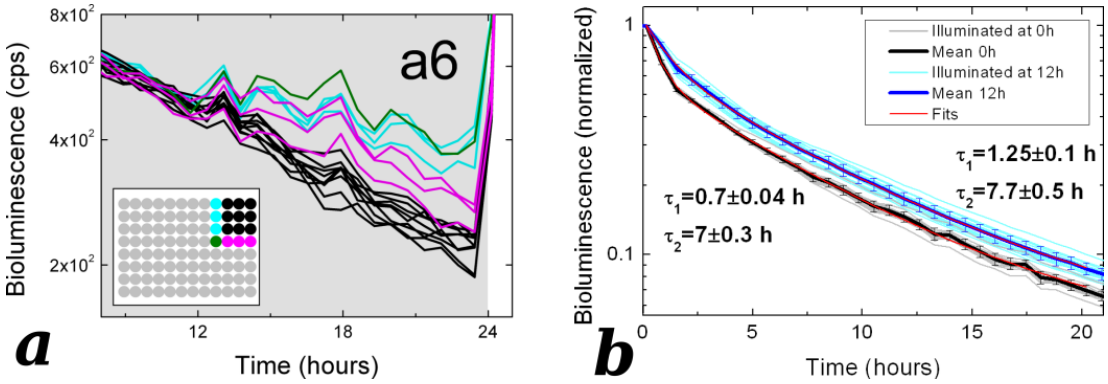

Figure 4.10: (a) Cross-illumination effects on cluster a6 in the 12 hours before direct illumination. The inset marks the emplacement of the wells on the micro plate. Cross-illumination began 12 hours before direct illumination. Cyan wells got cross-illuminated for a period of 12 hours from the cluster on the right, magenta wells for 6 hours from the cluster below and the green well from both of them. All 6 wells show an increase of bioluminescence activity under cross-illumination. At $t = 18\,h$ the magenta stop their increasing activity and decay with the same slope as the black wells again, while the green well now show the same behaviour as the cyan ones. (b) Different decays in function of the moment a 6 hour light pulse was applied.

During periods without direct illumination, the bioluminescence signal from all wells decreases roughly in the same way as described previously (ch. 4.3). A cross-illumination after direct illumination had no apparent effect (see Fig. 4.9 clusters a2 and a4), probably because the amount of bioluminescence after direct illumination was too high to detect such subtle variations. However, a cross-illumination that occurs before the light pulse does have some small effects, as can be seen on Fig. 4.9 clusters a3, a5, and best on cluster a6.

Figure 4.10a shows in detail how on cluster a6 the amount of detected bioluminescence first increases for cross-illuminated wells, indicating that these wells are no longer in total darkness. The direct illumination starts at 24h, but the wells neighbouring other clusters emit more bioluminescence form 12h on. The wells in magenta were cross-illuminated for 6 hours from 12h on, while the wells in cyan were cross-illuminated for 12 hours from 12h on. The green well is cross-illuminated from both neighbouring clusters. A second effect is that cross-illuminated wells show a slightly quicker decline of emitted bioluminescence (tab. 4.1). A double exponential fit of those curves shows that both the slow decay τ_2 and the fast decay τ_1 accelerate for the cross-illuminated wells. Besides that, all other clusters decline in similar ways: Clusters illuminated at 0h or 24h show the same behaviour, while clusters illuminated at 12h decrease slightly slower. The same double exponential fit shows here a slow decay $\tau_2 \simeq 7\,\mathrm{h}$ roughly unchanged and a fast decay τ_1 which accelerates from 1.25 h to 0.7 h for the wells illuminated

	τ_1	τ_2
a5	0.89 ± 0.08	5.9 ± 0.2
a5 X	0.79 ± 0.03	5.4 ± 0.1
a6	1.03 ± 0.09	7.9 ± 0.2
a6 X	0.97 ± 0.04	6.8 ± 0.1

Table 4.1: The different decay values for the cross-illumintaed wells in a5 and a6 (a5 X and a6 X) compared to the respective decay values of unperturbed wells.

at CT0 (fig. 4.10b). The sensitivity to light at least for the last decay seems to be slightly dependent on the circadian time.

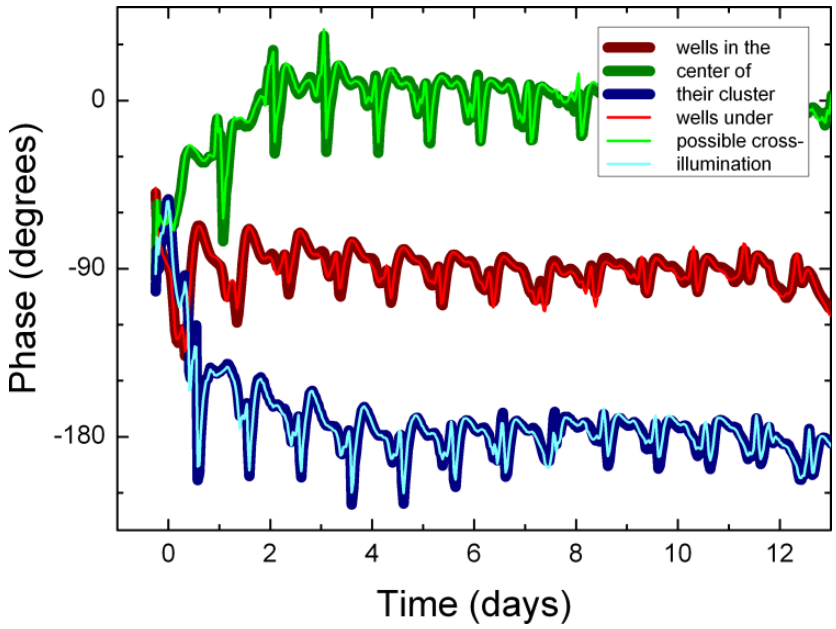

Figure 4.11: Comparison of corrected phases in a rotating time frame at $\omega_{Entrainment}$ obtained from wells without cross-illumination in the center of a cluster (the black wells in Fig. 4.9) and the wells under possible cross-illumination at the borders of it.

To verify that these effects, as small as they may be, have no influence on the phase we measure, we compared the phases obtained from wells that showed no cross-illumination effects during the light pulse experiment with the phases obtained from wells that do (see Fig.: 4.11). This comparison revealed no significant difference between these two groups, which led us to the conclusion that cross-illumination effects are too weak, compared to the direct illumination to perturbate the data.

Chapter 5

What do we measure?

In this section, we will discuss the measured signal (see 3.4) of the cyanobacteria (see 3.1) under entrainment (see 3.5), how it is composed, and how we extract the circadian information from it. We start with the circadian oscillation observed in single cell experiments and its description. Next, we extend this description to the signal measured from a population of oscillators, particularly by looking closer at the number of detected emitters and how they are distributed inside a well. We also show that, by starting with an initial number of $\approx 3 \cdot 10^7$ cells/well, we detect bioluminescence from a stable number of cells, regardless the ongoing cell division within a well during the experiment.

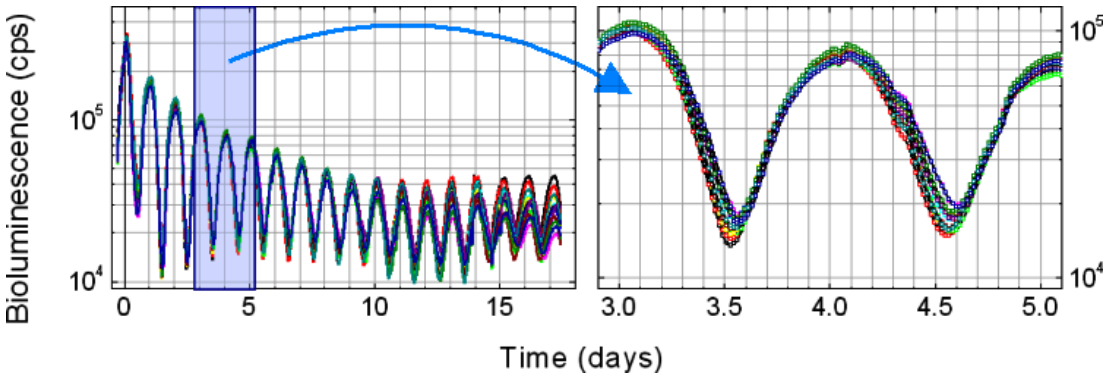

Figure 5.1: Raw signal from 16 independent wells under identical entrainment of an oscillating light signal done by individual illumination of each well by one white LED.

5.1 The bioluminescence signal of a population

Single cell experiments with bioluminescent cultures have shown that the circadian clock of a cyanobacterium reported by the density of bioluminescence $d_i(t)$

can be described as

$$d_i(t) = g \cdot [1 + b \cdot \cos(\omega_0 t + \varphi_i)] \tag{5.1}$$

with φ_i as the individual phase of each bacterium, ω_0 the proper frequency, b the relative amplitude of oscillation of the *PkaiBC* activity (with $b \geq 1$ as there is no negative bioluminescence) and g the reporter gain dependent on the illumination (ch. 5.3, fig. 5.3, [5]). We take ω_0 to be the same for the whole population, since single cell experiments showed that it is remarkably uniform inside a population of bacteria (ch. 1.3.1 and [35])

When observing a population of bioluminescent bacteria, we observe the sum of all emitters inside a well. We neglect here the absorption effects. This will be discussed in the next chapter. As oscillators within a population might have different phases, we observe the mean phase $\langle\varphi\rangle$ of the population. This also introduces a new variable, the order parameter ρ. It varies between 0 for a population with homogeneously distributed phases and 1 for a perfectly synchronized population. The signal of a population of N oscillators is thus given by:

$$\begin{aligned} i(t) &= \sum_{i=1}^{N} d_i(t) = N \cdot \langle d(t)\rangle = \sum_{i=1}^{N} g \cdot [1 + b \cdot \cos(\omega_0 t + \varphi_i)] \\ i(t) &= \overline{i(t)} \cdot [1 + b\rho \cdot \cos(\omega_0 t + \langle\varphi\rangle)] \end{aligned} \tag{5.2}$$

For longer experiment, the mean g cannot be taken as a constant anymore. Instead, a time dependent baseline of the oscillation $\overline{i(t)}$ is observed. As its varies much slower than the relatively fast oscillating circadian clock, these two components can be separated to keep only the circadian oscillation (ch. 6.3). We define the oscillatory signal as $s(t) = \frac{i}{\overline{i}} - 1 = b\rho \cdot \cos(\omega_0 t + \langle\varphi\rangle)$ with the amplitude of the oscillation signal as $A(t) = b\rho$ and the instantaneous phase $\langle\varphi\rangle$ as the average phase of the population of oscillators.

5.2 Measured signal

As already mentioned in 3.1.3, the cyanobacteria reabsorb a fraction of the emitted bioluminescence. This results in two detection regimes, a bulk detection regime where we detect all emitters inside a well, and a top detection regime with bioluminescence coming only from the upper layers. Each well may contain luminescent and non-luminescent cells. One example for non-luminescent cells are wildtype bacteria for the experiments described in chapter 1.3.2. Therefore we treat them independently here, although our experiments use only luminescent

populations.

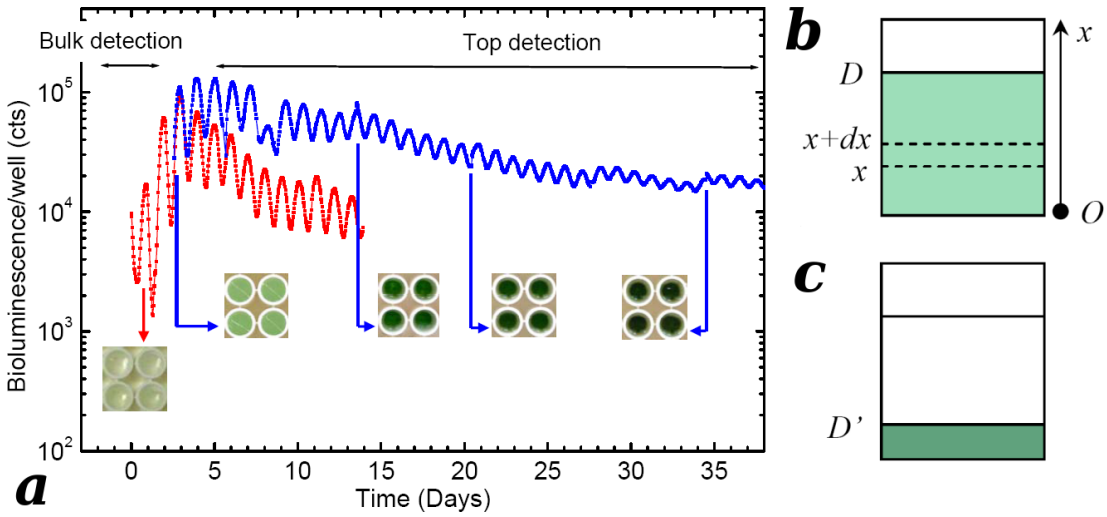

Figure 5.2: Evolution of population during the experiment. (a) Bioluminescence measurement for a population with different initial densities of cells. One with $OD_{750\,nm} = 0.1$ (blue line) and one with $OD_{750\,nm} = 0.01$ (red line). The later shows two detection regimes, first the bulk detection for the first 3 days where we detect the bioluminescence from the entire population under exponential growth. And then top detection from that point on when the population becomes too dense, so that the upper layers reabsorb all bioluminescence originating from the bacteria below. Well pictures: During the experiment the bacteria grow continuously (the wells becoming increasingly greener), but for the top detection regime the bioluminescence signal remains constant. (b) schema of a well containing cyanobacteria. For the first few days, the bacteria are distributed uniformly in the well. dx is a layer of bacteria which bioluminescence production can be described by 5.3. (c) During the experiment the cells sediment to the bottom of the well. As all bacteria are still in the well, only confined in a smaller space, the number of detected emitters doesn't change by this sedimentation process ([5]).

Each luminescent cell inside a well emits the same average signal $\langle d(t) \rangle$ towards the top of the well. For an absolute concentration of luminescent cells, n_E, the increase of the total light intensity I at a given depth x, measured from the bottom of the well (see Fig. 5.2b), is:

$$\frac{dI}{dx} = \langle d(t) \rangle \cdot n_E - \alpha \cdot I \tag{5.3}$$

Here α is the absorption coefficient of the culture inside the well and can be expressed roughly as proportional to the total concentration of cells (luminescent or not) $\alpha = n_T \cdot \sigma$, with $\sigma_{550nm} \cong 4 \cdot 10^{-9}$ cm^2 the absorption cross-section. Therefore, the total number of photons detected on the top of the well (at $x = D$) is:

$$i(t) = I(x = D) \cdot S\tau = \langle d(t) \rangle \cdot \tau \cdot \frac{n_E}{n_T} \cdot \frac{S}{\sigma} \cdot (1 - e^{-\alpha D})$$

With S as the well surface and τ the reading time.

For a transparent well with a low level of absorption ($\alpha D \ll 1$), this means that we detect the light emitted by all of the luminescent cells N_E present in the given volume (bulk detection):

$$i(t) = \langle d(t) \rangle \cdot n_E S D \tau = \langle d(t) \rangle \cdot \tau N_E$$

Otherwise, when the number of cells increases, the detected bioluminescence will increase up to a limit, given by:

$$i(t) = \langle d(t) \rangle \cdot \frac{n_E}{n_T} \cdot \tau \cdot \frac{S}{\sigma},$$

for $\alpha D \gg 1$. That corresponds to detection of the emitters located only on the top layers of the well. Even if the number of emitters continues to increase (visualized by an increasing green colour of the wells), the number of detected photons will remain constant as only the bacteria close to the surface can be seen (Fig. 5.2).

In a step closer to reality, two additional effects have to be taken into account, one is the fact that the bacteria sediment at the bottom of the well, and the other is the illumination dependent reporter gain (see next chapter). As sedimentation does not change the number of cells, the bottom layer contains the same total number of emitting (N_E) and absorbing centers (N_T), except that the cells previously dispersed in the entire well are now concentrated in a smaller region of the space D' (Fig. 5.2c). The detected bioluminescence rewritten as

$$i(t) = \langle d(t) \rangle \cdot \frac{N_E}{N_T} \cdot \tau \cdot \frac{S}{\sigma} \cdot \left(1 - e^{-\frac{\sigma}{S} N_T}\right),$$

therefore remains unchanged, whether for bulk or top detection regimes.

If we take the reporter gain g to vary linearly with the illumination intensity $\langle d(t) \rangle = g \cdot \langle y(t) \rangle$ (see next chapter), we can modify equation 5.3 to:

$$\frac{di}{dt} = \langle d(t) \rangle \cdot n_E \cdot e^{\alpha(x-D)} - \alpha I \tag{5.4}$$

g_0 is the reporter gain under the maximum illumination and $\langle y(t) \rangle = 1 + b \cdot \cos\left(\omega_0 t + \langle \varphi \rangle\right)$ the signal directly related to the circadian clock. Solving the equation yields an expression similar to that of independent light emitters, except for an apparent absorption that is twice as high. Therefore, starting from even lower optical densities, we detect mainly the top emitters.

In our case, an initial $OD_{750\,nm} = 0.1$ marks the beginning of a "top detection" regime. The detected bioluminescence will be then independent of the absolute number of cells, and depends only on the ratio emitters to the total number of cells:

$$i(t) = g_0 \cdot \langle y(t) \rangle \cdot \frac{N_E}{N_T} \cdot \tau \cdot \frac{S}{2\sigma}. \tag{5.5}$$

In addition, the nutrient resources shared among increasingly numerous members will counteract the gain g_0 of the biochemical luminescent reaction/cell. The baseline bioluminescence of a well therefore diminishes slowly in time as $g_0(t)$:

$$\overline{i(t)} = g_0(t) \cdot \frac{N_E}{N_T} \cdot \tau \cdot \frac{S}{2\sigma}. \tag{5.6}$$

The oscillatory signal can then be obtained by dividing the bioluminescence signal by the baseline and subtracting 1:

$$s(t) = \frac{i(t)}{\overline{i(t)}} - 1 \tag{5.7}$$

5.3 Reporter gain

The bioluminescence emitted by a cell $d(t)$ depends on its energetic resources (e.g., received light or nutrients). A cell at the bottom of the well will be less bioluminescent than another one, closer to the surface. The circadian clock is also affected (Katayama et al. [25]), but slightly compared to the bioluminescence reaction. To visualise the illumination-dependent variations of the bioluminescence, we separated a population of entrained bacteria and monitored their reaction to different intensities of constant illumination (LL) (see Fig. 5.3).

Both the absolute value of the bioluminescence intensity and the amplitude of oscillation (the peak to trough ratio) are light dependent (Fig. 5.3a). We quantify these changes separately for the luminescence reporter gain g (Fig. 5.3b) and the relative amplitude of oscillation of the *PkaiBC* activity b (Fig. 5.3c). This shows that the relative gain of the bioluminescent reporter increases with the external lighting. The relative amplitude of the circadian oscillation of the *PkaiBC* activity is also affected, diminishing when the external lighting decreases. The bioluminescence intensity for a maximum is $i_{max} = Kg \cdot [1 + b\rho]$ and for a minimum $i_{min} = Kg \cdot [1 - b\rho]$. This yields $Kg = \frac{i_{max}+i_{min}}{2}$ and $b\rho = \frac{i_{max}-i_{min}}{i_{max}+i_{min}}$, where i_{max} is the maximum at $t \cong 1.1$ days, i_{min} is the minimum at $t \cong 1.6$ days and $K = \frac{S\tau}{2\sigma}$ the factors independent of external lighting. The gain and the relative amplitude of oscillation/cell normalized to the optimal lighting conditions are

then $g_{rel} = \frac{Kg}{(Kg)_{1000\,lux}}$ and $b = \frac{b\rho}{(b\rho)_{1000\,lux}}$ with $b_{1000\,lux} \cong 1$. We take $b_{1000\,lux} \cong 1$ as single cell experiments show for exponentially growing cells a minimal density of bioluminescence close to $0 \Rightarrow b = 1$. However, when illumination diminishes, it appears that the minimal density of bioluminescence ≥ 0, and therefore $b < 1$. Figure 5.3c quantifies b in dependence of the applied illumination: as the illumination fades away, b decreases towards half its value.

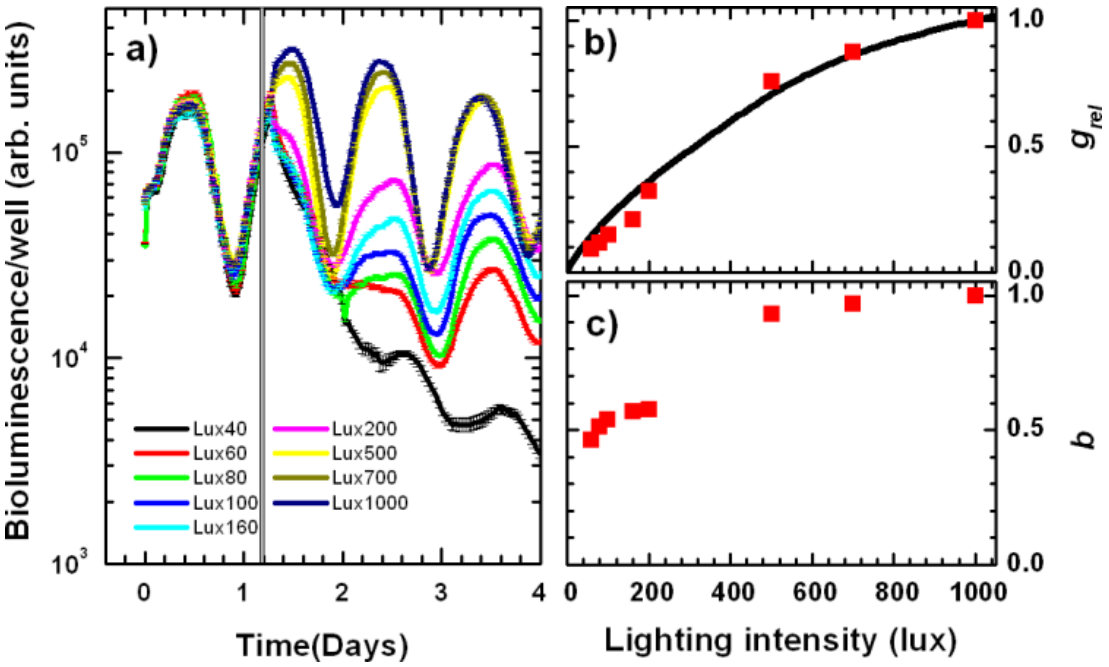

Figure 5.3: Experiments with light steps (for experimental details see 4.3.1) done with entrained bacteria. (a) Average for each cluster. The black line marks the beginning of the switch between 500 lux LL and a cluster depend LL value (light step). (b) The luminescence gain g. The continuous black line represents the calculated gain function obtained from the experiments described in chapter 4.3. (c) The relative amplitude of oscillation of the PkaiBC activity b ([5]).

Chapter 6

Data analysis

In this section, we detail the data treatment and methods we use. This is done in three steps: first a semi-manual correction of jumps in the measured bioluminescence at moments when media was added, second a signal correction related to the bioluminescence gain dependence on illumination and last extraction of relevant parameters and cleaning of the data. For these steps we used either Matlab 6.1 for the signal correction (chapter 6.2) or OriginPro 7.5, a scriptable calculus program. The information we are looking for is the frequency ω, phase φ and amplitude $A(t)$ of the circadian oscillation, which we want to extract from the experimental signal $s(t)$ using the Hilbert algorithm. For sinus-like oscillations it offers the great advantage to be sensitive to the phase and the amplitude of an oscillation all along, and not only relies on the extrema. The script also allows to clean the data before running statistics, based on several manually tunable parameters, which will be detailed in chapter 6.4. Cleaning is done as last step of the treatment on a copy of the data to allow for manual check and easy adaptation if needed.

6.1 Jump corrections on raw bioluminescence signal

When adding nutriments into a well, it can happen that the bioluminescence of the well rapidly increases (Fig. 6.1), which would perturb the extracted phase and amplitude. To correct these jumps, we look at the data from each well individually, and, where necessary, divide the value of all points from the jump on, to counteract the effects of the perturbations. This factor is calculated in three steps:

1. Manual definition of the last unperturbed point $i(t_j)$. This is the last measurement point before adding fresh media (chapter 3.1.2).

2. Detection of the jump width Δt. The width depends on the wells time response to the perturbation, usual values for Δt range from 30 to 110 min, which corresponds to 1 to 3 data points.

3. Calculation of the local derivative of the two closest data points around the jump $\frac{\partial i}{\partial t}\big|_{t_j}$

Calculus of α in case the jump happens on a single time point, where $\frac{\partial i}{\partial t}\big|_{t_j}$ is calculated as the average slope just before and after the jump:

$$\begin{aligned}\left.\frac{\partial i}{\partial t}\right|_{t_j} &= \frac{1}{2}\cdot\left[\left.\frac{\partial i}{\partial t}\right|_{t_{j-}} + \left.\frac{\partial i}{\partial t}\right|_{t_{j+}}\right] = \\ &= \frac{1}{2}\cdot\left[\frac{i(t_j)-i(t_{j-2})}{2\Delta t} + \frac{i(t_{j+3})-i(t_{j+1})}{2\Delta t}\right] \\ &= \frac{1}{4\Delta t}\cdot[i(t_j)-i(t_{j-2})+i(t_{j+3})-i(t_{j+1})]\end{aligned}$$

With this information we now can calculate where the next data point would have been without the jump:

$$i^*(t_{j+1}) = i(t_j) + \underbrace{\left.\frac{\partial i}{\partial t}\right|_{t_j}\cdot\Delta t}_{\alpha} = i(t_j)+\alpha$$

where

$$\alpha = \frac{i(t_j)-i(t_{j-2})+i(t_{j+3})-i(t_{j+1})}{4}$$

We use this to calculate the scaling factor between the points which we will then use to correct all points after the jump:

$$\beta = \frac{i^*(t_{j+1})}{i(t_{j+1})} = \frac{i(t_j)+\alpha}{i(t_{j+1})}$$

The definition of new corrected points is then:

$$\Rightarrow i^*_{jump\,corrected}\,(t_m)_{\,m>j} = \beta\cdot i(t_m)_{m>j}$$

We use a multiplicative correction as the jump amplitude depends on the moment in the circadian cycle. Jumps on an oscillation peak are bigger than on a minimum. It also avoids to shift the bioluminescence signal below zero.

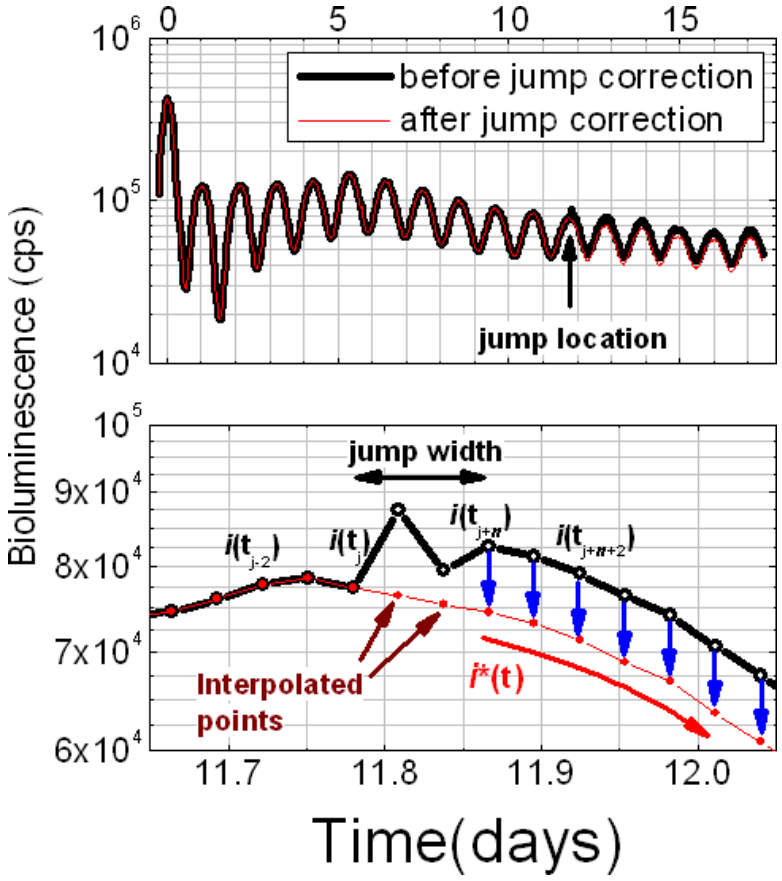

Figure 6.1: Bioluminescence jump correction. (left) the raw bioluminescence oscillation with an intensity jump due to adding media. (right) Zoom on the same jump. $i(t_j)$ is the last unperturbed point before the jump, $i(t_{j+n})$ the first point after a jump of width n. The local derivative is calculated between $i(t_{j-2})$ & $i(t_j)$ and $i(t_{j+n})$ & $i(t_{j+n+2})$. This allows to calculate the shift due to the phase jump and correct it (blue arrows) to obtain $i^*(t)$. Points in between $i(t_j)$ and $i^*(t_{j+n})$ get replaced by interpolated values.

In case the jumps happen over more than one data point, jump with n data points:

$$i^*(t_{j+n}) = i(t_j) + n \cdot \underbrace{\left.\frac{\partial i}{\partial t}\right|_{t_j}}_{\alpha} \cdot \Delta t$$

$$\begin{aligned} \Rightarrow i^*(t_{j+n}) &= i(t_j) + n\alpha \\ \beta = \frac{i^*(t_{j+n})}{i(t_{j+n})} &= \frac{i(t_j) + n\alpha}{i(t_{j+n})} \end{aligned}$$

$$\Rightarrow i^*_{jump\,corrected}\,(t_m)_{\,m>j+n} = \beta \cdot i(t_m)_{m>j+n}$$

As the data points between $i(t_j)$ and $i(t_{j+n})$ hold no valid data, we replace them by linear interpolated values. As mentioned before, these bioluminescence jumps have a limited jump width, so these interpolations concern only one or two points (fig. 6.1).

6.2 Applying the Bioluminescence correction

As shown in 5.3, the bioluminescence gain varies as a function of the incident light the bacteria are exposed to. In this step of the data treatment we unmask this effect based on the light step experiments (see chapter 4.3.1). For that, we calculate the bioluminescence gain $g\left(E(t)\right)$ (chapter 4.3) for each individual well as a function of the LED illumination applied to it.

$$i_{biolum\,corrected}(t) = \frac{i_{jump\,corrected}(t)}{g\left(E(t)\right)}$$

To do this, the data from both plates and the illumination device are interpolated to a common time line before calculating the relative reporter gain for each applied light signal, based on the dependency found in the light steps experiments. By dividing the measured signal by the relative gain we unmask the reporter effects.

6.3 Oscillatory signal extraction: $s(t)$

6.3.1 2-step time average calculus of the signal

As shown in chapter 5.2 the signal from a well is described by

$$i(t) = \overline{i(t)} \cdot \left[1 + b\rho \cdot \cos\left(\omega_0 t + \langle\varphi\rangle\right)\right].$$

This can be separated into the slow $\left(\overline{i(t)}\right)$ and the fast changing components $\left[1 + b\rho \cdot \cos\left(\omega_0 t + \langle\varphi\rangle\right)\right]$ to obtain $s(t)$ (eq. 5.7). To obtain the slow varying component of the signal $\overline{i\,(t)}$, which we also call "baseline", we use, for each individual well, a low pass FFT smooth of approximately 28 h width in two consecutive steps. First a raw smooth $b_1(t)$ on the logarithm of the signal, and

then a second smooth $b_2(t)$ in linear scale on the remaining signal:

$$\begin{aligned} b_1(t) &= \text{smooth}\left[\ln\left(i(t)\right)\right] \\ b_2(t) &= \text{smooth}\left[\frac{i(t)}{e^{b_1(t)}}\right] \\ \Rightarrow \overline{i(t)} &= e^{b_1(t)} \cdot b_2(t) \end{aligned} \tag{6.1}$$

The choice of the baseline is an important step, as it affects all data extracted later during the procedure. The fast oscillating parts belonging to the circadian clock are then obtained by dividing the raw signal by its baseline. This way we get $s(t) + 1 = \frac{i(t)}{\overline{i(t)}}$, from which we subtract 1 to obtain the oscillatory signal $s(t)$. Figure 6.2 shows the effect of the baseline. The upper left panel shows the raw bioluminescence signal (orange) and baselines calculated by using only the first step $b_1(t)$ (cyan) and the combination of $b_1(t)$ & $b_2(t)$ (black). The other panels show how the combined approach improves the quality of the extracted oscillation in the respective colour code. The circadian oscillation shown in the upper right panel, is obtained by dividing the raw oscillations by the baseline, and the instantaneous amplitude (lower left panel) and phase (lower right panel) are extracted from this oscillatory signal via the Hilbert transformation (see next chapter 6.3.2). The oscillation of the instantaneous amplitide and the instaneous phase are smaller when using the combined baseline. This shows that the baseline is an important step of the data extraction. As the baseline is calculated with the help of data smoothes, we need to reduce 'border-effects' that appear at the beginning and the end of the experimental data. We do this by duplicating the first and the last oscillations, this process is described in more details in chapter 6.4.4.

6.3.2 Instantaneous phase and amplitude extraction

Now we come to the core part of the data treatment script, the extraction of the instantaneous phase and amplitude. We do this by reconstructing the complex oscillation signal from $s(t)$ by using the Hilber transform:

$$\zeta(t) = s(t) + is_{HT}(t) = A(t)e^{i\varphi(t)}$$

where $s(t)$ is our measured signal and $s_{HT}(t)$ is given by the Hilbert transform of $s(t)$:

$$s_{HT}(t) = \pi^{-1}\mathcal{P}\int_{-\infty}^{+\infty}\frac{s(\tau)}{t-\tau}d\tau$$

As the imaginary part of an oscillation is perpendicular to the real part, the easiest numerical way to calculate the Hilbert transform is by performing a Fourier transform, shifting all components by 90° and then transforming it back by an inverse Fourier transform. Note that in order to use the fast Fourier transform (FFT) algorithm, the vector data have to be previously interpolated to an exact power of 2 length (2^n).

As introduced in 5.1, the instantaneous amplitude extracted from the measurements contains two parameters, the mean individual amplitude b and the order parameter of the population ρ, which cannot be separated by this experimental approach. It can then be obtained by (Fig. 6.3b):

$$A(t) = \sqrt{[s(t)]^2 + [s_{HT}(t)]^2}$$

In chapter 9.1 we show a possibility to separate them with the help of simulations. The instantaneous phase is given by:

$$\varphi(t) = \begin{cases} \arctan\left(\frac{s_{HT}(t)}{s(t)}\right) & , \text{if } s(t) > 0 \\ \arctan\left(\frac{s_{HT}(t)}{s(t)}\right) \pm 180^{\circ} & , \text{if } s(t) < 0 \end{cases}$$

This gives us the wrapped phase going from $-180°$ to $+180°$ with a jump discontinuity for each cycle (Fig. 6.3c). We unwrap it by correcting all discontinuities by 360° (Fig. 6.3d). Figure 6.4 shows the evolution of the phases of 16 independent wells belonging to the same condition. It shows how reproducible the bacterial circadian clock reacts under the influence of an entrainment. The instantaneous phase gains 360° per cycle (Fig. 6.4a). To better visualise the phase dynamics due to the entrainment, we put all clusters belonging to an experimental condition into the same rotating reference frame by subtracting $\omega_e t$ (for one entrainment phase: Fig. 6.4b, all entrainment phases of this experiment: Fig. 7.5 left side). We will refer to this phase representation as phase deviation.

6.4 Data cleaning

Now the principal parts of the data treatment are completed and we proceed to clean the data. For this we copy the data sheets and remove the data points marked by the cleaning sheets made during the data treatment. This allows to compare the cleaned data with the original one, and also to easily go back in case an error occurred. We use three different criteria to clean the data from

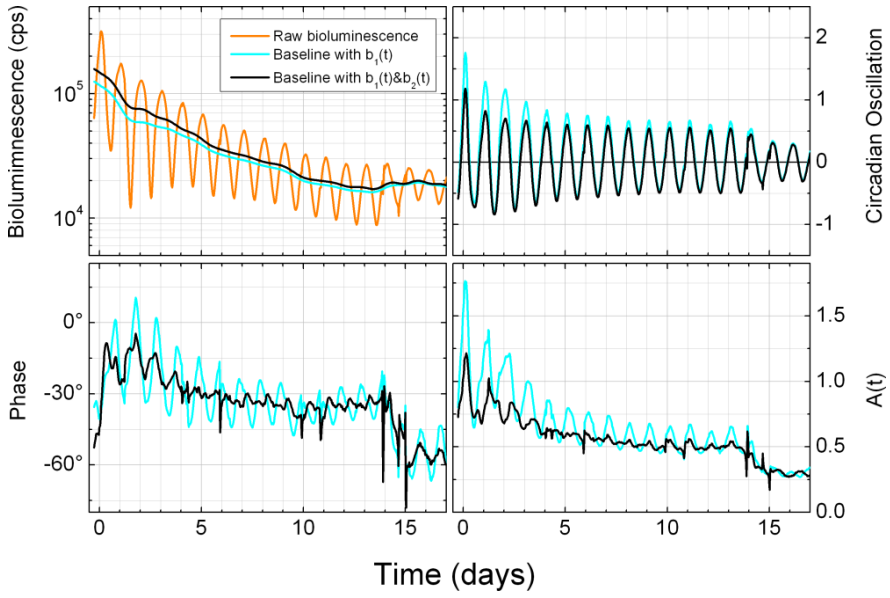

Figure 6.2: Comparison of the 2-step time average calculus of the signal vs. a 1-step calculus. (top left) Baselines calculated from the raw bioluminescence (orange) by using only the first step $b_1(t)$ (cyan) and the combination of $b_1(t)$ & $b_2(t)$ (black) (eq. 6.1). The other graphs show the effect the choice of the baseline has on the extracted data: the circadian oscillation (top right), the extracted phase in an ω_e-rotating frame (bottom left) and the extracted instantaneous amplitude (bottom right).

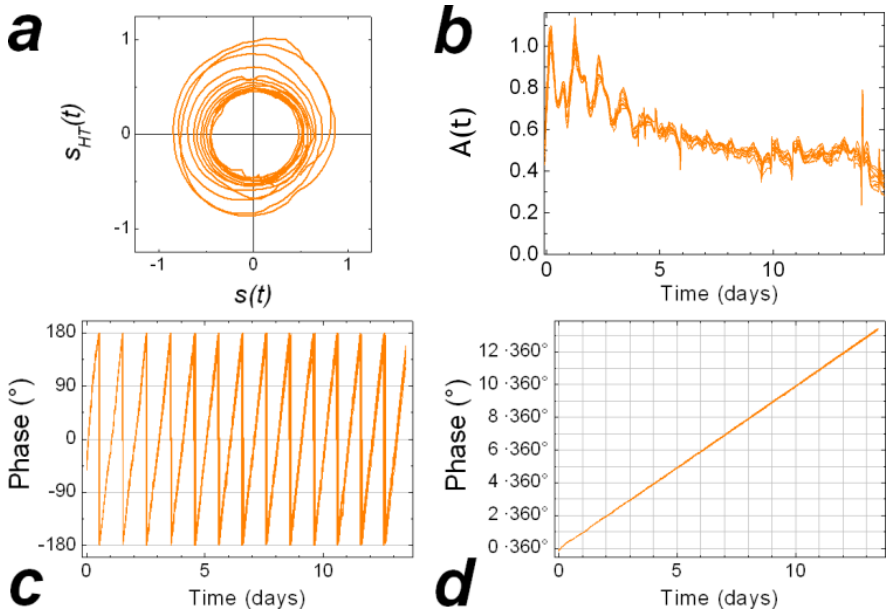

Figure 6.3: Construction of the complex signal and extraction of instantaneous amplitude and phase from it. (a) The complex components $s_{HT}(t)$calculated via the Hilbert transformation in function of the real signal $s(t)$ measured during the experiment. (b) The instantaneous amplitude $A\,(t)$ for 16 wells from a cluster. (c) The wrapped phase with values in$]-180°; 180°]$ (d) The unwrapped phase where the discontinuities of the wrapped phase are corrected by $360\,°$ each. For circadian clocks it gains around $360\,°$ per day.

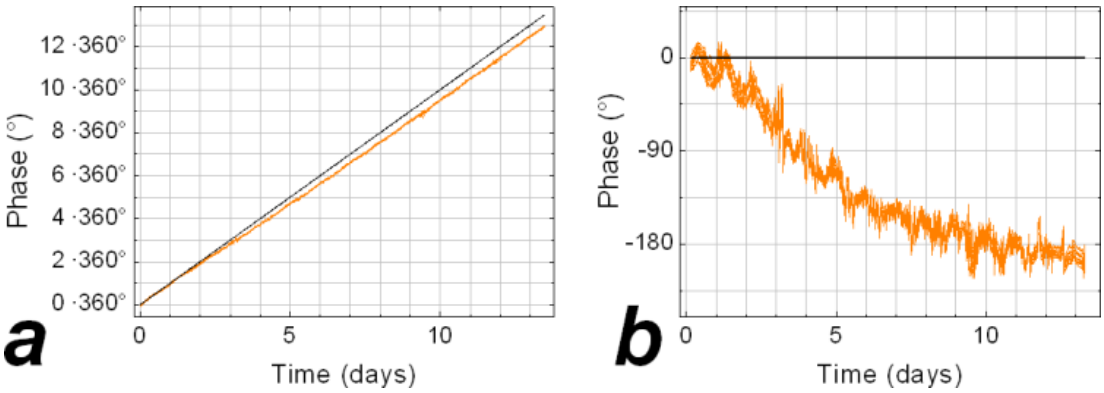

Figure 6.4: Representation of the phase in a rotating frame. Here shown are 16 independent wells of an identical conditions. This demonstrates the reproducibility of the experiment. (a) The unwrapped phase, gaining $\sim 360°$ per day. We subtract $\omega_{entrainment} = 360°{\cdot}t$ represented in black to keep only the variations compared to our reference frame. (b) The phase deviation in the rotating reference frame. The phase of the reference frame in black is constant and equal zero by definition.

dried or contaminated wells. First the baseline criteria (ch. 6.4.1), with which we verify that a wells baseline is not too far away from a manually chosen reference baseline of its cluster. Second the amplitude criteria for entrained wells (ch. 6.4.2) with which we detect areas where instantaneous amplitude of a well is too low to extract the phase. And finally a jump detection (ch. 6.4.3), which locates 360° phase jumps that have their origin in the phase extraction procedure rather than in the circadian clock. So far we apply the cleaning to the phase deviation in the rotating reference frame (fig. 6.4b), the instantaneous amplitude $A(t)$ (fig. 6.3b), the raw bioluminescence data (fig. 5.1) and the oscillatory signal (fig. 6.2 upper right panel).

6.4.1 Baseline criteria

As shown in chapter 6.3.1, the baseline represents the general evolution of a well $\overline{i(t)}$. As this is roughly the same for all wells of a cluster, it can also be used to detect problematic wells during the experiment. A dried up or contaminated well shows a different general evolution than a healthy well and should not be considered to determine the relevant information.

To find this type of wells, we plot all baselines of a cluster together and manually choose a reference line for this cluster with which all other baselines will be compared. In case a baseline is found to leave the corridor given in percent (here 20%) around the reference line (fig. 6.5), its coordinates (line and data point number) are logged in a separate data-sheet. This information is then

used to remove all later data.

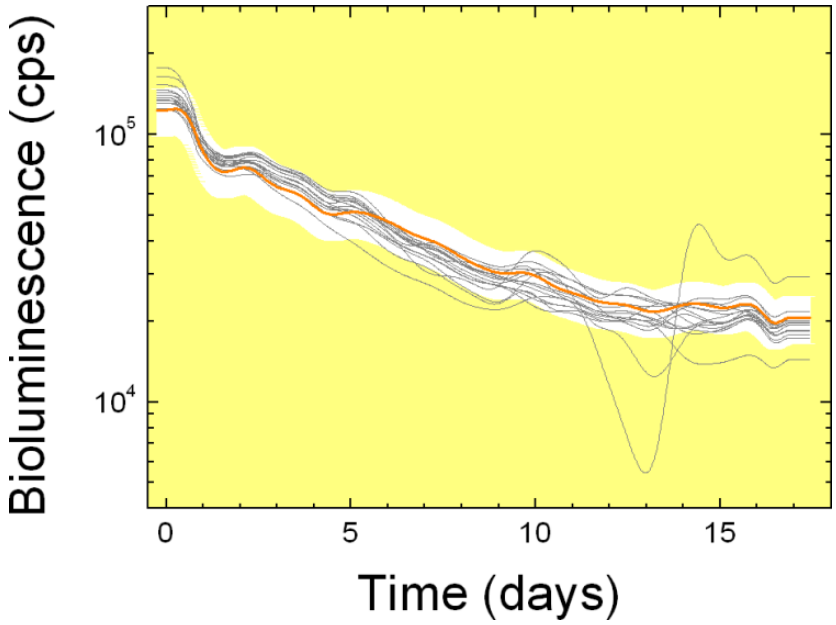

Figure 6.5: The reference baseline criterium. For each cluster we manually choose one baseline as reference. Each other well whose baseline leaves a 20% corridor (white) around that reference will not be considered for the statistics from that point on (gray line entering yellow area), regardless if it rejoins the corridor again or not. Baselines in gray with the reference line in orange.

6.4.2 Amplitude criteria for entrained wells

With the help of the instantaneous amplitude $A(t)$ we gain information about the periods where the algorithm cannot properly extract the phase, due to a too low instantaneous amplitude compared to experimental noise. This can happen for example when the distribution of individual oscillation result in a low order parameter ρ. As this is only an intermediate effect due to the entrainment, we only remove affected points.

We locate these periods for each well independently by applying a 28 hour smooth to the relative amplitude, and compare it with a reference threshold of 0.1. If the smoothed amplitude of a well falls below this value, we track areas where it is below and log them for later cleaning (fig. 6.6). In case the amplitude oscillates around the threshold value, we mark the whole period for later cleaning. The log file is an independent data sheet that holds the line number and the definite starting and ending point. Points in-between will later be removed on the final data by the cleaning process. With this criteria we locate periods with detection difficulties that have their origin in the phase distribution inside a well rather

than actual biological problems. Once the oscillators inside a well are sufficiently synchronised to determine the phase of the population, we continue to track it.

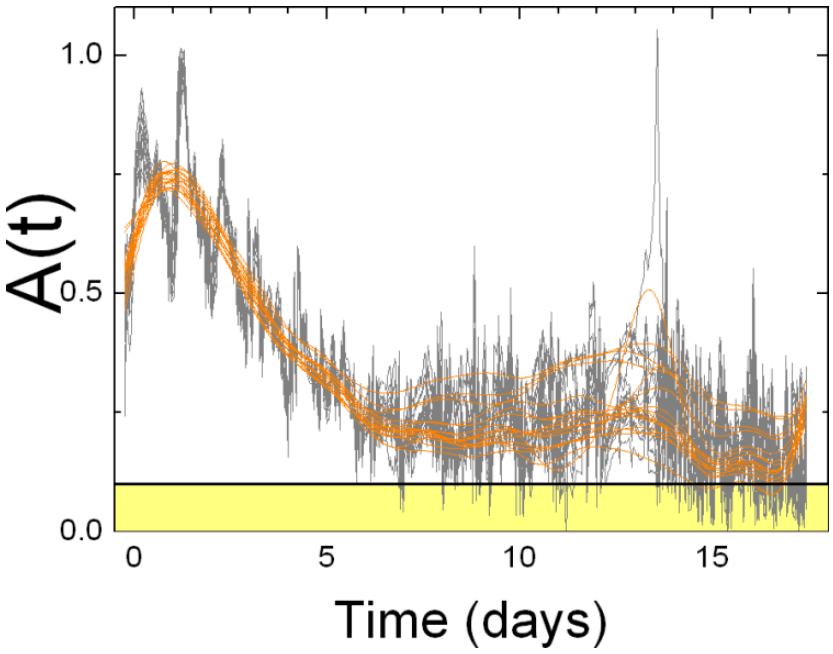

Figure 6.6: Minimum instantaneous amplitude cleaning criterium. Very low amplitude below 0.1 is a sign for a difficult to detect oscillation and also increased sensibility towards noise. All data from wells whose smoothed instantaneous amplitude $A(t)_{smoothed} \leq 0.1$ (yellow area) at that moment will not be taken into account for the statistics. Once it gets above that threshold it will be taken again, as this is merely a detection handicap than a sign for a biological problem. Relative amplitudes for a cluster in gray, their smooth in orange.

6.4.3 Jump detection

The circadian clock of the cyanobacteria is not totally a sinusoidal oscillation. This and possible remaining reporter effects and detection noise can introduce additional discontinuities. We detect them by looking at the short time evolution of the phase. First, we look at the difference between direct neighbors. In case it exceeds 300°, we correct the phase from this point on by ±360° (fig. 6.7). The threshold of 300° instead of 360° was chosen because it is already largely superior to the phase advancement for an oscillator with circadian rhythm, but is small enough to detect jumps, even under the presence of noise on the phase. Because of the stretching to 2^n data points, necessary for the phase extraction, not all phase jumps occur between only two points. To find these we perform 4 runs, looking at the difference between points that are 2, 4, 8 and 16 points apart from each other. If a phase jump is detected, we detect the location of the biggest difference between two data points; within the observed section we correct it by

360°. This information will later be used to remove data points in close proximity to these jumps. Figure 6.8 shows the effect of this phase jump correction on an entire cluster. The yellow lines mark areas where a jump on one of the phases was detected and corrected as shown in figure 6.7.

6.4.4 Effects of the baseline borders

The baseline is calculated by a FFT smooth with a length of 28 hours (ch. 6.3.1). This method gives the best results, as it separates fast and slow evolving parts in the measured signal, but it is less sensitive at the borders. At the beginning and the end of a data line, the FFT runs with a smaller time window and is thus more sensible to the fast oscillating parts. To overcome these reduced windows and reduce these border effects, we add two oscillations from a manually chosen well under constant illumination, and add them at the beginning of each oscillatory signal curve. As the bacteria are entrained to different phases during the experiment, we cannot add the same wells oscillations at the end. Instead, we replicate the last two oscillations of each well. This additional data will be cut away again after the data treatment.

To evaluate the effects the baseline has on the extracted phase, we created a set of 12 oscillations centered around a common baseline (fig. 6.9). We then calculated the base line of this signal in several different ways: by double FFT smooth (eq. 6.1) without any other treatment, same smooth and additional oscillations on both ends and same smooth and additional constant mean value for several days.

We then compared the phase extracted from this signal with the phase of the created signal. This showed that adding a constant value does not solve the problem, but adding oscillations improves the precision. We found that adding more than 2 oscillations does not significantly improve the precision (fig. 6.10).

In the next step we verified that data interpolation does not influence the precision. For this we created a data sheet with $2^8 + 1$ data points. We processed it once without stretching by cutting the last point, and once by stretching it to 2^9 data points. Then once again we added 2 oscillations on both ends and processed this data once with 2^9 data points without stretching and once with $2^9 + 1$ points stretched to 2^{10}. We repeated the process with $2^8 + 2^7$ data points stretched to 2^9. In all cases the stretching does not influence the extracted phase, and the data processed with additional oscillations show better precision.

Figure 6.11 compares the effect of the baseline extraction on experimental data. The baselines were extracted with (dark blue) and without (cyan) ad-

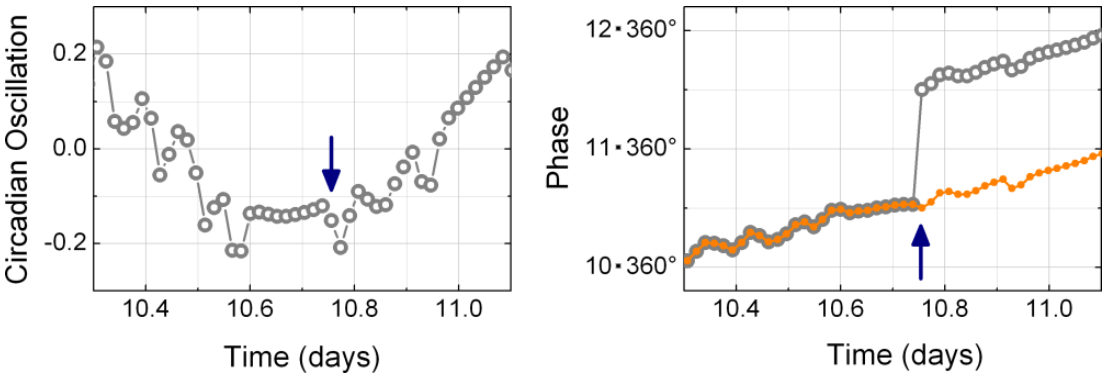

Figure 6.7: Origin of sudden phase jumps. Under certain conditions, noise on the bioluminescence signal is detected as an additional oscillation, which leads to a $360°$ jump on the instantaneous phase. We detect these jumps and correct them by $360°$ to obtain the original phase. (left) the bioluminescence signal (grey). (right) the instantaneous phase extracted from this well uncorrected (grey) and corrected (orange). The arrows mark the instant where a variation of the bioluminescence signal is detected as an additional oscillation that leads to a $360°$ phase jump.

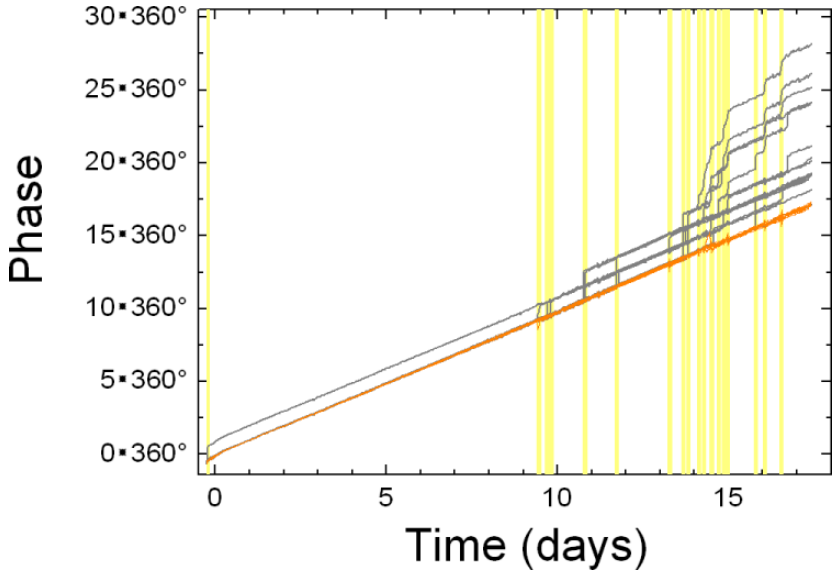

Figure 6.8: Phase jump correction. Phase fluctuations due to noise or reporter effects can be detected as additional oscillation. They show up as $360°$ phase jumps on the unwrapped phase and can be found and corrected by comparing the local derivative to the overall derivative. Unwrapped phases before (gray) and after (orange) correction. Areas with detected jumps (yellow). Points for lines with a jump within these areas will be deleted as jumps can extend about a few data points ($5 - 15$).

ditional oscillations (fig. 6.11a) and the circadian oscillation (fig. 6.11b) was calculated by dividing the raw bioluminescence signal by the baseline. The two lower panels show the effect on the instantaneous phase (fig. 6.11c) and the instantaneous amplitude (fig. 6.11d). The insets zoom on the beginning and the end of each respective graph. This approach allows to determine the initial phase with better precision than before.

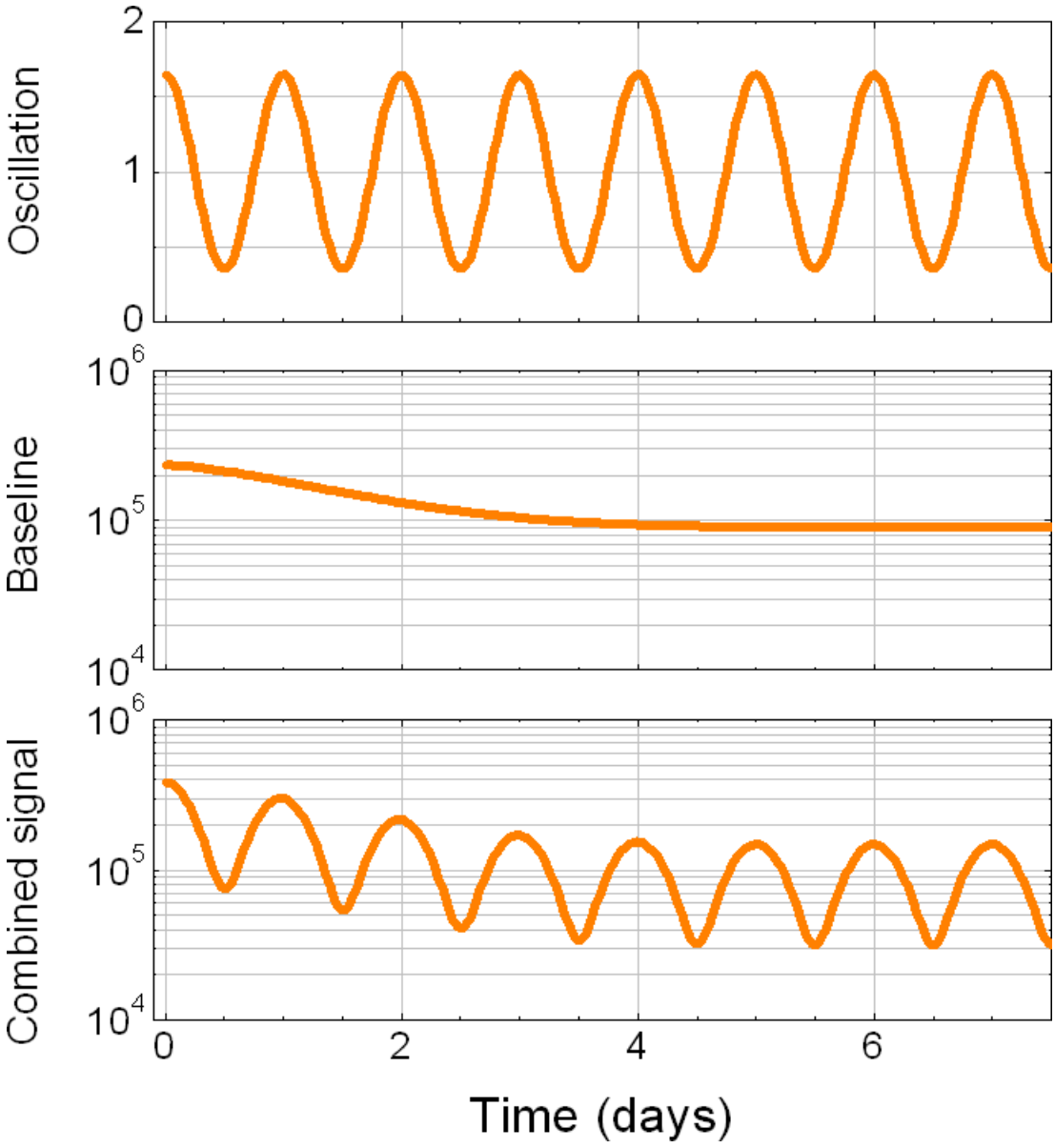

Figure 6.9: 3 steps of artificial signal generation. (top) one oscillation out of a set of 12 different phases. (middle) common baseline for all 12 oscillations. (bottom) combination of both.

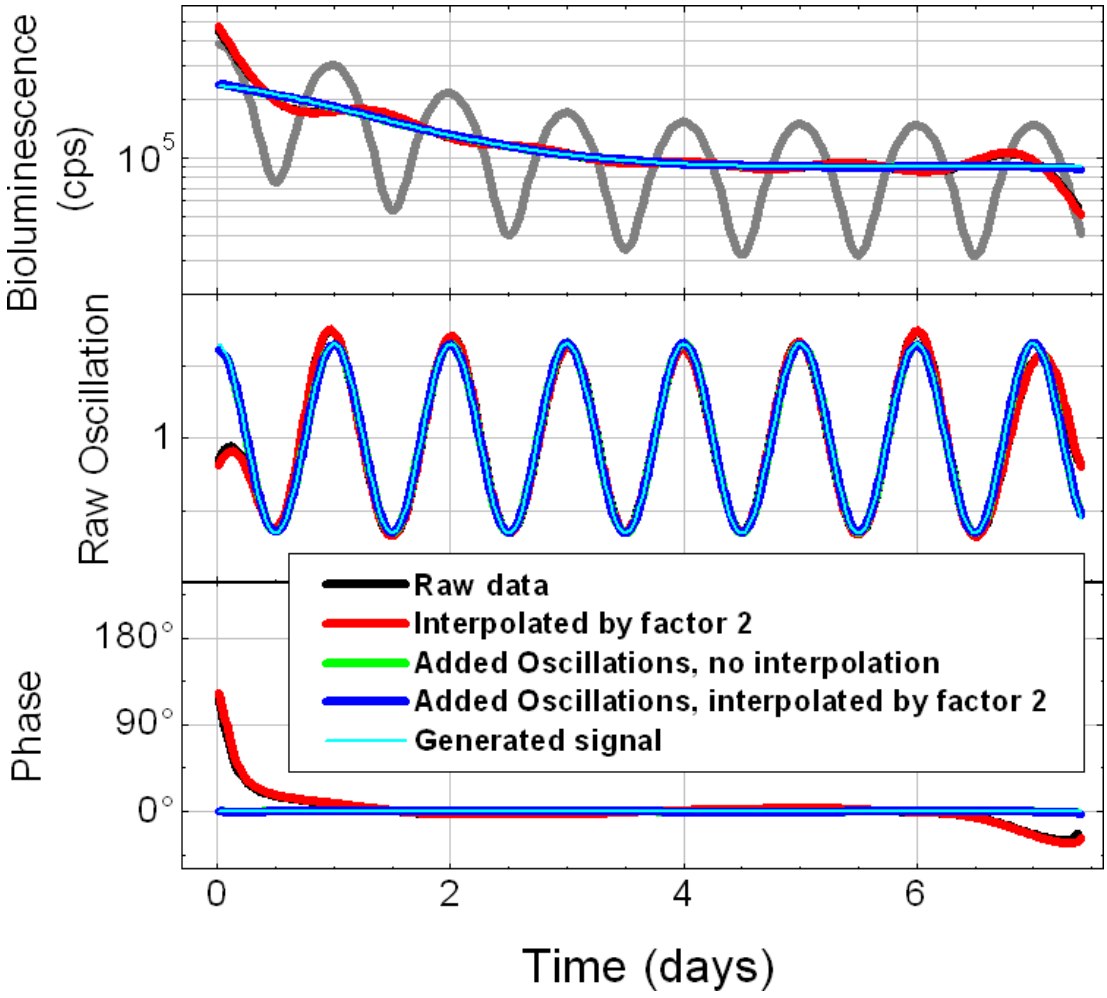

Figure 6.10: Signal extraction from the generated oscillations (fig. 6.9). (top) The oscillations with baselines calculated by different methods. (middle) The oscillatory signal $s(t)$ obtained by dividing the raw oscillations by the different baselines. (bottom) The instantaneous phases extracted form the oscillatory signals.

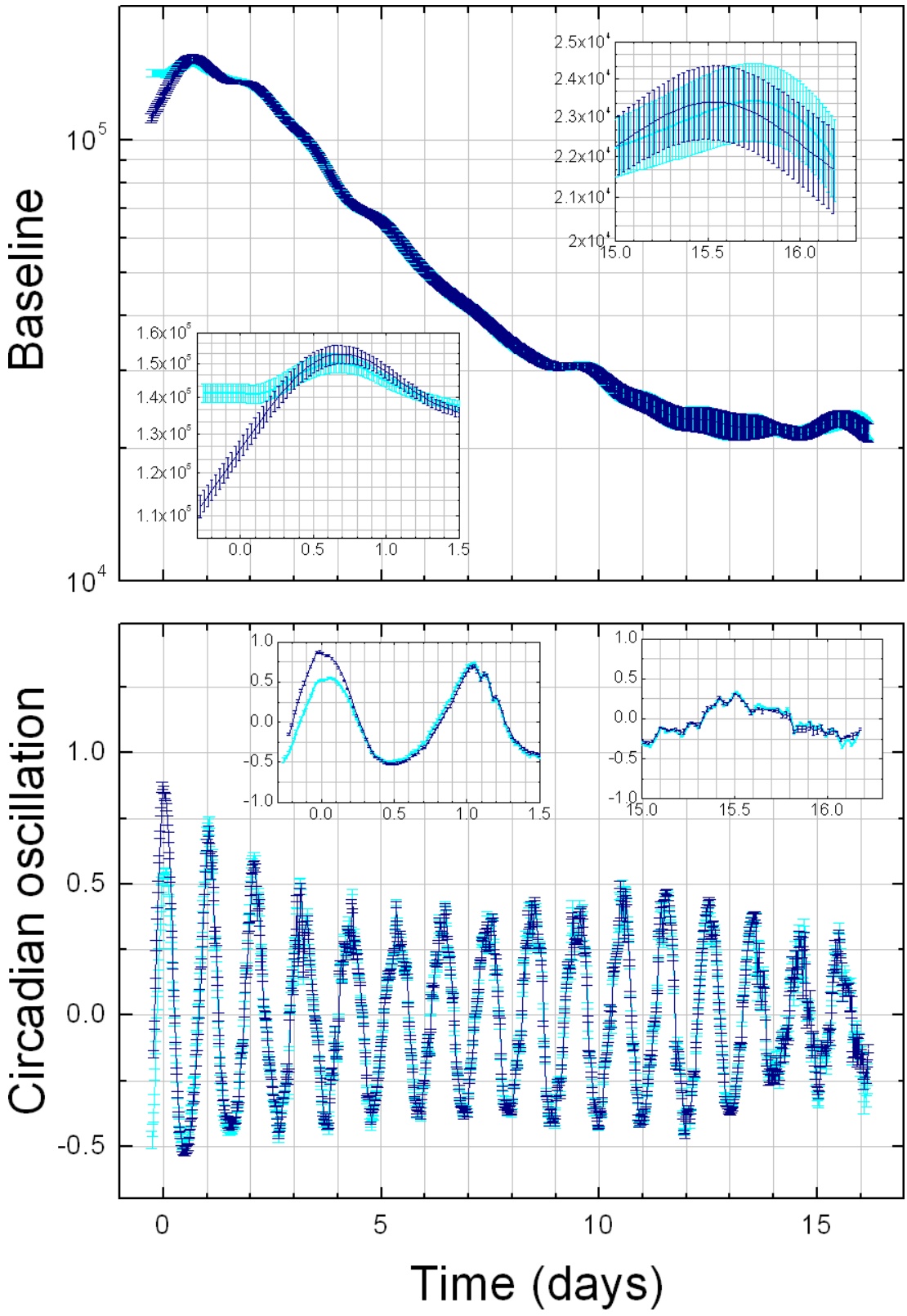

Figure 6.11: Comparison between base line extraction with (dark blue) and without added oscillations (cyan). The inset graphs zoom on the beginning and the end of the respective large graph. (top) The baseline itself. (bottom) The circadian oscillation obtained by dividing the raw bioluminescence signal by the baseline. The corresponding instantaneous phase and instantaneous amplitude are shown in figure 6.12.

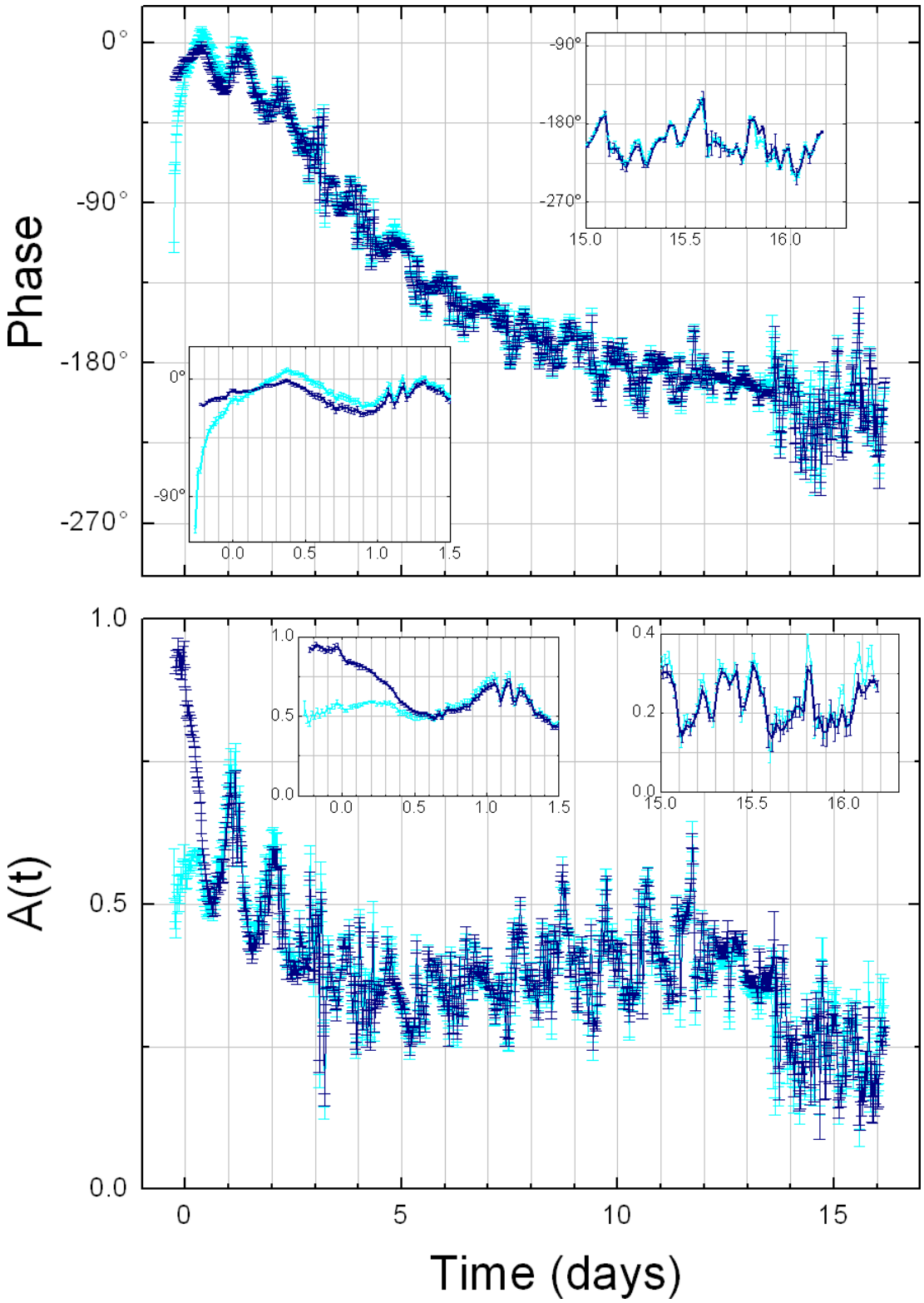

Figure 6.12: Comparison between base line extraction with (dark blue) and without added oscillations (cyan). The inset graphs zoom on the beginning and the end of the respective large graph. (top) The instantaneous phase. (bottom) The instantaneous amplitude. The corresponding baseline and oscillatory signal are shown in figure 6.11.

Part III

RESULTS: Dynamic description of the response of a cyanobacterial population to a periodic forcing

English introduction

In the qualitative description we first discuss the difficulties in defining the phase of the circadian clock via a bioluminescence reporter before showing the results of the entrainment by illumination forcing. We show experiments with entrainment to various phase shifts by sinusoidal illumination oscillations with a relative amplitude ranging from 0.2 to 1.0. We show examples for frequency and phase locking, and discuss the importance of the perturbation strength versus the difference of proper frequencies between the entrainment and the bacterial clock, in order to distinguish between synchronisation and pseudo-entrainment. We show examples for both cases with relative phase shifts of 90° and 30° between the different perturbation phases. We also briefly discuss a comparison of the entrainment efficiency of sinus shaped versus square shaped perturbation. We end the qualitative description by showing the effect of temperature forcing and compare it to the illumination results.

In the quantitative description we demonstrate how the experimental values are obtained, associate them with the theoretical variables of the Adler model and modify the model to the experimental needs by adding variables for strain and reporter related phase shifts and the phase of the entrainment forcing. We then apply the resulting fit function to a homogeneous population of oscillators, and show how the parallelisation of the experiment can be used to eliminate free fitting parameters. Based on the fits of experiments with synchronisation and pseudo-entrainment, we show how the coupling constant ε depends on the relative amplitude of the forcing and discuss the experimental distribution of the observed initial phase ψ_0^{lum}, and the strain and reporter related phase shifts α. We proceed with the discussion of the temperature forcing and its description with the same model, before enlarging our view and considering a population of oscillators with distribution of initial phases. We simulate its behaviour and compare the results with the experimental data. We close this chapter with the discussion of the applicability of the phase oscillator model to describe the cyanobacterial circadian clock.

We then take the next step and consider the effect of a stochastic noise on each individual member of a population. To do this, we first discuss the limitations of getting information about the instantaneous amplitude via the approach with population experiments and show a possibility to get an impression of it with the help of the numerical simulations. We extend the simulation and individualise the behaviour of the oscillators inside a population by adding a stochastic noise or a distribution of proper frequencies. By comparing those two types of approaches we highlight the importance of single cell experiments to answer remaining questions.

With this as initial point we propose an experimental set-up to answer those questions and show a possibility to solve the technical problems. For this we imagine a bacteria trap that allows to observe bacteria over many generations, and then present our technical approach and preliminary experiments with fluorescent cyanobacteria. We close this chapter with an outlook to further development of these devices and sketch some additional possible applications with these devices beyond the scope of cronobiology with cyanobacteria.

We close this work with a brief summary and a general outlook on possible follow up experiments.

Introduction en français

Dans la description qualitative nous examinons d'abord les difficultés à définir la phase de l'horloge circadienne par un rapporteur de bioluminescence avant de montrer les résultats de l'entraînement par l'illumination de forçage. Nous montrons des résultats d'expériences avec entraînement vers différentes phases par des oscillations sinusoïdales d'éclairage avec une amplitude relative allant de 0.2 à 1.0. Nous montrons des exemples de verrouillage de fréquence et de phase, et discutons l'importance de la force de perturbation par rapport à la différence de fréquences propre entre l'entraînement et l'horloge bactérienne, afin de distinguer entre la synchronisation et le pseudo-entraînement. Nous montrons des exemples pour ces deux cas, avec des décalages relatives de phase de 90° et 30° entre les différentes phases d'entraînement. Nous discuterons aussi brièvement une comparaison d'efficacité entre un signal d'entraînement sinusoïdal et un autre en forme de carré. Nous terminons la description qualitative en montrant l'effet de la température comme force d'entraînement et comparons ceci aux résultats obtenus par entraînement d'illumination.

Dans la description quantitative, nous démontrons comment les valeurs expérimentales sont associées aux variables théoriques du modèle d'Adler, et nous modifierons le modèle aux besoins expérimentales en ajoutant des variables aussi bien pour les déphasages liés à la souche et le rapporteur et pour la phase d'entraînement. Nous appliquons ensuite la fonction d'ajustement numérique résultant à une population homogène d'oscillateurs, et montrons comment la parallélisation de l'expérience peut être utilisée pour éliminer les paramètres libres. Sur la base des ajustements numériques des expériences avec synchronisation et pseudo-entraînement, nous montrons comment la constante de couplage ε dépend de l'amplitude relative du signal d'entraînement, et nous discutons la distribution expérimentale de la phase initiale observée ψ_0^{lum} et du décalage interne dépendant de la souche et du rapporteur α. Nous procédons à la discussion d'entraînement par température, et montrons que le modèle d'Adler est également valable dans ce cas-là avant d'élargir notre point de vue en tenant compte d'une population

d'oscillateurs avec une distribution des phases initiales. Nous simulons son comportement et comparons les résultats aux données expérimentales. Nous terminons ce chapitre par la discussion de l'applicabilité du modèle de l'oscillateur de phase pour décrire l'horloge circadienne des cyanobactéries.

Dans l'étape suivante, nous examinons l'effet d'un bruit stochastique sur chacun des membres d'une population. Pour ceci, nous examinons d'abord les limites des informations que nous pouvons obtenir sur l'amplitude instantanée via l'approche avec des expériences en population et montrons la possibilité d'obtenir une impression de celle-ci à l'aide des simulations numériques. Nous développons la simulation en rajoutant des possibilités d'individualiser le comportement des oscillateurs à l'intérieur d'une population par un bruit stochastique individuel ou une distribution de fréquences propres. C'est en comparant ces deux types d'approches que nous démontrons l'importance des expériences cellule unique pour répondre aux questions restantes.

Partant de ce point initial, nous proposons un dispositif expérimental pour répondre à ces questions et montrons une possibilité de résoudre les problèmes techniques. Pour cela, nous imaginons un piège à bactéries qui permet de les observer pendant plusieurs générations, et présentons notre approche technique et des expériences préliminaires avec des cyanobactéries fluorescentes. Nous terminons ce chapitre par une perspective de développement de ces dispositifs et envisagons certaines applications supplémentaires possibles avec ces dispositifs, au-delà du domaine de la chronobiologie avec des cyanobactéries.

Nous terminons ce travail par un bref résumé et des perspectives générales pour de possibles expériences dans l'avenir.

Chapter 7

Qualitative description

In this section we focus on a qualitative description of our experiments. A quantitative description follows in the next chapter (ch. 8). We start by showing how periodic forcing by illumination can entrain the cyanobacterial clock, how this is represented in the phase graphs and how the amplitude of the forcing influences the entrainment speed. We proceed by looking closer to the case when an external periodic forcing is present, but does not succeed into entraining the circadian clock, this is the so called pseudo-entrainment. Next we compare sinusoidal shaped to rectangular shaped forcing of the same amplitude. Last we look at the effects of a different type of forcing and its effect on the phase: the temperature entrainment.

7.1 Time delays in the system

When observing the circadian clock of cyanobacteria via a reporter, it is difficult to define the real oscillation state of the clock. There are several possible candidates: the phosphorylation state of KaiC, the mRNA expression, the protein expression of either KaiC or the Luciferase and finally the bioluminescence production. All belong to the same chain of events, and all of them oscillate in function of the circadian clock. But they are phase-shifted one to another. On top of that, mRNA and the proteins have their own degradation times which induces additional time lags. Each of them peaks at different moments during the cycle, phosphorylated KaiC reaches its peak level typically at circadian time[1] CT=12h, mRNA concentration peaks at CT=14h, the KaiC concentration usually 4-6 hours later at CT=19h and the Luciferase at CT=16, due to its shorter

[1] Circadian Time =0 is the moment when the illumination switches back to LL, after usually several cycles of LD.

degradation time.

In our case this reporter is the bioluminescence produced by the Luciferase protein complex, which was added to the genome of the bacteria. We use it as reporter, as it is the only non-invasive measurement method and thus allows for long time experiments. Since the bioluminescence production is at the end of the signal chain, we have to deal with the inherent phase shifts (fig. 7.1). As to which degree these lags are affected by the circadian clock can not be determined by this experiments. So we group all internal shifts into one single parameter α, which describes the phase shift between the circadian clock and the bioluminescence reporter we measure.

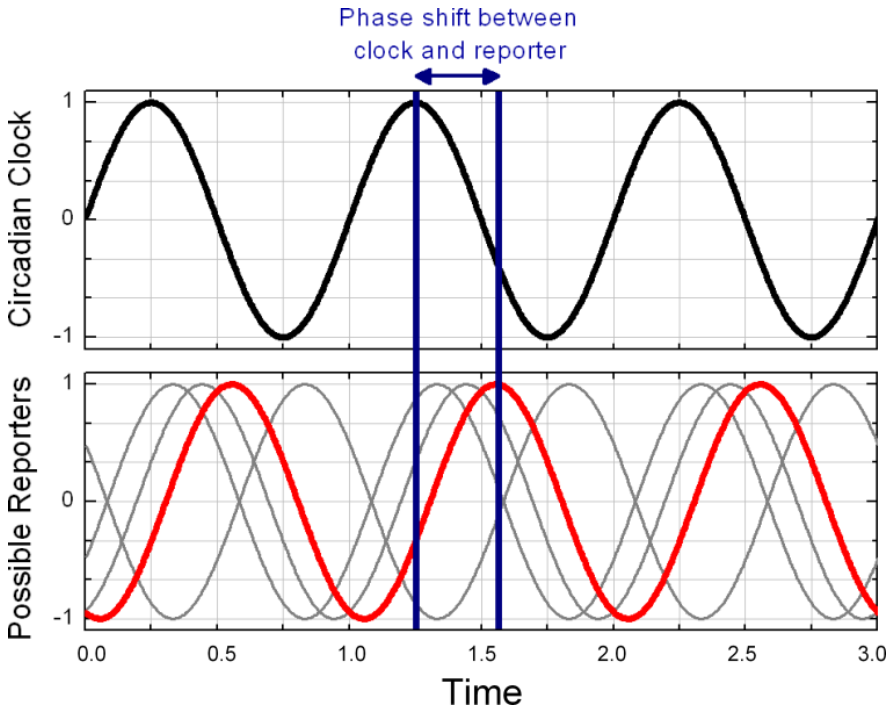

Figure 7.1: Phase shift between the circadian clock and possible reporters. As we cannot read the circadian clock directly, we have to measure it via a reporter. As all of these reporters are further down the signaling chain, we have to take into account that the phase we measure via this reporter is shifted. The amount of this shift is reporter dependent. (top) the rhythm of the circadian clock in vivo. (bottom) a series of possible reporters cycles dependent of the circadian clock. An arbitrary reporter is shown in red to highlight the phase shift it has with the circadian clock.

7.2 Periodic forcing by light

In this part we present the experiments we did using periodic light perturbation to entrain the circadian clock of cyanobacteria. An example is given in fig. 7.2. We

create the forcing with our illumination devices (ch. 3.5.1) with an entrainment period of $\omega_e = 360^o/24h$, which serve both as an entrainment device and as an energy source for the bacteria. The other crucial parameters to describe the behaviour of the bacteria under entrainment are the initial phase of the clock ϕ_0, and the initial phase measured via the bioluminescence reporter ψ_0^{lum} at $t = 0$ the moment when the entrainment begins. As we entrain bacteria to different phases simultanously, we also use the phase of the entrainment force θ_{e0} to name the different conditions. The difference between the proper frequency of the bacteria ω_0 and the proper frequency of the entrainment ω_e gives us the detuning $\nu = \omega_e - \omega_0$. During our experiments we always kept the illumination entrainment signal oscillating around a time average of 500 lux. This ensures that the bacteria always receive the same energy/day. We first show how frequency locking is achieved and how to read it in the phase representation. Next we extend the description with phase locking to describe a set of experimental conditions that were entrained to the same frequency but with different phases.

7.2.1 Frequency locking

We speak of frequency locking when a self-sustained oscillator does not oscillate with its own proper frequency ω_0, but with the frequency of an external zeitgeber ω_e. As soon as this is achieved, the oscillator has reached a stable final phase within the reference frame of this zeitgeber. This behaviour is shown in fig. 7.2, where an entrained condition (red) is compared with a condition in free-run (black). The different conditions were created by separating a population of bacteria entrained in the incubator for several days. Right after separation they were microplated and put under light entrainment. Each experimental condition is reproduced 16 times. This allows to remove corrupted wells and run statistical analysis. The entrained condition (red) illuminated by gradual intensity changes centered around 500 lux shows frequency locking. This can be seen either by the constant peak to peak ratio between the entrainment signal (top) and the measured oscillation (middle) or by the horizontal phase of this oscillation in the rotating frame of the zeitgeber. The free-run condition illuminated by constant light at 500 lux oscillates with its own proper period ω_0, different from the proper period of the zeitgeber ω_e. This leads to a gradual deviation between the entrained and the free-run condition.

7.2.2 Phase locking

Phase locking is quite similar to frequency locking as it describes the fact, that an entrained oscillator reaches a final stable phase induced by an external zeitgeber. Here we introduce this separately, as in our experiments we entrain several experimental condition to the same frequency (in general 24h) but to different phases. As example we show in fig. 7.3 two experimental conditions, taken from the same population that are entrained to opposite phases during a 15 days experiment. Initially in phase at $t = 0$, they gradually shift until both reach their respective final stable phase, separated from each other by 180°. The figure shows how the 12h shift of the entrainment can be found in the circadian oscillations measured from both conditions, and how this is represented by the phases in the rotating frame at $\omega_e = 360^o/24\text{h}$. The conditions keep these entrained phases, even under free-run conditions. When looking at the oscillations of the entrainment signal compared to those of the oscillator, we see that they are almost in phase oposition at the end of the experiment period. The reason for this is the time delay between the peak of the entrainment and the peak of the bioluminescence reporter mentioned in chapter 7.1. We will take these into account in our model in chapter 8.1.1.

7.2.3 Perturbation strength

Besides the phase of the entrainment signal we varied two other parameters: the relative amplitude of the illumination, which produces a stronger zeitgeber signal for the bacteria, and the period length via which will be determined the detuning ν. We did most of our experiments with zeitgeber signals of 24h period length. Note that the proper frequency ω_0 can vary from one experiment to another, therefore even for ω_e one can have different $\nu = \omega_e - \omega_0$.

Depending on the chosen parameters we can classify the experiments in two categories (fig. 7.4): one where the circadian clock synchronises with the illumination (fig. 7.4 left side, more details in ch. 7.2.4) and one where the perturbation was not important enough to act as zeitgeber (7.4 right side, more details in ch. 7.2.5), but still has some influence on the system. We call these cases pseudo-entrainment. Figure 7.4 shows three perturbation conditions with the same detuning ν but perturbed by different illumination amplitudes. As it can be seen in the upper panels that show the perturbation signal, the illumination amplitude decreses from left till right. The lower panels show the phase of the bacteria exposed to these illumination patterns. The connection between the amplitude

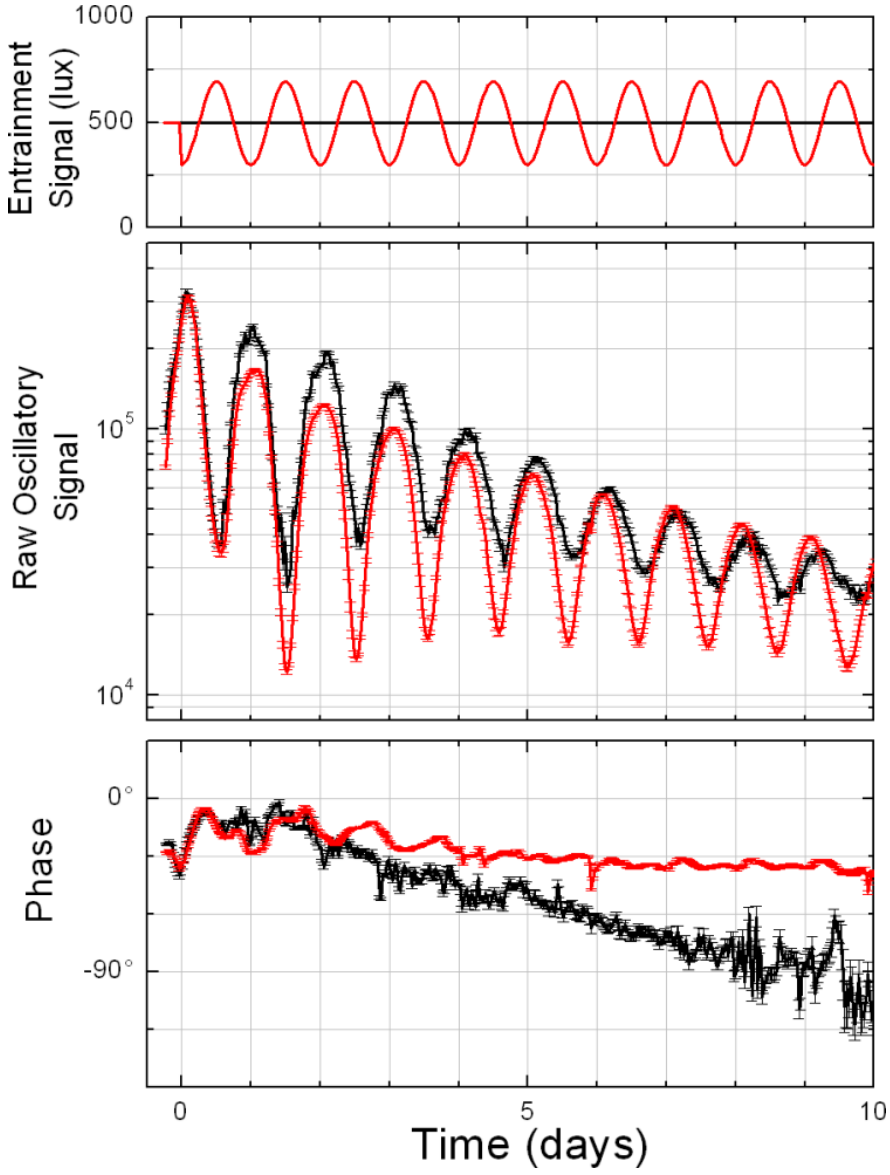

Figure 7.2: Entrainment by light perturbations (red) vs. free run (black). Initially identical due to the same pre-experimental treatment, the conditions show the same raw mean bioluminescence signal (middle) before they separate under influence of their respective different illumination signal (top) applied to them. While the entrained oscillation keeps the same phase shift with the entrainment signal, indicating frequency locking with the zeitgeber, the unentrained oscillations slowly shift as they oscillate with their own proper frequency. (bottom) Representation of the phases in the rotating frame of the zeitgeber. The entrained phase becomes horizontal once frequency locking is achieved, while the free-run condition follows a straight line, which inclination is given by the difference between the proper frequencies ($-\nu = \omega_0 - \omega_e \cong -10$ %/day).

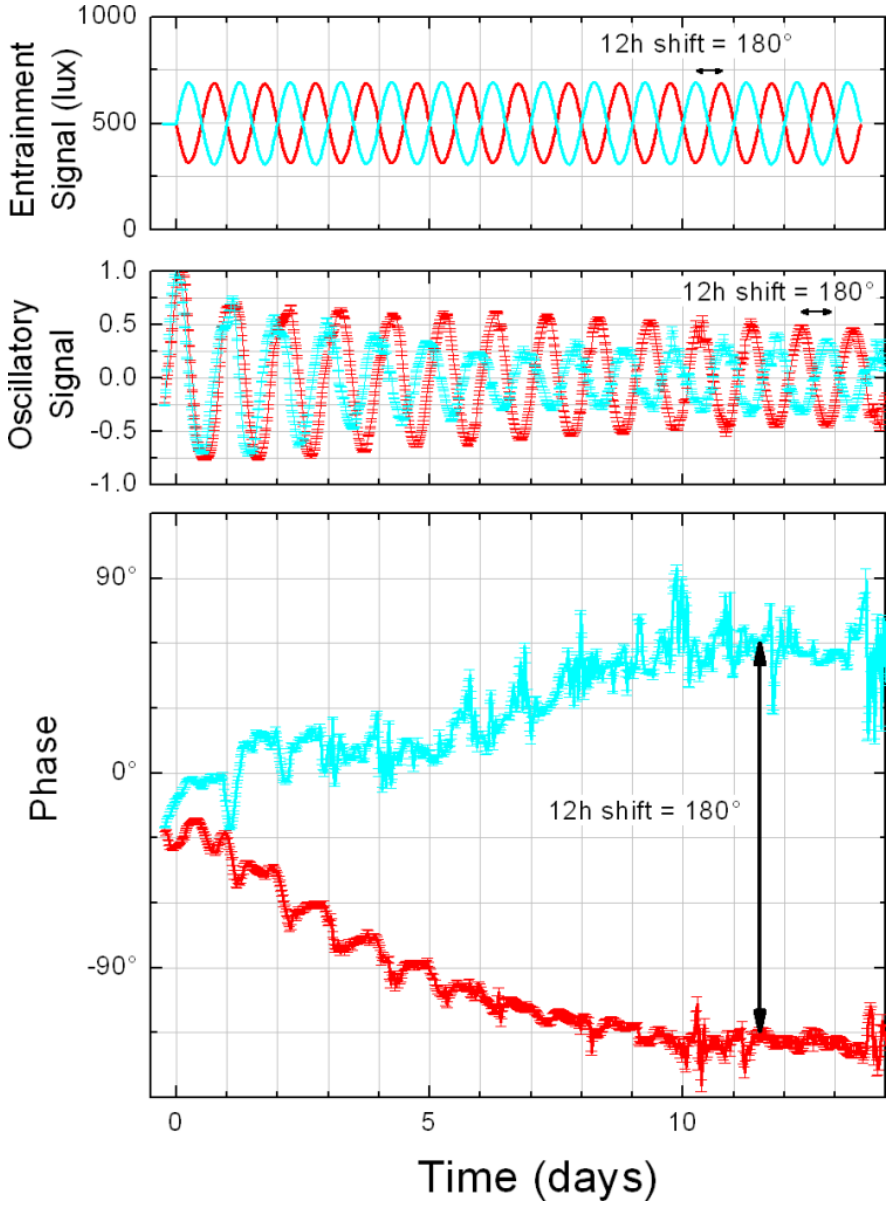

Figure 7.3: Entrainment by light perturbations. Here we show two different experimental conditions (middle) that are entrained to different phases by illumination perturbations (top) of identical amplitude. Both illumination patterns oscillate around 500 lux with a relative amplitude of 0.4. Their phases are shifted by 12h or $180°$. (bottom) The instantaneous phase extracted from the bioluminescence signal of bacteria under influence of these illumination signals are shown in the lower graph. They possess a common origin and separate to a stable phase shift of $180°$ under influence of the external perturbation.

of the perturbation and its ability to entrain the circadian clock of the cyanobacteria is obvious. While in the left condition the final stable phases are reached within ~ 3 days, the bacteria in the middle condition take much more time and those in the right condition are not entrained (pseudo-entrainment). A side effect of the better entrainment is also, that the fluctuations of the phase become more important. There are two main reasons for this. First the circadian clock is not necessarily sinusoidal, it thus appears to fluctuate in a rotating reference frame. The better a population is synchronised, the clearer these fluctuations become. The second effect is related to the bioluminescence reporter and its correction. The correction of the bioluminescence signal is more complicated for low illumination, which occurs mainly for large relative entrainment amplitudes.

7.2.4 Synchronisation

In our experiments we observe synchronisation over a wide range of illumination amplitudes, ranging from 0.2 to 1.0 of the common mean illumination of 500 lux. All of these experiments lead to phase locking of the circadian clock, but the amount of time needed to reach these stable phases varies from few periods up to over 2 weeks. Generally speaking, synchronisation can occur when the zeitgeber can force the circadian clock to its own frequency. This means that the entrainment force needs to overcome the difference between the proper frequencies of the zeitgeber and the oscillator (the detuning ν). The bigger the coupling force is, compared to the detuning, the quicker it will entrain the circadian clock. The amount of time to reach the final phase depends also on the total phase shift the entrained oscillator has to overcome. Another effect of a stronger entrainment is that the entrained phases follow more closely the entrainment phase. All of these effects are demonstrated in fig. 7.5, where we compare an experiment under weak external perturbation with an experiment that was under strong external influence. The phases of the zeitgeber signal are identical for both experiments. One sees clearly the different amount of time entrainment to the different phases can take in a single experiment. But they generally are quicker in attaining their final phase in the experiment entrained by larger light oscillations (left).

The last effect, the different final phases of the entrained oscillator, despite being entrained by identical entrainment phases, can be explained via the strength of the coupling force. As an illustration, we can imagine the coupling force to be like a spring that connects the oscillator with the entrainment (fig. 7.5 schema on the right hand side). The strength of the coupling will be given by the stiffness of the spring. An oscillator that is entrained via a weak coupling force will have a

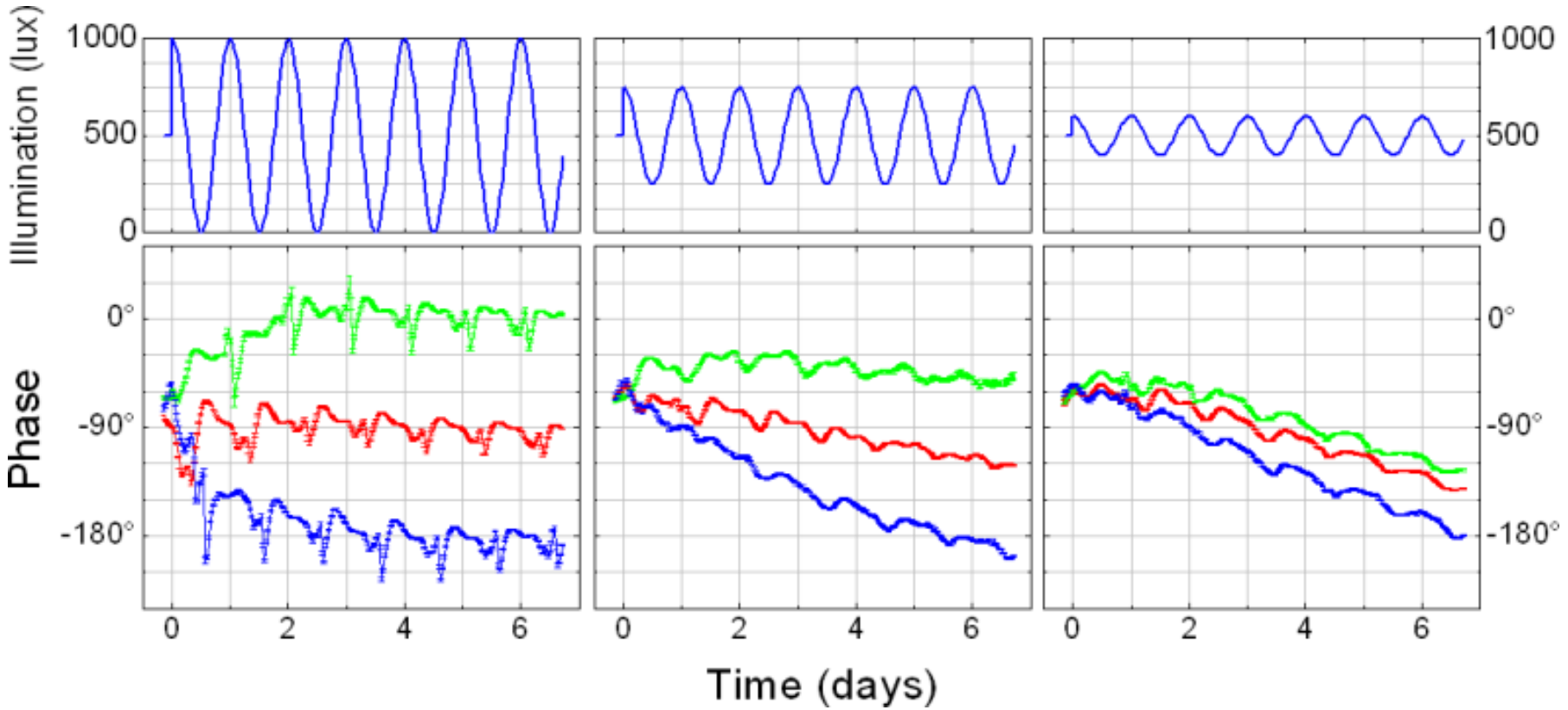

Figure 7.4: Perturbations of different relative amplitude. These graphs show a set of parallel experiments that were done with the same population. Just before the detection start, the population was split up and the different subpopulations were entrained to different phases using perturbations of 3 different relative amplitudes (1.0, 0.5 and 0.2 of the common mean 500 lux). The bigger the relative amplitude of the perturbation is, the better it entrains the circadian clock of the bacteria. The perturbation with 1.0 relative amplitude (left) quickly entrains the bacteria in 3 oscillations or days, while the 0.5 perturbation (center) hasn't fully entrained the bacteria after 6-7 days. The weakest perturbation here with 0.2 relative amplitude (right) does not succeed in entraining the clock, we see here a case of pseudo-entrainment. The phases separate only slightly from each other and keep essentially their own frequency. The fluctuations of the extracted phase become also more important with increasing relative amplitude of the entrainment signal. There are two main reasons for this. First, the circadian clock is not necessarily sinusoidal, and the better a population is synchronised, the clearer these fluctuations become. Second, the correction of the bioluminescence signal is more complicated for low illumination, which occurs mainly for large relative entrainment amplitudes.

large lag behind the entrainment phase. The stronger the coupling force becomes the closer the oscillator will follow the phase of the entrainment.

The circadian clock reacts very precisely to external perturbations. Phases entrained to phase differences of only 30° (which corresponds to 2h) are clearly distinguishable. Figure 7.6 shows an example where the perturbation amplitude was 0.8, centered around 500 lux.

7.2.5 Pseudo-entrainment

In cases when the detuning exceeds the coupling force we observe pseudo-entrainment. This means that the perturbation still has an effect on the circadian clock and its phase, but the proper frequency remains the dominant parameter of the equation. Cases of pseudo-entrainment are easily recognisable as all different phases show a common behaviour governed by their common proper frequency. The faster rotating system (entrainment or oscillator) will thus periodically overtake the slower one. In the rotating frame of the perturbation this leads to alternate periods of slow and fast decreasing phases (fig. 2.5b). They mark the periods when the entrainment force holds back or accelerates the oscillator. In function of the entrainment phase, the switch points are time shifted to each other. The period of one of these cycles is called the beat frequency. It depends on the strength of the coupling force and the detuning between the entrainment and the oscillator. Figure 7.7 shows two different experiments with pseudo-entrainment. The left panel shows an experiment with 4 different perturbation phases, one every 90°. The beat frequency is plotted as thick dark blue. The right panel shows a similar experiment, but this time with perturbation phases shifted by only 30°. Again we see how the different pseudo-entrained phases oscillate around the common beat frequency, without attaining a stable phase.

7.2.6 Comparison of the entrainment efficiency of sinus shaped versus square shaped perturbation

During all our experiments we use sinusoid entrainment signals instead of the rectangular ones commonly applied. While both have been shown to successfully entrain the circadian clock of cyanobacteria, it remains to show whether the inclination of the slope plays a role and how the bacteria react to these different entrainment signals. Our illumination device allows us to apply all kind of signals, so we set up an experiment with different inclinations as well as some clusters, that slowly vary the inclination from pure rectangular to pure sinus over a course

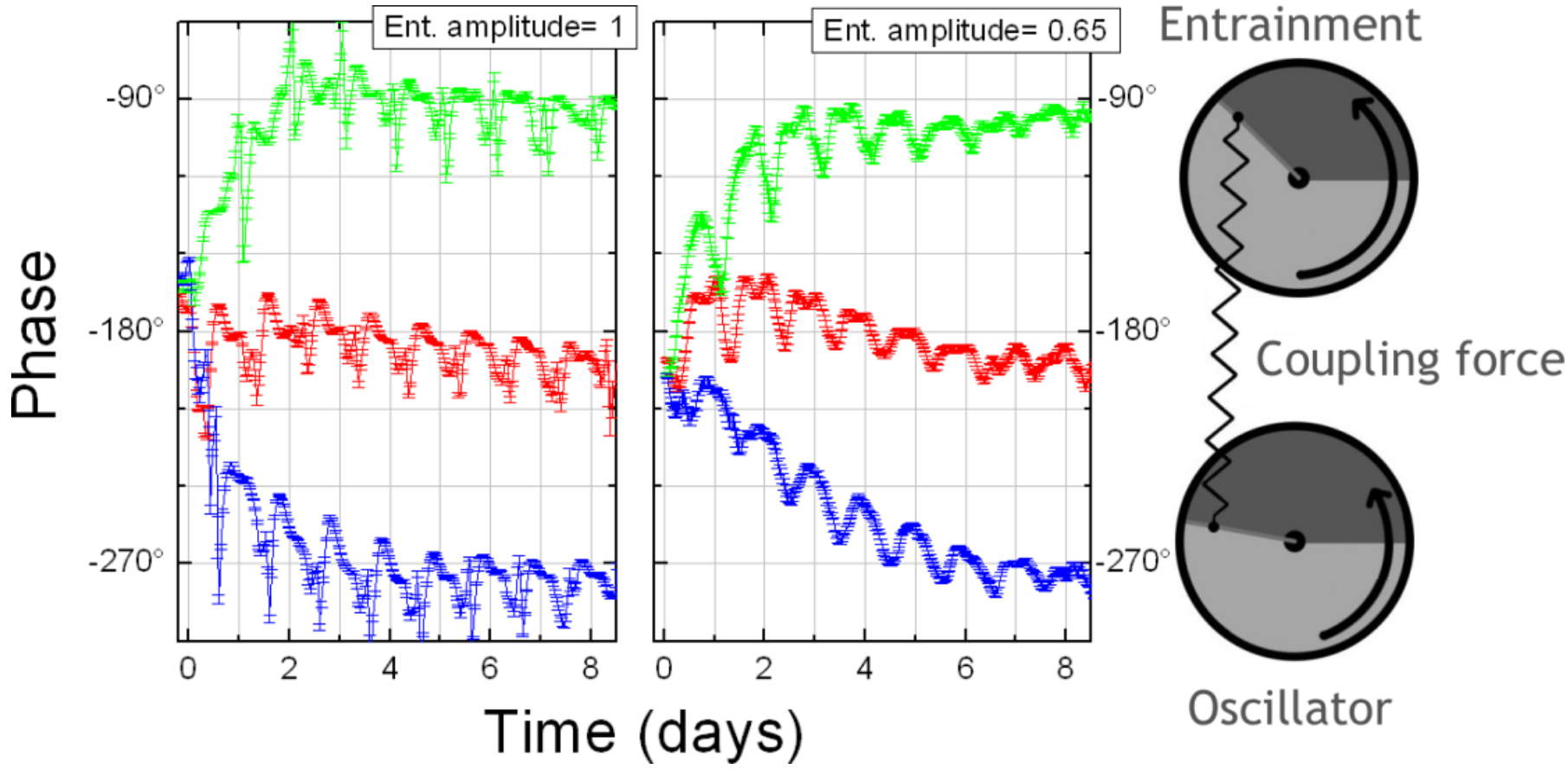

Figure 7.5: Two examples for entrained phases of different relative perturbation amplitude (left: 1.0, right: 0.65, both centered around 500 lux) and initial phase of the bacteria. Note that the phases take different time to reach the final state and that those entrained by a weaker coupling force (center) take longer and are consistently lower than those entrained by a stronger coupling force (left). The entrainment phases are identical, but due to the difference in coupling force the phase of circadian clock follows the external phase more or less closely. It is sligtly closer when the coupling is stronger. (right) Schema of how the coupling force acts on the oscillator. The weaker it gets, the bigger the phase shift between the entrainment and the final phase becomes.

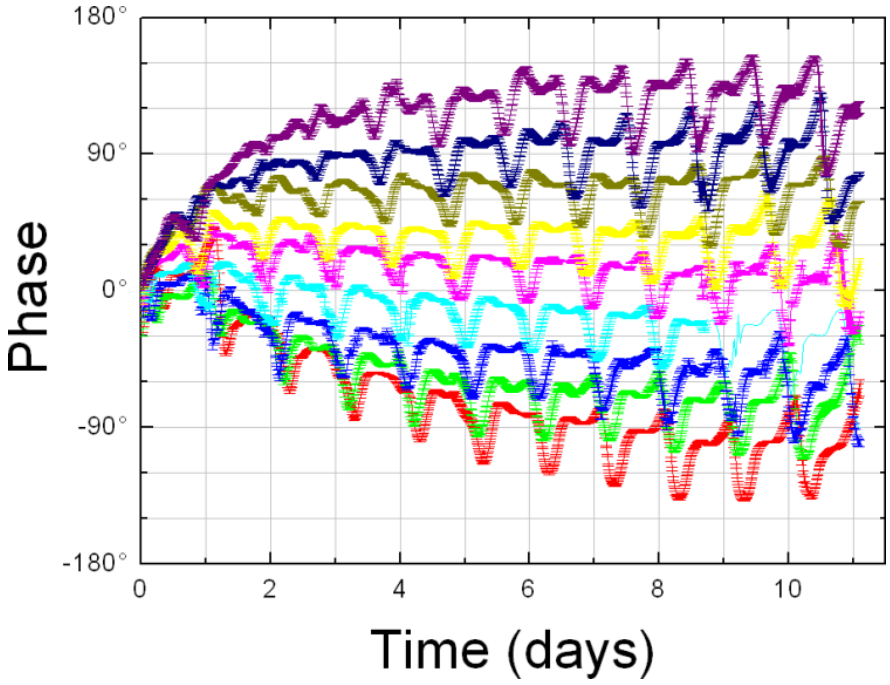

Figure 7.6: Example of entrained phases entrained to phase shifts of 30°. The perturbation amplitude was 0.8 centered around 500 lux.

of 10 days. This was done both for an 0.8 entrainment to be sure to successfully entrain and see the effects, and a 0.5 entrainment (see 7.8) to see the more subtle details, and escape possible detection problems during the zeitgeber night (see 4.3.3). During a period of 15 days, the phases showed very similar behaviour, regardless of the shape of the signal for a given amplitude and mean illumination. A small lag of bacteria exposed to the rectangular entrainment signal (cyan line) in the 0.5 entrainment amplitude experiment could be a sign that the bacteria entrain slightly better with gradual intensity changes at dusk and dawn. In our case, the speed of the illumination variation between night-day and day-night does not seem to play an important role.

7.3 Temperature periodic forcing

To evaluate whether the entrainment behaviour of the cyanobacterial circadian clock depends on the zeitgeber cue or is a genuine reaction, we used a similar experimental setup and replaced the illumination perturbations by temperature perturbations. As our set-up does not allow to control the temperature of each single well, independently the experiments with temperature as zeitgeber (Fig. 7.9) are therefore different than the ones with light entrainment. The temperature forcing we apply is not limited to a single experimental condition, but

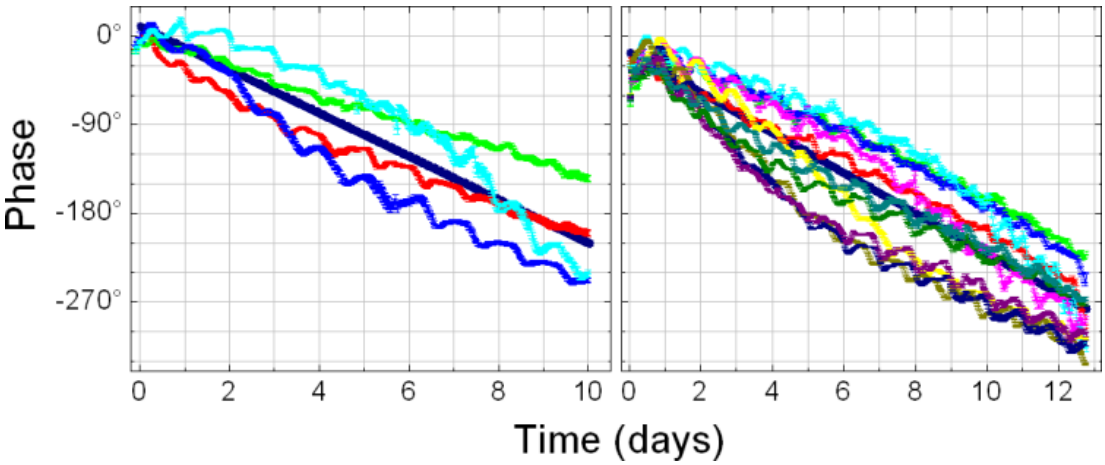

Figure 7.7: Two examples for pseudo-entrained phases of different relative perturbation amplitude (left: 0.4, right: 0.5) and initial phase of the bacteria. The approximate beat frequency depends on the coupling strength and the detuning. It is plotted as thick dark blue graph below the measured phases. The phases continuously oscillate around this beat frequency without developing a stable phase shift with the entrainment phase. (left) an experiment with only 4 perturbation phases, one every 90°. (right) an experiment with perturbation phases every 30°. In both cases we see how the different pseudo-entrained phases oscillate around the common beat frequency, without attaining a stable phase.

acts on all conditions at once. To still use the capacity for parallelisation of our experimental set-up, we use a strong illumination forcing to create populations with separated initial phases ψ_0^{lum} before putting them under influence of the temperature forcing. This approach offers the same qualities of redundancy (16 independent populations per experimental condition) and exploration of the phase space (12 different initial phases per experiment) as the experiments with illumination forcing. It does however limit our possibilities to vary the amplitude and the period length of the temperature forcing, and we also cannot keep one condition as control under constant conditions. Instead, we measure the detuning during the illumination perturbation period.

When looking at the experimental phases, we can clearly distinguish between the three periods of the experiment (separation of the phases by illumination forcing, free-run for all clusters, reunification of the phases by temperature forcing). This shows, that the circadian clock is sensible to both forcing types and that our set-up posseses the necessary resolution to detect the different behaviour during those experiments. For our temperature experiments with a forcing period of 24h, the populations showed pseudo-entrainment like behaviour (see ch. 7.2.5). Figure 7.9 shows a set of conditions under LL illumination with different initial phases at t=0. After 2 days under constant temperature, the temperature oscilla-

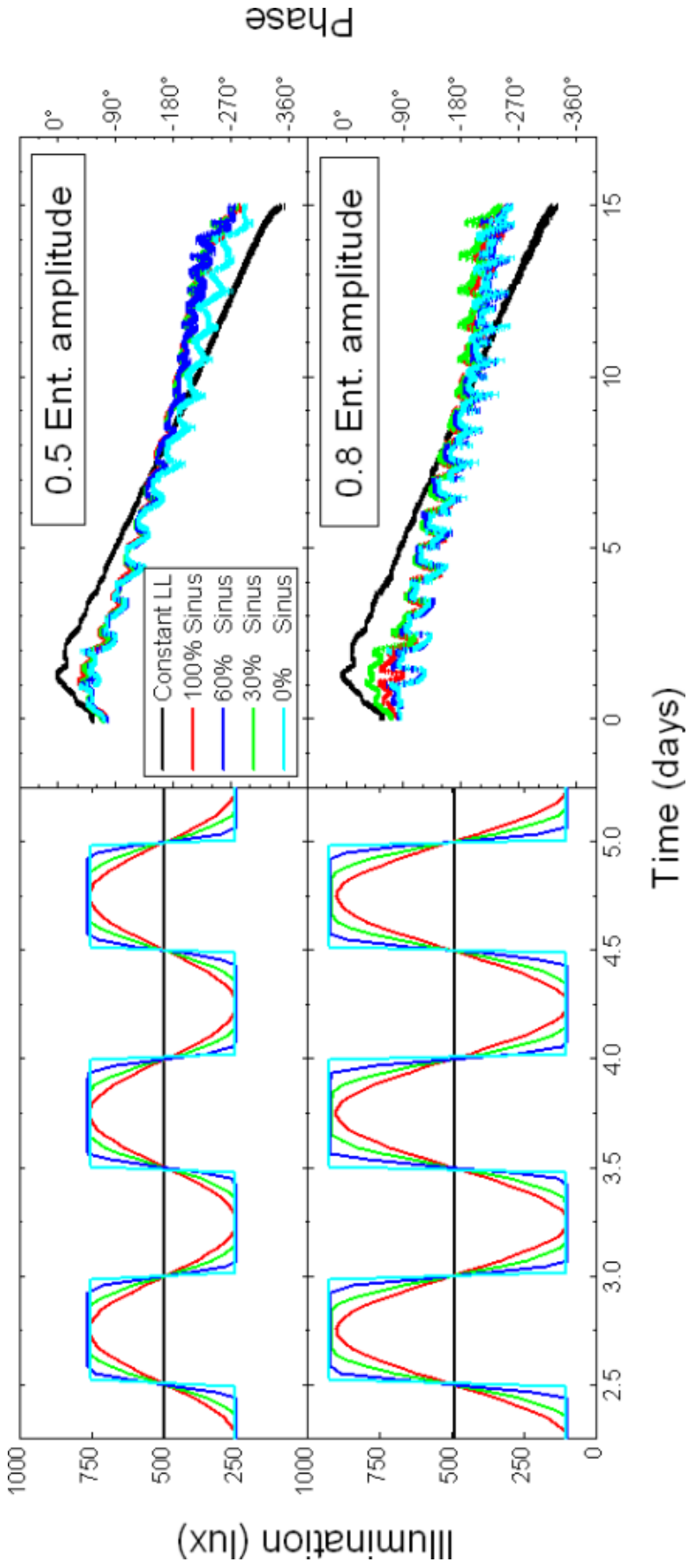

Figure 7.8: Illumination signal applies during the slopes experiment. In this experiment each plate is set to a certain entrainment amplitude to minimize cross-talking. (left) The applied entrainment. All clusters were entrained to the same phase by light oscillations with the same relative amplitude, but different shapes. (right) The corresponding phases in a rotating frame at 360°/24h. No big variation can be detected in both experiments, but the small lag of bacteria exposed to the rectangular entrainment signal (cyan line) in the 0.5 entrainment amplitude experiment could be sign that that the bacteria entrain slightly better with gradual intensity changes at dusk and dawn.

tion begin and we observe how the phases of the different experimental conditions unite under the influence of this common zeitgeber signal. A screenshot from the control program for a similar experiment is shown in figure 3.14.

This shows that the behaviour of the bacteria is generally comparable for temperature and illumination perturbations.

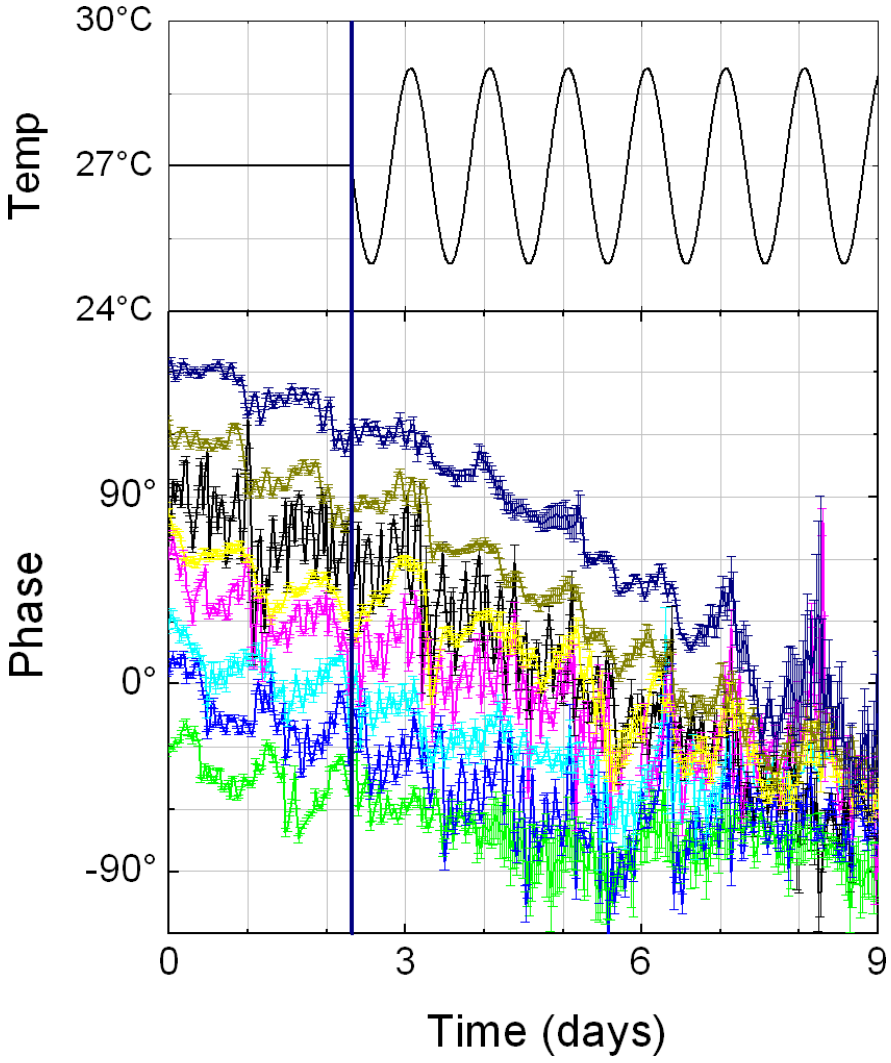

Figure 7.9: Entrainment with a temperature zeitgeber. (above): the temperature signal applied on all populations uniformly. (below): mean phase of 8 different clusters. They were initially entrained to different phases by illumination perturbations (not shown here), then kept under constant conditions for 2 days to measure the phase ψ and proper frequency ω_0 and finally submitted to the common temperature perturbations. The phases then show a pseudo-entrainment like behaviour (see ch. 7.2.5).

Chapter 8

Quantitative description

Our experiments were done using a homogeneous population of bacteria that underwent all the same pre-experimental treatment. To compare the experimental data with the Adler model, we first assume a homogeneous population of oscillators and include possible effects due to initial phase distribution inside the population later. For that we modify the Adler equation to take into account strain and reporter related parameters. Next we use this adapted model to fit the experimental data and get a first impression of the different parameters and dependencies between them.

8.1 Adler equation parameters

8.1.1 Entrainment vs strain and reporter related phase shifts

For the phase of the oscillator in the entrainment reference frame $\psi = \phi - \omega_e t$ we obtain (ch. 2.3.1.1) the Adler equation:

$$\frac{\mathrm{d}\psi}{\mathrm{d}t} = -\nu - \varepsilon \sin(\psi).$$

It predicts a certain phase shift between the entrainment and the entrained oscillator when phase locking is reached ($\frac{\mathrm{d}\psi}{\mathrm{d}t} = 0$):

$$\psi|_{t\to\infty} = -\arcsin\left(\frac{\nu}{\varepsilon}\right).$$

This describes the final phase shift between the entrainment and the circadian clock itself. To include the reporter dependent phase shifts described in chapter 7.1, we group these effects into a new variable α. This shift α is at first considered independent of ω_0 or the amplitude of the forcing. Therefore our mesurable

variable is

$$\psi^{lum} = \psi + \alpha = \phi - \omega_e t + \alpha$$

and the corresponding Adler equation becomes:

$$\frac{\mathrm{d}\psi^{lum}}{\mathrm{d}t} = -\nu - \varepsilon \sin\left(\psi^{lum} - \alpha\right) \tag{8.1}$$

At steady-state the phase shift between the reporter and the entrainment will be the combined effects of $-\arcsin\left(\frac{\nu}{\varepsilon}\right)$ and α (fig. 8.1 top):

$$\psi^{lum}\big|_{t\to\infty} = -\arcsin\left(\frac{\nu}{\varepsilon}\right) + \alpha$$

The combined effect of $-\arcsin\left(\frac{\nu}{\varepsilon}\right)$ and α is large in our case as is shown in figure 8.1 bottom where the entrainment signal (blue) and the circadian oscillation stabilise at almost opposite phases.

8.1.2 Entrainment to different phases

As we observe the circadian clock only indirectly, we compensate for the uncertainty we have on the parameters by entraining bacteria from the same initial population to different phases with the same forcing strength. This allows us to have several independent measurements of common parameters.

The entrainment phase will therefore be:

$$\theta_e(t) = \theta_{e_0} + \omega_e t$$

and with $\psi^{lum} = \phi - \omega_e t + \alpha$ the Adler equation (eq. 8.1) becomes:

$$\begin{aligned} \frac{d\psi^{lum}}{dt} &= \underbrace{\omega_0 - \omega_e}_{-\nu} - \varepsilon \sin\left(\psi^{lum} + \omega_e t - \alpha - \theta_{e_0} - \omega_e t\right) \\ \Longrightarrow \frac{d\psi^{lum}}{dt} &= -\nu - \varepsilon \sin\left(\psi^{lum} - \alpha - \theta_{e_0}\right) \end{aligned} \tag{8.2}$$

This equation describes the evolution of the phase difference ψ^{lum} between the phase of the oscillator and its respective entrainment phase θ_{e_0}. The whole set of entrainment phases is shifted by the bioluminescence reporter shift α, while its dynamics depends on the detuning $\nu = \omega_e - \omega_0$ between the frequency of the entrainment ω_e and the proper frequency of the oscillator ω_0, and the strength of the coupling force ε between them.

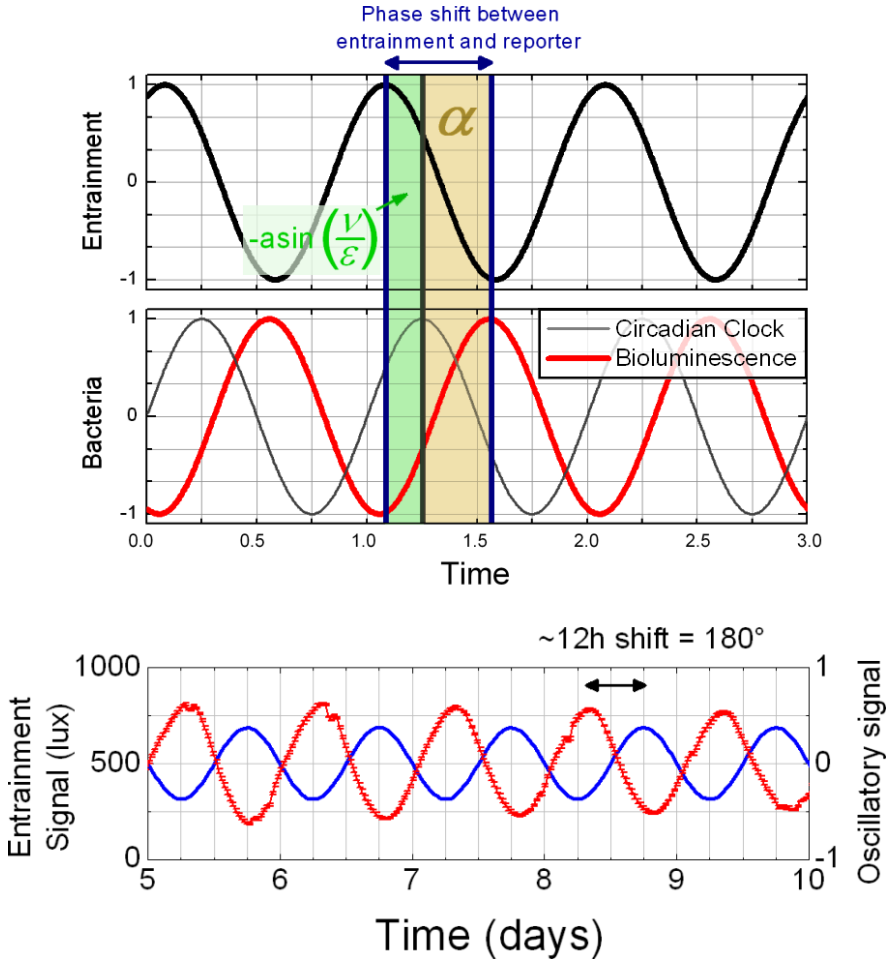

Figure 8.1: (bottom) When observing the circadian clock we observe a phase shift between the entrainment signal (blue) and the bioluminescence (red+error bars). This shift consists of two components. (top) First a phase lag between the entrainment and the circadian clock (grey oscillation) that depends of the ratio of the detuning ν over the coupling constant ε ($\psi|_{t\to\infty} = -\arcsin\left(\frac{\nu}{\varepsilon}\right)$, eq. 2.14) and second the reporter shift α discussed in chapter 7.1 and figure 7.1.

For a set of experimental conditions all parameters except θ_{e_0} are the same. We will take this into account during the fit by sharing these parameters between the different conditions.

8.1.3 Fit function

The initial fits are done under the assumption that we observe a homogeneous population of oscillators. We use the analytical solution of eq. 8.2 to fit the experimental data. These fits follow the mean instantaneous phase and allow to describe the behaviour of most entrainment conditions very well.

Since the value under the square root has to remain positive we distinguish

between two cases, first for $\varepsilon > \nu$:

$$\tan\left(\frac{\psi^{lum} - \psi_0^{lum}}{2}\right) = \begin{cases} \frac{[\varepsilon\sin(\Delta\theta) - \nu]\cdot\tanh\frac{\Omega t}{2}}{\Omega + \varepsilon\cos(\Delta\theta)\cdot\tanh\frac{\Omega t}{2}} & , \varepsilon > \nu \\ \frac{[\sin(\Delta\theta) - 1]\cdot\varepsilon t}{2 + \varepsilon t\cos(\Delta\theta)} & , \varepsilon = \nu \\ \frac{[\varepsilon\sin(\Delta\theta) - \nu]\cdot\tan\frac{\Omega_b t}{2}}{\Omega_b + \varepsilon\cos(\Delta\theta)\cdot\tan\frac{\Omega_b t}{2}} & , \varepsilon < \nu \end{cases} \tag{8.3}$$

where:

$$\begin{aligned} \Delta\theta &= \alpha + \theta_{e_0} - \psi_0^{lum} \\ \Omega &= \sqrt{\varepsilon^2 - \nu^2} \\ \Omega_b &= \sqrt{\nu^2 - \varepsilon^2} \end{aligned}$$

8.2 Homogeneous population of oscillators

In this section we discuss the results obtained from fitting the experiment results with the modified Adler model described in the section above. We focus here on the main fit parameter, the coupling constant ε and its relation with the detuning ν and the reporter shift α. Fig. 8.2 shows by the example of a single entrainment phase how the fit extracts these parameters from the measured data.

With the exception of the entrainment phase θ_{e_0} which is set in advance by the applied illumination, ψ_0^{lum} and ν are shared between several experimental conditions, entrained or not, including the LL condition. For the shift α we constrain it to be the same for a given amplitude of entrainment, but let it free for a different entrainment force.

8.2.1 Shared fit parameters

Our experimental set-up allows us to apply 12 different illumination patterns simultaneously (ch. 3.5.1). To keep an independent control of ν we kept one condition under constant illumination and used the other 11 possible conditions to either entrain bacteria to 11 different phases by the same periodic illumination forcing (eg. fig. 7.6 and fig. 7.7 right graph) or to apply different forcing strength by reducing to fewer different phases. This allows to apply 3 types different illumination amplitudes at a time. For example, we applied oscillations 0.4, 0.65 and 0.8 of the common mean illumination 500 lux. Both the 0.4 and the 0.65 sets had 4 different entrainment phases (0°, 90°, 270° and 180°) while the 0.8 set had only 3 (0°, 90° and 270°) to keep the last condition for the continuous control. A

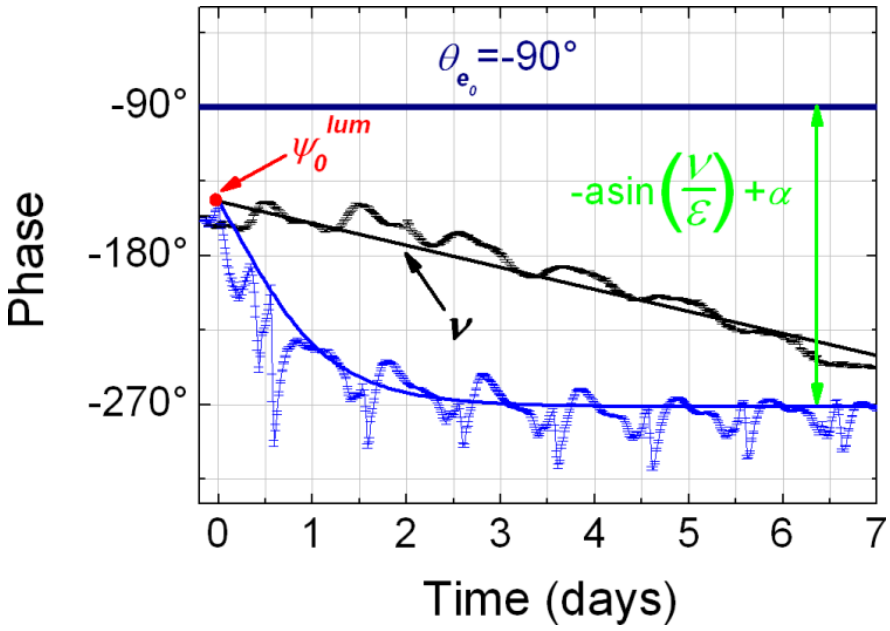

Figure 8.2: This figure illustrates how the fit extracts the different fit parameters from the measured data. The entrainment phase θ_{e_0} is set in advance by the applied illumination forcing. The detuning ν can be directly measured by keeping one experimental condition under continuous environment (LL). The initial phase of the population ψ_0^{lum} is the common starting point of all conditions. The coupling constant ε is the main adjustable parameter which describes the strength of the external forcing.

selection of light entrainment experiments with different illumination amplitudes is shown in figure 8.3.

For experiments with different forcing amplitudes we shared the detuning ν and the initial phase of the population ψ_0^{lum} between all 12 conditions, while the bioluminescence reporter lag α and the coupling constant ε were only common parameters inside a set with common forcing strength.

8.2.2 Fit results

The coupled fits describe the experimental data very well. Fits for different illumination forcing and detuning are shown in fig. 8.3. The illumination amplitudes used in this experiments ranges from 0.2 to 1.0 and the detuning ν from 5 to 25.3°/day. All fits were executed with the same fit function (eq. 8.3) by adjusting the different parameters. As discussed before, the experiments can be classified into two groups: one where the bacteria synchronise with the entrainment and their phases become horizontal in the rotating frame (see for example fig. 8.3 top right graph or the entire second line, ch. 8.2.2.1), and one with pseudo-entrainment when the external forcing is too weak to synchronise the bacteria (fig. 8.3 top left and lower right graphs, ch. 8.2.2.2). The fits show that the

Adler model describes well the phase evolution of the cyanobacterial circadian clock under external forcing whether synchronisation with the external forcing is reached or not. As can also be seen from the graphs, the illumination amplitude is not the only factor that decides between entrainment and pseudo-entrainment. Figure 8.3 shows the phases of two different experiments that were entrained by a 0.5 amplitude illumination forcing, while one (top center graph, 4 different entrainment phases and LL) is about to reach synchronisation while the other one (lower right graph, 11 different entrainment phases and LL) clearly is not about to reach it. The value of the detuning of case with the pseudo-entrainemnt 25.3°/day is almost twice the detuning of the entrained case with 13.3°/day.

8.2.2.1 Synchronisation

We observed synchronisation with illumination amplitudes ranging from 0.4 till 1 (fig. 8.3 all graphs except upper left and lower right graph). While the fits describe very well the behaviour of most synchronised populations, we regularly observe that one or two entrainment conditions undergo sudden phase jumps that can only partially be reproduced by the fits (fig. 8.3 second row: green phases; lower left graph: cyan phase; lower center graph: dark green and dark cyan phase on the the top and the bottom of the graph). This happens for conditions where the entrainment and the circadian clock are close to phase opposition. These phase jumps can be understood by keeping in mind that in fact we do not observe a single oscillator, but a population of independent oscillators where we measure the mean bioluminescence signal. These jumps can be explained by population effects where subpopulations take different routes along the limit cycle. It will discussed in more detail in chapter 8.3.

To avoid falsification of the entire fit by these phase jumps, we limit the fit range on these entrainment conditions to the data before the jump. This can be seen in fig. 8.3, the graph of the fit function does not cover the entire timeline of jumping conditions.

8.2.2.2 Pseudo-entrainment

Because the entrainment force ε is too weak to overcome the detuning ν between the clocks' proper frequency and the entrainment frequency, the circadian oscillator will alternate between periods when the entrainment holds back the clocks phase and periods when it advances it. This happens either for weak forcing amplitudes (fig. 8.3 upper left graph: entrainment amplitude=0.2) or strong detuning (fig. 8.3 lower right graph: $\nu = 25.3$). The switch from the advancing

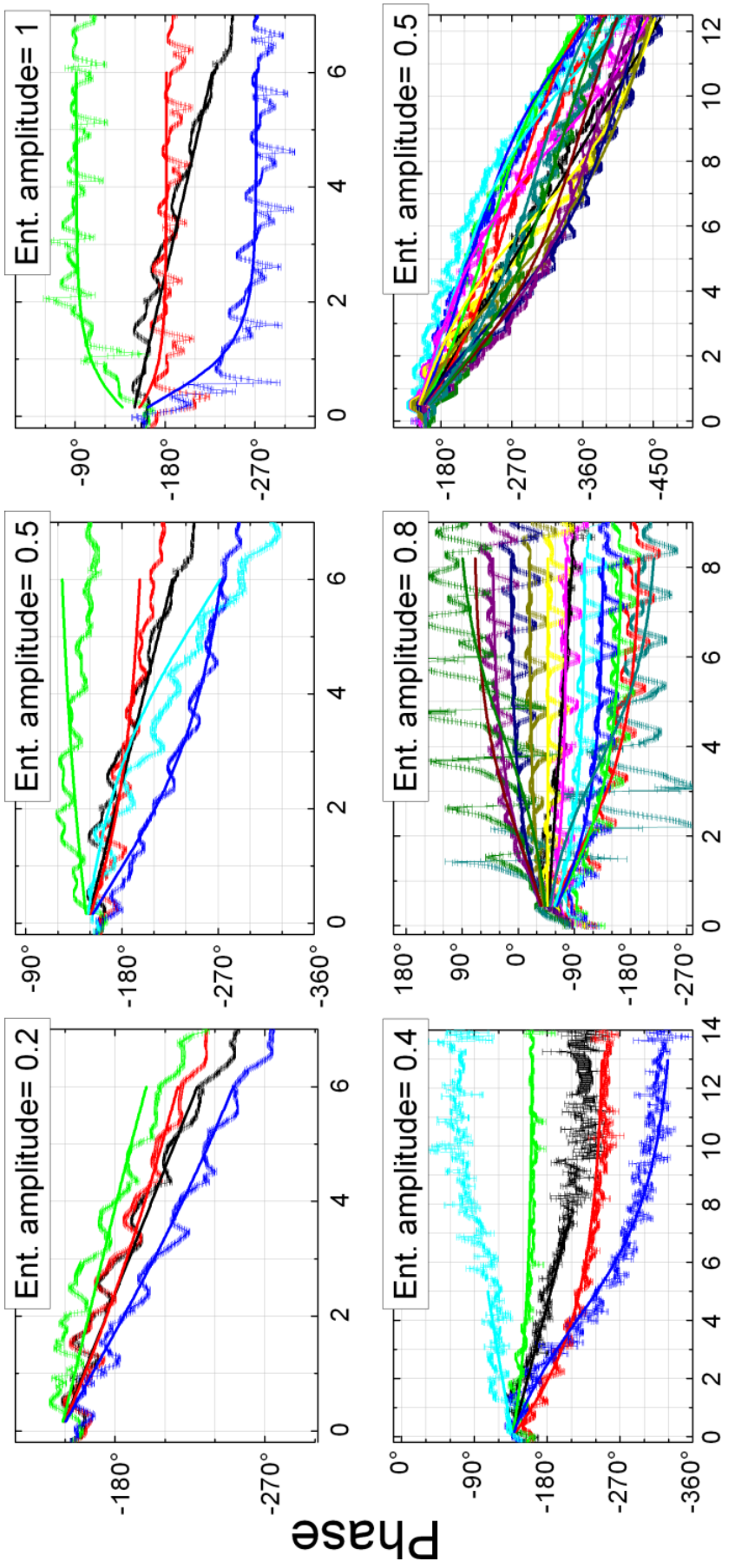

Figure 8.3: Fits of different illumination sets. The illumination amplitudes used in these experiments ranges from 0.2 till 1.0 and the detuning ν from 5 till 25.3 °/day. Experiments with pseudo-entrainment: upper left and lower right graphs, all other graphs show synchronisation using different amplitudes of illumination forcing. Except for the last two experiments all experiments used 3 or 4 different entrainment phases separated by 90°. The other two experiments had 11 different entrainment phases separated by 30°. All experiments have an LL condition (black) that allows to directly measure ν.

regime to the retarding regime occurs when the clock is in phase with the entrainment. The switch back occurs when they reach phase opposition to each other. All phases oscillate then around the so called beat frequency which is given by $|\Omega_b| = \sqrt{\nu^2 - \varepsilon^2}$. It describes the arythmetic mean of all phases and depends thus only on the entrainment force ε and the detuning ν. In our case $\nu > 0 \Rightarrow \Omega_b < 0$ so take $\Omega_b = -\sqrt{\nu^2 - \varepsilon^2}$.

8.2.2.3 Variation of ε

When looking at the values for the coupling constant ε in function of the applied illumination we find an exponential variation with values ranging from 5.3°/day for the 0.2 entrainment till 86.4°/day for the 1.0 entrainment. This is shown in figure 8.4. The values corresponding to experiments with pseudo-entrainment are shown as red squares, those from experiments with successful synchronisation are in black. At illumination amplitudes of 0.4 and 0.5 we find both types of experiments; in one case, at illumination amplitude=0.5, the ε-value of an experiment with pseudo-entrainment is bigger than one found under synchronisation. For this we have to keep in mind that the distinction between those regimes is not determined by the the ε-value alone, but also the detuning ν.

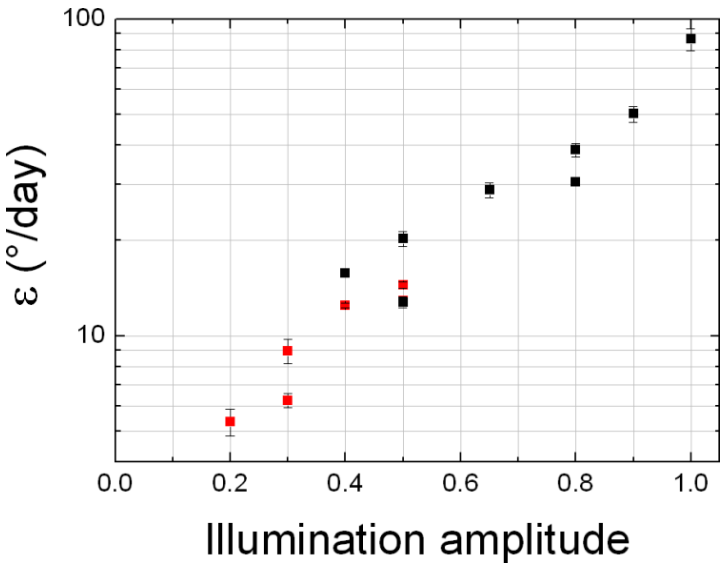

Figure 8.4: The values found for the coupling force ε in function of the relative amplitude of the periodic illumination forcing for synchronised conditions (black squares) and conditions with pseudo-entrainment (red squares). Examples for the fits are shown in fig. 8.3. ε clearly grows with increasing amplitude of the illumination forcing.

8.2.2.4 Experimental distribution of ψ_0^{lum}

We observe a distribution of initial phases although all cultures were entrained in the same incubator. What varied from on experiment to the other was the age of a culture and its optical density. There was no significant dependency between the optical density measured right before the experiment start and the detuning observed in the respective experiment, which shows that the light entrainment under constant steering reached all bacteria in a cell culture. Also the dilution, we do right before the experiment start to begin each experiment with an OD of 0.1, might induce PRC like patterned phase shifts. Figure 8.5 shows the initial phase of the bioluminescence reporter ψ_0^{lum} in function of different factors. Looking at it in function of the initial OD, the bacteria had before been diluted to an OD of 0.1 and put into the experiment show a general phase lag with increasing OD probably due to bacteria being less exposed to the day-night rhythm of the incubator (fig. 8.5a). In function of the dilution time, we find the possible beginning of a PRC-like behaviour, but do not have enough datapoints to give a final answer to that question (fig. 8.5b). There does not seem to be a easy relationship with the detuning ν, as we observe large variations of ψ_0^{lum} for small variations of ν (fig. 8.5c).

8.2.2.5 Experimental distribution of α

As the bioluminescence shift α (fig. 8.1) has an important influence on what we measure, we show here how it depends on several experimental parameters. First in function of the OD of the bacteria in the incubator, measured just before diluting them to an OD of 0.1 for the experiment (fig. 8.6a). It shows an increase of α with increasing preexperimental OD that is of the similar range as the variation of ψ_0^{lum} (fig. 8.5a). On the other hand, α is not sensitive to the dilution time (fig. 8.6b), the detuning during the experiment (fig. 8.6c), the initial amplitude(fig. 8.6d) and the coupling constant ε (fig. 8.6e)

8.2.2.6 Fit of the temperature forcing experiments

To fit these experiments we use the same model and equations as before, just that all conditions begin their evolution at different points and get entrained by the same driving force. This means that the initial phase $\psi_{0,i}^{lum}$ becomes an individual parameter for each experimental condition and the zeitgeber phase θ_{e_0} of the temperature forcing is a common parameter for all. We also extended the approach with the shared variables to fit at once the 12 experimental conditions

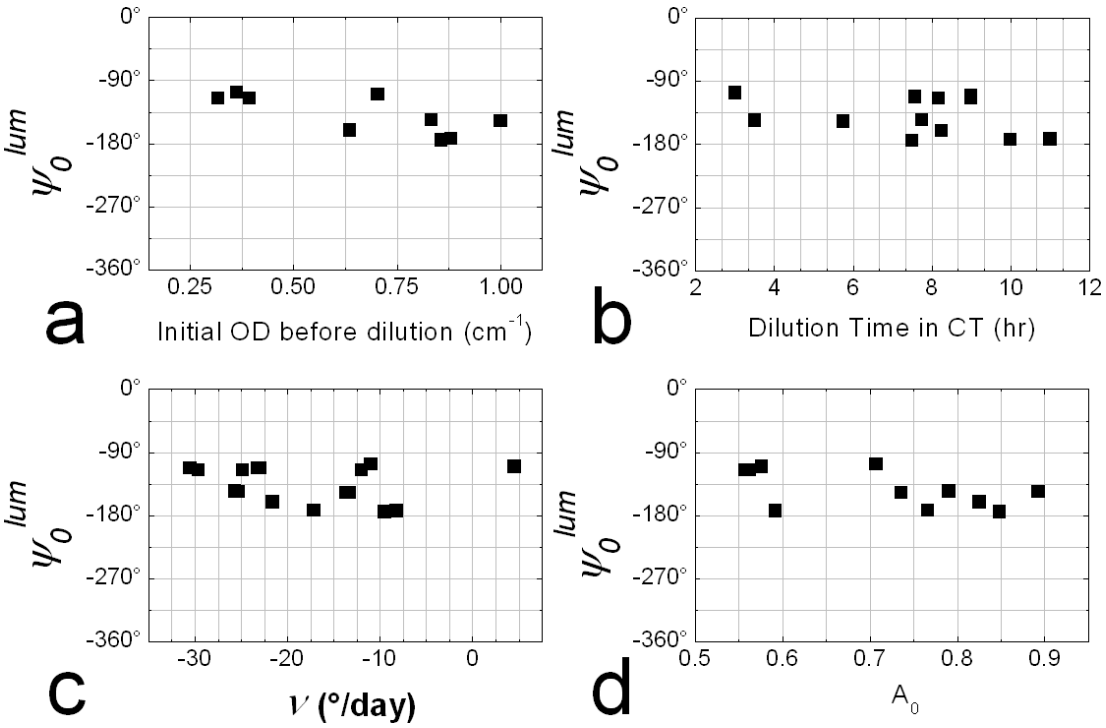

Figure 8.5: The initial mean phase in function of several pre-experimental parameters. (a) In function of the OD of the culture right before the dilution. (b) In function of the dilution time in CT before being platted and put into the experiment. There might be PRC-like behaviour due to the dilution process. But since most of our experiments were done with similar dilution times this does not affect the results much. (c) In function of the detuning ν. (d) In function of the initial amplitude. This shows that there is no significant correlation between a possible random perturbation of the population due to the dilution and the measured initial mean phase. The observed variability must be due to other non, or at least, less reproducible factors, like age of the population since defreezing, possible contamination or temperature shocks during the experiment preparation.

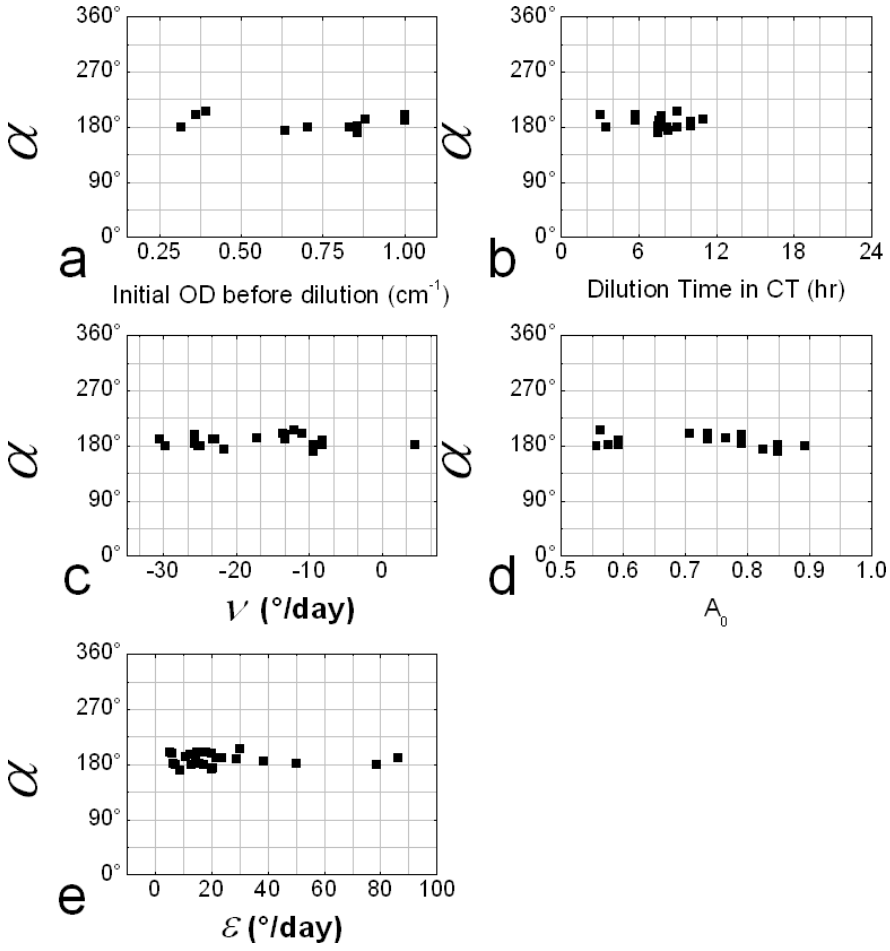

Figure 8.6: The bioluminescence shift α in function of several experimental parameters. (a) In function of the OD of the culture right before the dilution. (b) In function of the dilution time in CT before being platted and put into the experiment. (c) In function of the detuning ν. (d) In function of the initial amplitude. (e) In function of the coupling constant ε.

in the periods under constant conditions and under temperature forcing. The fit function consists of two parts: first a linear function to fit the phase evolution under constant conditions, and second the Adler equation to fit the phase evolution under temperature forcing. The fit ranges are set in a way that the final point of the linear fit acts also as initial phase value for the Adler equation. The detuning ν is a shared parameter for the 2 functions. This allows to have a good precision for the detuning and the initial phases $\psi_{0,i}^{lum}$ of the 11 entrainment condition.

The fit confirms the first impression that we observe phase evolution under pseudo-entrainment (fig. 8.7). The coupling constant ε_{temp} for temperature entrainment was 7.9°/day and the detuning ν=13.7°/day, which results in a beat frequency of $\Omega_b = -11.2°$/day. This confirms that the applied temperature forcing was not strong enough to overcome the detuning. But this result nevertheless demonstrates the validity of the Adler model for this type of zeitgeber. The inset shows the initial phases $\psi_{0_i}^{lum}$ of the 11 entrained phases in function of the applied entrainment phase θ_{e_0}. We find a very good reproducibility for all clusters, shifted by bioluminescence shift $\alpha = 150°$ here. In general bioluminescence shift of the temperature entrainment has similar values and distribution as for the illumination entrainment.

8.3 Population of oscillators with distribution of initial phases

To better understand the phenomena of the jumping phases, we first need to look closer at the instantaneous amplitude $A(t)$ we measure during the experiment. Sudden jumps of the instantaneous phase are generally accompagnied by low values of the instantaneous amplitude (fig. 8.8).

The experimental amplitude $A(t)$ consists essentially of two components $A(t) = b\rho$ (see ch. 5.1), where $b\epsilon[0,1]$ is the relative amplitude of the P_{KaiBC} reporter oscillation and ρ the order parameter of the population. Even after the strong entrainment in the incubator, the bacteria inside a population are not perfectly synchronised, which is represented by a $\rho_0 < 1$ ([6, 5]). Since there is no intercellular coupling[1], the external forcing acts as single zeitgeber on each oscillator in function of its individual phase difference $\psi_i - \theta_{e_0} = \phi_i - \omega_e t - \theta_{e_0}$. For small phase shifts, each oscillator will take the same way in the phase space. This can be seen in figure 8.10 in the upper series of graphs. A group of oscillators,

[1]Prior experiments revealed no intercellular coupling for cyanobacteria. For more information see chapter 1.3.2.

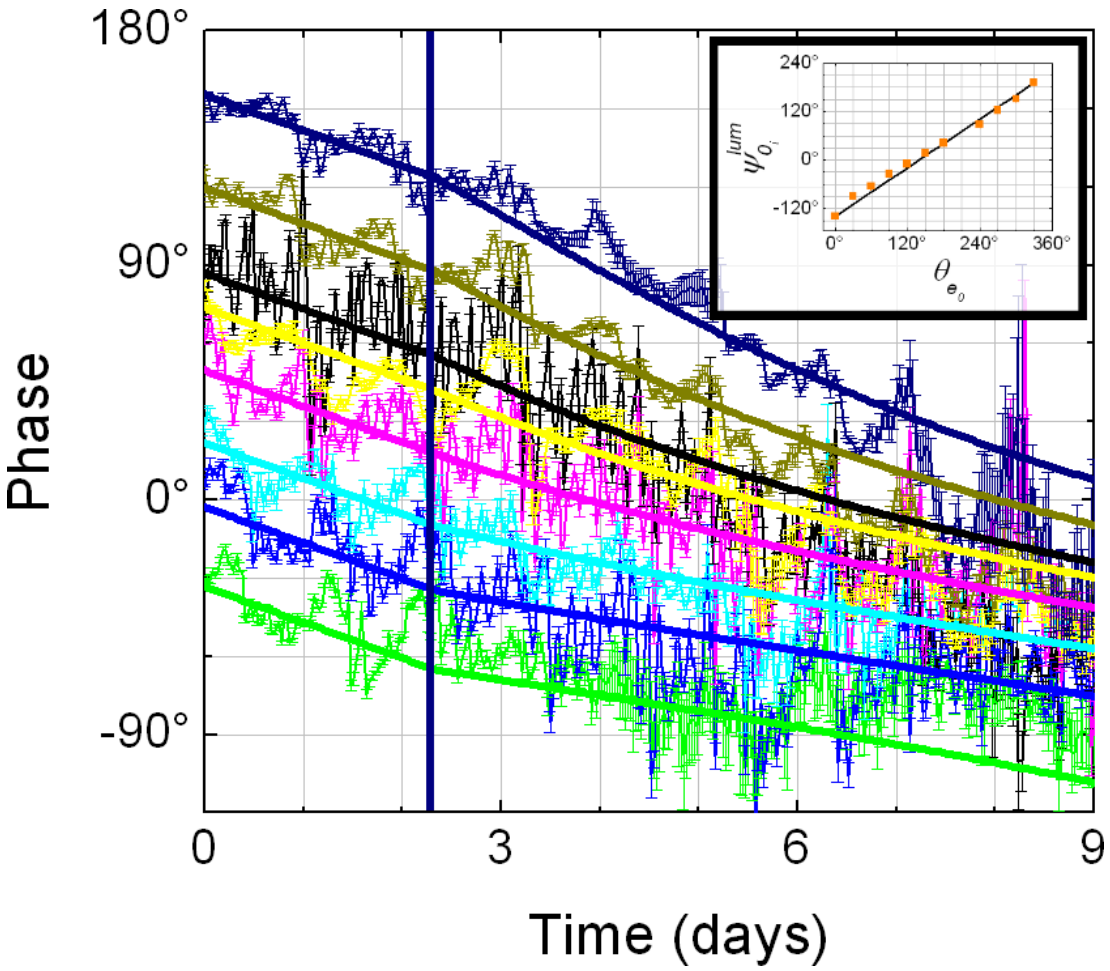

Figure 8.7: Pseudo-entrainment by a common temperature zeitgeber. The fit covers two regimes, a LL regime when all conditions are under constant conditions (left side) and the forcing regime when they unite under influence of the temperature forcing (right side). The inset shows the initial phases $\psi_{0_i}^{lum}$ of the different phases in function of the applied entrainment phase θ_{e_0}.

represented by their phase is entrained by a 90° phase shifted external force. As the shortest way along the phase circle is the same for all oscillator inside this population, the population stays together while undergoing the phase shift. For entrainment to the opposite phase and/or large distribution of initial phases inside a population, it can happen that two subpopulations are formed that follow opposite ways on the phase circle before reuniting at their final stable phase. This is shown in figure 8.10 in the lower series of graphs. The same population as before is now entrained by a 180° phase shifted external force. Depending on their individual phase, the oscillator split up to take different ways along the phase circle. When observing the mean phase of the population this splitting up leads to jumps in the mean phase. This behaviour can be reproduced by simulation, see figure 8.11. It shows the behaviour of the mean phase $\langle\varphi\rangle$ of a population,

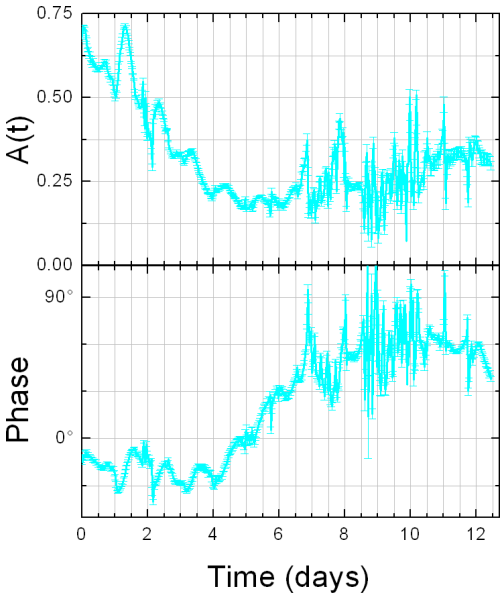

Figure 8.8: Correlation of a jump of the instantaneous phase (bottom) with low values of the instantaneous amplitude $A(t)$ (top). This is due to a separation of the different oscillators inside the population that take different ways along the limit cycle when entrained to opposite phases (see also fig. 8.10).

entrained to different phases (upper four panels), under constant conditions (LL, lower left panel) and compares this simulated mean phases with a real experiment (lower right panel). Mean phases where a large majority of oscillators take the same way along the limit cycle follow almost the same trajectory as the fits (fig. 8.3), while the condition with a separation (fig. 8.11, top left frame) initially does not seem to change its mean phase before suddenly undergoing a positive phase change. As we observe only the mean instantaneous phase of a population, we do not have the resolution to follow these subpopulations independently. As the phase of these subpopulations cancel each other when measuring the mean phase, this leads to the observation of sudden phase jumps, once the majority of the oscillators approach their final phase.

Since $b_0 \approx 1$ we can use the value of $A(0)$ as a measurement of the initial synchronisation ρ_0 inside the population. With this information we set up a simulation of a population of $N = 2000$ independent oscillators with the same initial phase distribution around ψ_0^{lum} as measured experimentaly. The width of this distribution is obtained from the instantaneous amplitude of the LL condition at $t = 0$. As the instantaneous amplitude fluctuates, this is done by linear fitting the first few days of the measured $A(t)$, as value for A_0 we use the value of this fit at $t = 0$ (see fig. 8.9). With this we can calculate the initial width of the phase distribution $\sigma = \sqrt{-2\ln(A_0)}$. When recreating the periodic forcing of the

experiment we also recreate very accurately the phase behaviour of the bacteria, including the phase jumps. We run this simulation for all our experiments to refine the parameters found by the initial fit. As this adds another parameter we adapt the other ones to fit the experimental results. The simulations corresponding to the fits shown in figure 8.3 are shown in figure 8.12.

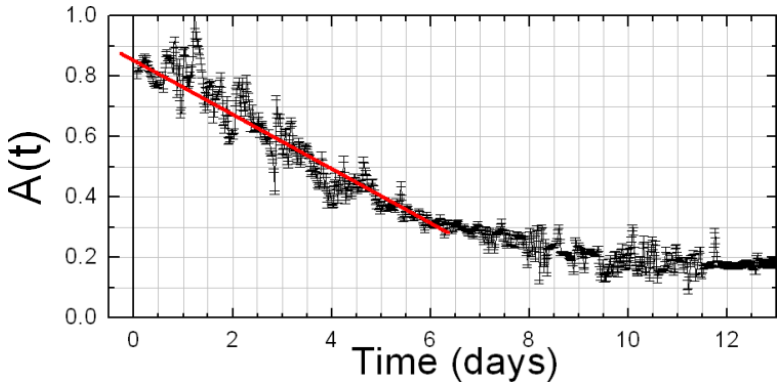

Figure 8.9: Determination of $\rho_0 \cong A(0)$ by linear fit of the instantaneous amplitude of the LL cluster.

8.4 Description by phase oscillator model

Both the light and temperature entrainment experiments are well fitted by the Adler model, which shows that the circadian clock of the cyanobacteria can indeed be seen as a phase oscillator. When we plot the coupling strength normalised by the proper frequency of the oscillator ω_0 vs. the relative amplitude of the light entrainment in the different experiments, we find a rough exponential dependency in the first approximation (fig. 8.13 left panel). To interpret this result we have to keep in mind that all tested entrainment was still within the weak coupling limit, and thus other dependencies are likely to arise when trying stronger coupling. Stronger coupling could be realized by combining different types of entrainment forces, for example a synchronized zeitgeber signal of both temperature and light entrainment.

If we plot the normalised coupling constant ε/ω_0 for each experiment vs. the normalised entrainment frequency ω_e/ω_0, we get an impression of the conditions under which the in vivo circadian clock of the cyanobacteria can be entrained (Fig. 8.13 right). The shape of this plot is called an Arnold tongue, which regroups the entraining conditions and separates them from those that fail to successfully entrain the system. The separation limit is given by the black line where $\varepsilon = \nu$, above this line the coupling force ε exceeds the detuning ν and the oscillator are

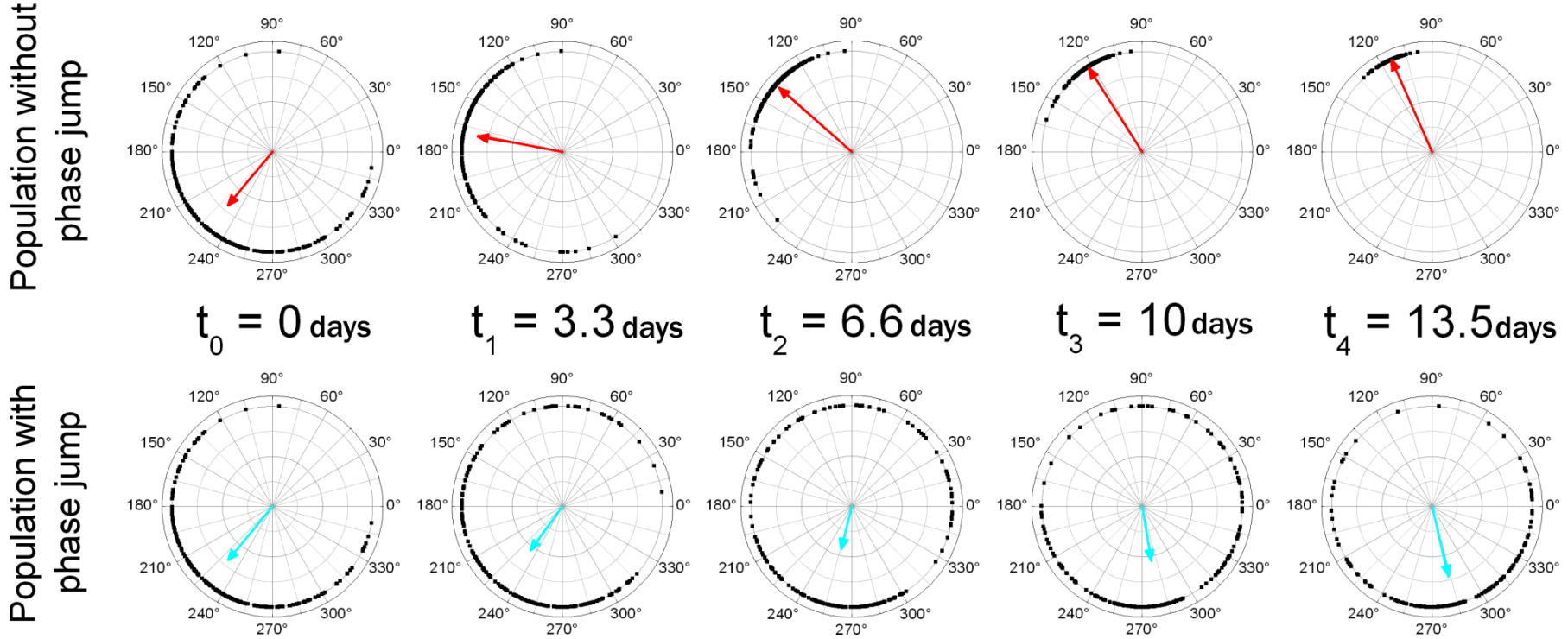

Figure 8.10: Mean phase, order parameter and origin of phase jumps. Snapshots of the evolution of a population of oscillators under external forcing at different moments. The entire phase evolution is shown in figure 8.11. The angle of the vector indicates the mean phase $\langle\varphi\rangle$ of the population, its length is given by the order paramter ρ which represents the level of synchronisation. Phase jumps occur when a population of oscillators with distributed phase splits up into two subpopulations that take different ways in the phase space to rejoin the phase of the entrainment force. (top) An example of a population without phase jump. The whole population follows the same way in the phase space. We observe a smooth evolution of the mean phase and the order parameter increases with the continuous synchronisation inside the population. (bottom) An example of a population that seems to undergo a phase jump. Each oscillator takes the shortest way in the phase space to reach the phase of the entrainment. This leeds to a population split. The mean phase varies slowly at the begining and then jumps rapidly. The order parameter initially decreases when the individual oscillators of the population spread over the phase space and regrows when more and more oscillators reach their final phase and resynchronise.

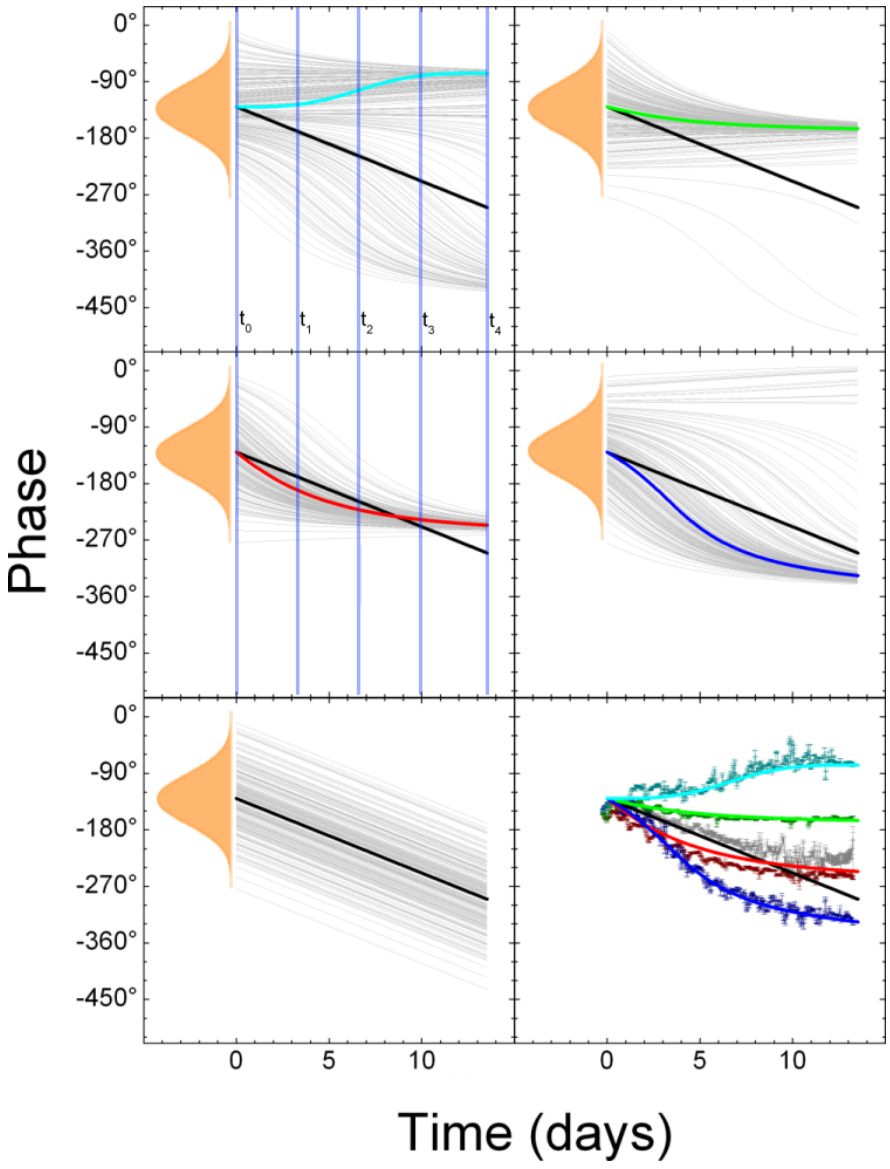

Figure 8.11: The effect of the initial phase distribution $\langle\varphi_0\rangle$ for entrainment to different phases. The blue lines in two of the panels mark the moments when the snapshots from figure 8.10 were taken (at $t_0 \ldots t_4$). (top & middle) Each graph shows 500 (out of the 2000) phases simulated for each condition. The large coloured line represents the mean phase of this 2000 oscillators while the large black line shows the detuning for this experiment the entrainment has to overcome. Oscillators taking different ways around the phase cycle are most commonly seen for entrainment to almost opposite phases ($\pm 120°$), but can also be observed on other phases though much less frequently. Entrainment to phases close to the initial phase (red, green) is much quicker than for phases with larger shifts (cyan, blue) as 13 days were not enough to fully synchronize the population with this parameters. (bottom left) The free run control. (bottom right) The 5 mean phases from the simulation plotted on top of the experimental data.

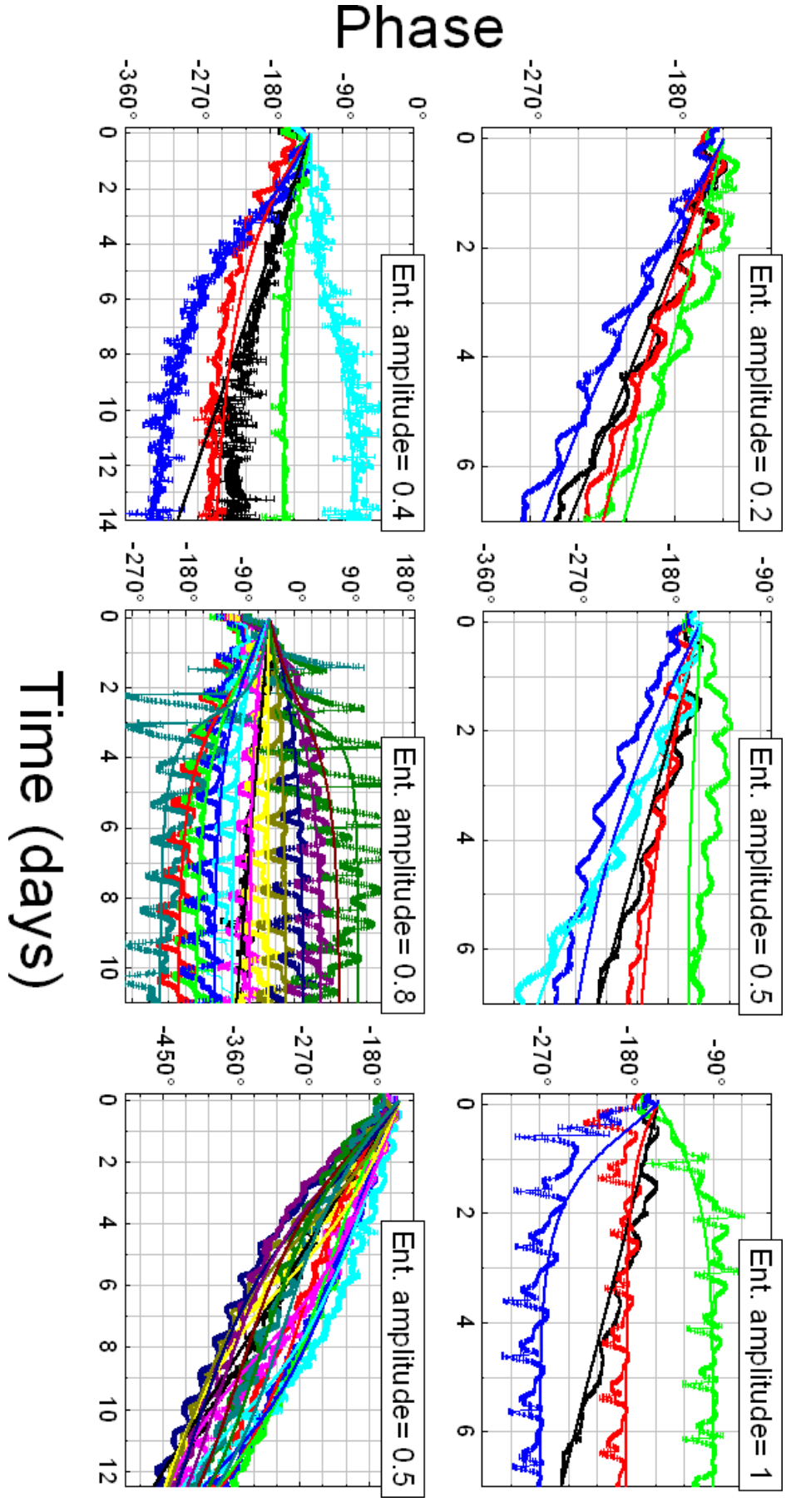

Figure 8.12: Simulations for the experiments shown in figure 8.3. The bold lines plotted on top of the experimental data represent the mean phase of a simulated population of 2000 independent oscillators with a distribution of initial phases.

thus entrained by the external force. Below this separation the coupling force is not sufficient to overcome the difference between the proper frequencies, and we observe pseudo-entrainment. The theoretical separation between entrained and unentrained conditions is reproduced by the experimental results.

Taking everything into consideration, these results demonstrate that the circadian clock of cyanobacteria can indeed be accurately described using the phase oscillator model and that their behaviour under entrainment can be explained with the strongly simplified Adler model.

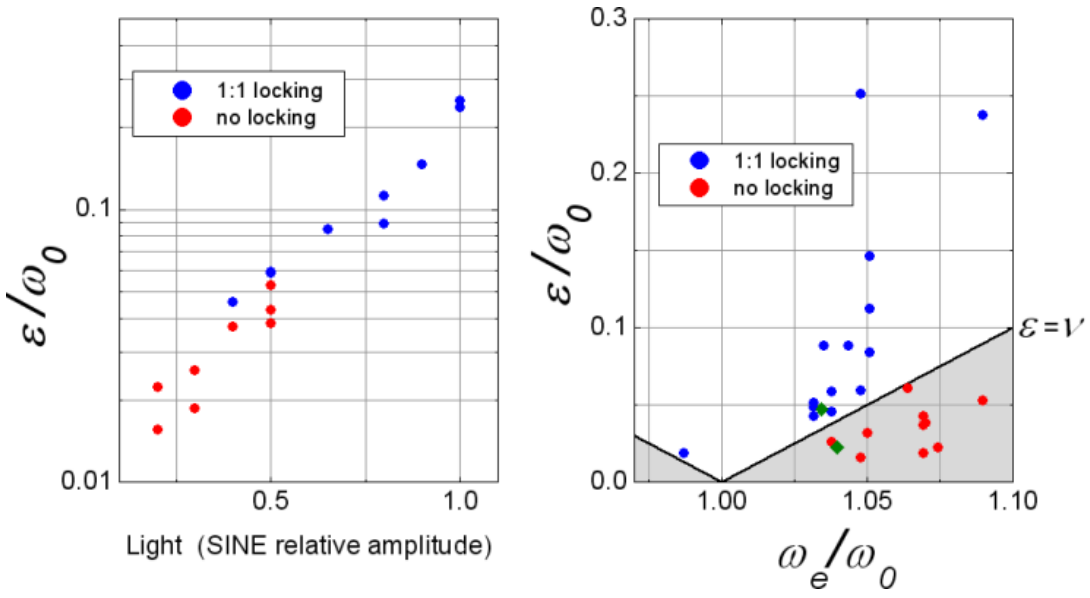

Figure 8.13: (left) The coupling constant ε in function of the relative entrainment amplitude. (right) Arnold tongue. Blue points represent successful entrainment, while red points stand for pseudo-entrained populations. The green points marks values obtained from temperature entrainment experiments.

Chapter 9

Noise considerations

After showing that the circadian clock can be described by the phase oscillator model and that the Adler equation reproduces well its phase behaviour under external forcing, we proceed by looking at the effects noise can have on the system.

The information about it can be found mostly in the instantaneous amplitude $A(t)$. It contains both the relative amplitude of oscillation per cell b and the order parameter of the whole population ρ. As those parameters cannot be separated experimentally without single cell experiments, we use the order parameter from our simulations ρ_{Simul} to separate them from each other. So, before looking at the noise itself, we show how to separate them and get an impression of the evolution of b during the experiment (ch. 9.1).

We then extend our numerical simulations and include diffusion noise into it, that acts directly on the phase of each single oscillator (ch. 9.2). This allows to test the reaction of the population in presence of noise and to compare it with the experimental variation of phase and amplitude. Next, we replace the white noise by a distribution of proper frequencies and compare the results from both approaches with each other.

9.1 Information in the instantaneous amplitude

As already shown in equation 5.2 and brought up in chapter 5.3, the instantaneous amplitude of the measured signal depends essentially on two parameters: the mean individual amplitude of an oscillator b, and the order parameter ρ that describes the level of synchronisation inside the population.

Here we discuss a possible strategy to separate these parameters under the assumption that the evolution of b has a similar time-scale as the evolution of the baseline and is not dependent of the applied entrainment phase. In this way $\frac{A(t)}{\rho_{Simul}}$

should be the similar for all clusters belonging to an experimental condition.

Figure 9.1 illustrates the process. From our simulation we obtain both the simulated mean phase that reproduces the experimental data (fig. 9.1 top left), and the order parameter of the simulated population ρ_{Simul} of oscillators (fig. 9.1 lower left). By dividing the experimental $A(t) = b\rho$ (fig. 9.1 top right) with ρ_{Simul} we obtain an estimation of b during the experiment (fig. 9.1 lower right). To properly divide, them we first copy and cut both the experiment and the simulation data to the same time period, before interpolating them to the same time line. We then divide the experimental amplitude by the order parameter of the simulation ρ_{Simul} to obtain what may be b. We apply a low pass filter to remove fast oscillating parts and detection noise from the bioluminescence photon detectors. Finally we plot $\frac{A(t)}{\rho_{Simul}}$ with $\left(\frac{A(t)}{\rho_{Simul}}\right)_{Filtered}$ on top for all clusters. The so extracted b behaves similarly for all clusters in an experimental condition, independent of the phase the bacteria are entrained to (fig. 9.2).

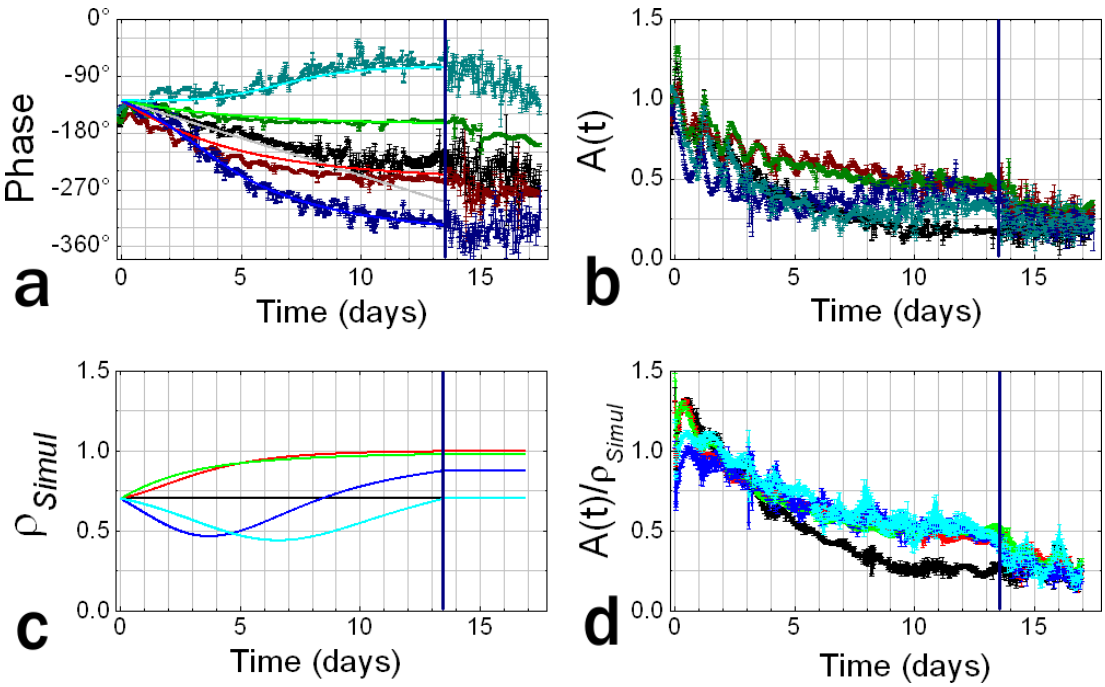

Figure 9.1: How b is extracted from the signal. Here we show an experiment entrained with an relative illumination amplitude of 0.4. Experimental data is shown in darker colours, while simulated or calculated data is shown in lighter colours. The vertical blue line marks the moment when the entrainment is replaced by constant illumination. (a) The measured instantaneous phase with the simulation. (b) The measured instantaneous amplitude $A(t)$. (c) The simulated order parameter for all 5 conditions. With the transition to constant conditions it does not change anymore. (d) b is then obtained by dividing the experimentally measured instantaneous amplitude by the order parameter from the simulation. Under constant illumination all conditions show similar values as the LL control.

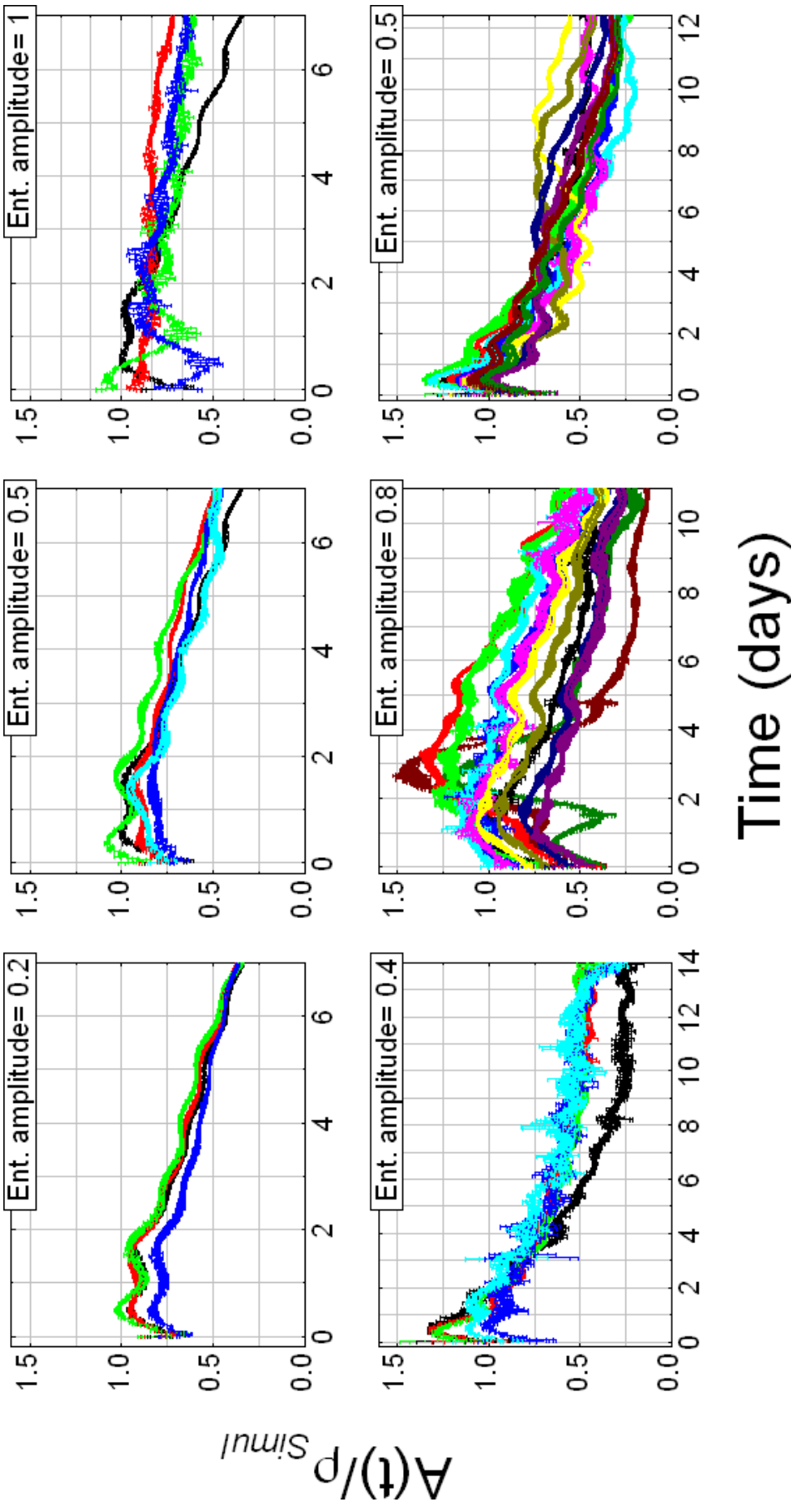

Figure 9.2: Different values of extracted b. The values for the calculated b superpose for the different conditions. With increasing entrainment amplitude and thus coupling force, the difference between the entrained conditions (in colour) and the respective freerun condition (in black) also increases. This could be a hint, that the bacteria prefer an oscillating environment.

In fact this is a behaviour we observe for our simulations (fig. 9.2). The remaining big question is how the evolution of b really is. To measure this similar entrainment experiments, need to be done on single cells. A possible strategy how to perform this kind of long time single cell experiments will be presented in the next chapter (ch. 10).

When comparing values from experiment different entrainment amplitudes we find that b is proportional to the entrainment amplitude (fig. 9.3). This suggests that bacteria under the influence of a strong day-night rhythm produce a stronger oscillation.

9.2 Effect of white noise on the instantaneous phase

Besides their use to further refine the fit quality, the simulation also offers a possibility to investigate the effects of noise on the system, as suggested by single cell experiments. Another choice would have been to consider a distribution of proper frequencies ω_{0_i}. In this paragraph we wanted to test if the resolution of entrainment experiments with populations of cyanobacterial oscillators were sufficient to discriminate between the two hypotheses.

9.2.1 Same proper frequency ω_0, gaussian noise on the phase

For this we consider a white noise that randomly acts on the phase of each oscillator independently, like a one-dimensional random walk along the limit cycle with a predefined step length $\xi_j = \pm\sqrt{D \cdot \Delta t}$ ([5]). So the Adler equation including the noise term becomes:

$$\frac{d\psi_j^{lum}}{dt} = -\nu - \varepsilon \sin\left(\psi_j^{lum} - \alpha - \theta_{e_0}\right) + \xi_j$$

The noise scatters an initially well entrained population of oscillators and maintains a certain amount of phase variation under entrainment. Figure 9.4 shows the phases for different entrainment conditions under the influence of different noise levels. We scanned the parameter space for the diffusion constant from 0 (no noise) to $D = 0.192$ day^{-1} and found a slightly better fit for the value of $D = 0.012$ day^{-1} found via single cell experiments ([35]). See figure 9.4 for comparison of the two extrema and $D = 0.012$ day^{-1}.

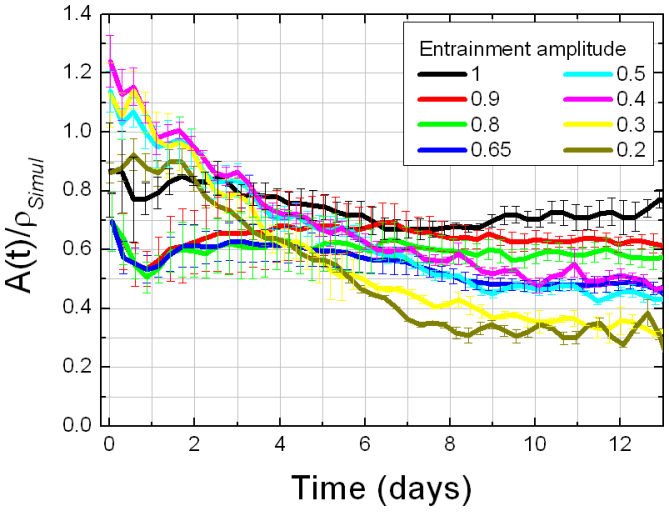

Figure 9.3: Tendency of b dependent on the entrainment amplitude. Stronger entrainment seems also to produce a higher amplitude on the level of each single cell. Some of the graph start above 1, which should not be the case. This is due to remaining uncertainties in the calculation of the baseline close to experiment beginning and does only affect the data for the first ≈ 1.5 days.

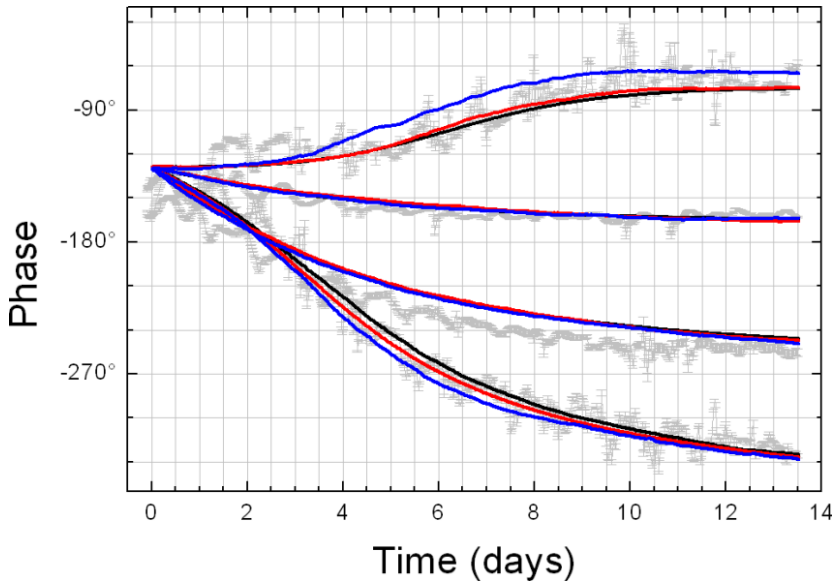

Figure 9.4: Simulation with noise on the phase of each individual oscillator with the experimental data in the background. Here we plot the 4 entrainment conditions (grey) with errorbars with 3 simulations: $D = 0.003$ day^{-1} (black), $D = 0.012$ day^{-1} (red) and $D = 0.192$ day^{-1} (blue). The three simulated sets are very close to each other, only the cyan graph for the strongest noise value $D = 0.192$ day^{-1} is clearly distinguishable from the other sets.

9.2.2 Distribution of ω_0, no noise

Another way to individualise the oscillators inside the population is to consider a distribution of proper frequencies $D(\omega_{0_i})$. Just like the white noise on the phase of each individual oscillator, a distribution of proper frequencies scatters an initially well entrained population and also maintains a phase distribution under entrainment as the detuning ν_i depends directly on it. Figure 9.5 shows the phases for different entrainment conditions. This approach leads to very similar results as the simulation with white noise.

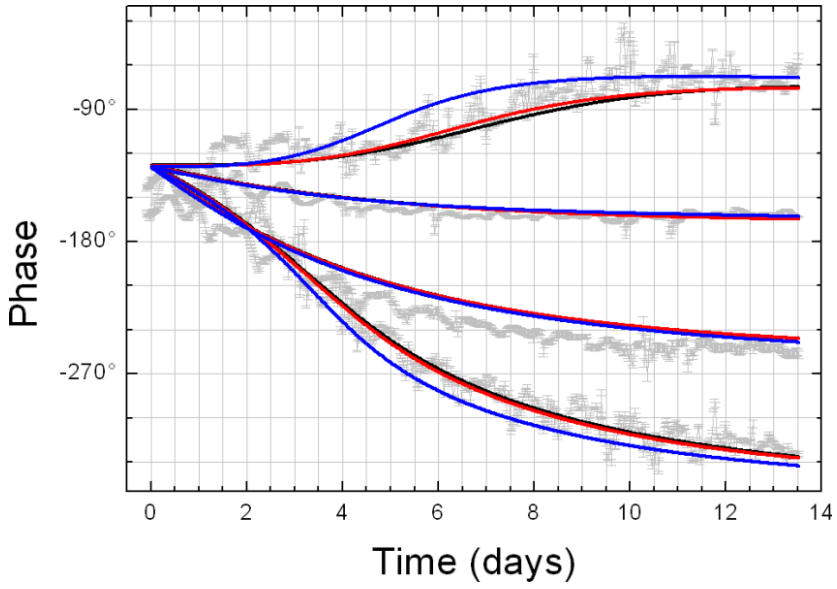

Figure 9.5: Simulation with a distribution of proper frequencies ω_0 with the experimental data in the background.Here we plot the 4 entrainment conditions (grey) with errorbars with 3 simulations: $\sigma_{\omega_0} = 0.0011$ day^{-1} (black), $\sigma_{\omega_0} = 0.0088$ day^{-1} (red) and $\sigma_{\omega_0} = 0.0704$ day^{-1} (blue).

9.2.3 No distinction between phase noise and frequency distribution

As the effects of noise and the frequency distribution are similar, it is difficult to distinguish between them. This is shown in Fig. 9.6, where we show that either of these parameters can be used to accurately reproduce the experimental measurements. This shows that with this experimental set-up we can estimate the amount of noise which acts on the system, but cannot determine its origins.

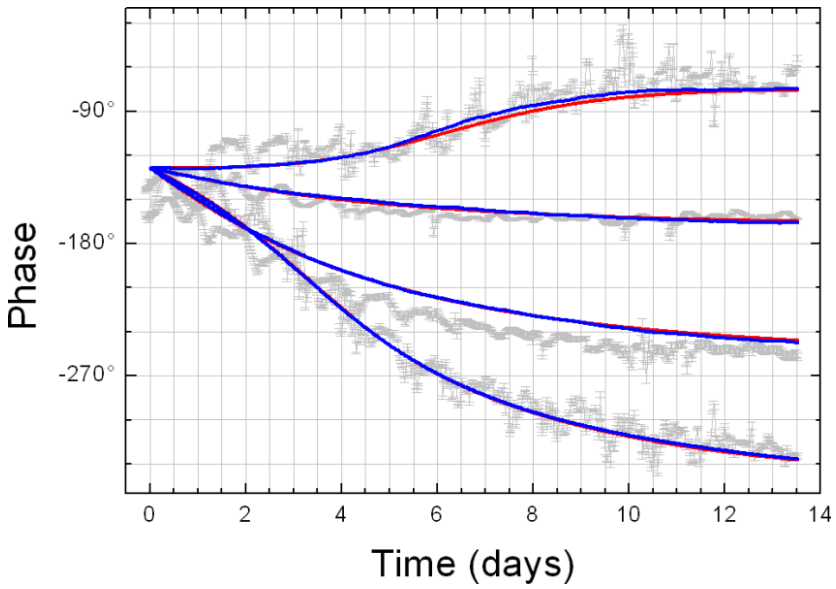

Figure 9.6: Comparison between different source of noise. The experimental data (grey) with the best fitting simulations considering noise ($D = 0.012$ day^{-1}, red) and a distribution of ω_0 ($\sigma_{\omega_0} = 0.0088$ day^{-1}, blue). As can be seen, both scenarios fit well the experimental data. This shows that we can estimate the amount of noise in the system, but cannot locate its source using experiments on populations.

Chapter 10

Single cell devices

As discussed, the population experiments have their limitations. To overcome them it is necessary to follow the circadian clock of individual cells inside a population over several cycles. The major problem here is the continous growth of the population, that makes it impossible to track the individual bacteria of a population over more than 5 to 10 cell divisions. Other problems are possible drifts within the liquid medium, the supply of fresh medium during the experiment in order to keep the environment constant, and 'loss' of bacteria due to vertical movements. The solution to all these problems is a sort of channel with a constriction at one end, through which the culture medium flows. Bacteria inside this medium are carried with it inside the channel until they get hold back by the constriction at the end. A constant flow of medium ensures that a bacterium stays imobile inside the channel and aliments it with all necessary nutritions. Some additional features are necessary: the material of the channel needs to be biocompatible and transparent. As cleaning and re-usage of channels of the size of a bacterium is labour intensive, their production should also be cheap and quick.

Polydimethylsiloxane (PDMS) is a commercial polymer with all these features. It is commonly used in many microfabrication processes, especially in biological research. Initially it is composed of the liquid PDMS and a liquid curing agent. When mixed together and baked for some time (generally 65°C for 1.5 hours) it stiffens out. To create channels, one first creates a negative mold on which the PDMS is poured. After the baking, the mold is removed and the PDMS is attached to a glass slide by plasma bonding. The mold is not destroyed in the process and can be reused. The main challenge consists in creating a mold with channels as fine as a single bacterium. For cyanobacteria we need channels of width and height of about 2µm and constrictions of about 0.5µm. The process of

the mold production is described and discussed in section 10.1. We then continue with the device production in section 10.2 and in section 10.3 we show images from preliminary experiments and the problems encountered in these experiments. We close this chapter with section 10.4, where we show ways to further develop these devices and imagine possible utilisation beyond the scope of circadian research.

10.1 Mold production

The molds we use are made from pure silicon. The structures are directly carved out of the silicon wafer in three stages: Lithography, Lift-off and Etching (fig. 10.1 right). The first step is classic lithography. We spincoat a photoresist (wine red) on the wafer (grey) and remove the insolated areas (yellow) that later shall form the channels (fig. 10.1a). Next we perform a lift-off, for that we apply a layer of $\sim$ 100nm of aluminium (blue) (fig. 10.1b) and dissolve the remaining photoresist. The aluminium layer on top of the photoresist is removed together with the photoresist (fig. 10.1c). Only the areas that will later form the channels are still covered by aluminium, which will protect them from the etching plasma. The thickness of the photoresist in this process does not really matter as long as it is thick enough to allow the lift-off.

During the etching we remove 2µm from the silicon wafer, except on the areas that are protected by the aluminium. The direction of the etching depends on the used process. We tried several etching processes on silicon wafers with a crystal orientation 100.

We first tried an etching process that is homogenous and produces very clean and smooth surfaces. On the other hand it has also a strong horizontal etching capacity which gives the channels a triangular shape (fig. 10.2a). In our case this resulted in channels too small for cyanobacteria, but it offers the possibility to finetune the size of the channels if necessary.

The second etching process we used is quite the opposite of the first one. It etches almost vertically but also creates a very rough surface (fig. 10.2b) that looks a bit like grass. These strong irregularities cause two problems when using this as a mold. The PDMS is very difficult to remove from the mold with a high risk of breaking it, and also the PDMS does not bond properly to a glass surface anymore. This creates devices with a tendency to leak, even at low pressures.

The last etching process we used is a combination of the two previous ones. Strong vertical etching for about 2µm and then a brief application of uniform etching to 'cut the grass' (fig. 10.2c). This leaves us with distinguished channels of

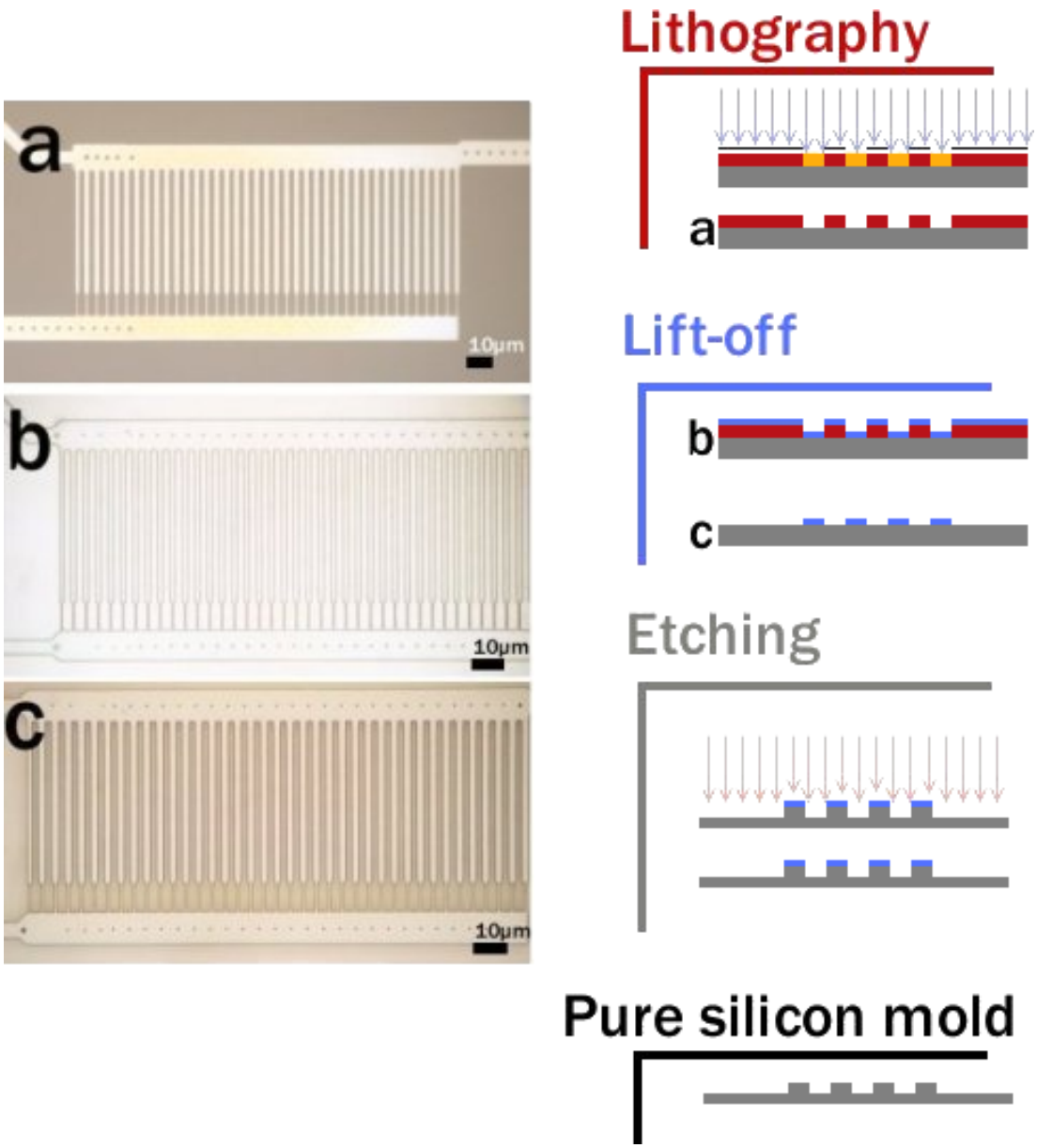

Figure 10.1: (a) The wafer after exposure and development. Dark areas are covered with photoresist, light areas show the pure silicion. (b) After the application of ~ 100nm aluminium layer. (c) Lift-off of the remaining photoresist together with the aluminium on top of it. The aluminium covers now the areas that will later form the channels and protects it against the etching plasma. (righ) Schema of the different steps of mold production. From the top: Lithography: with photoresist (wine red), development of the insolated areas (yellow). Lift-off: aluminium deposition (blue), lift-off of the remaining photoresist. Etching: removal of 2µm unprotected silicon, etched wafer with aluminium protection. Pure silicon mold: after the removal of the aluminium protection.

almost rectangular shape and a reasonably smooth surface for the following device production with PDMS. The molds we used for our preliminary experiments were made with the third etching process. In the end we remove the aluminium protection to keep a pure silicon mold.

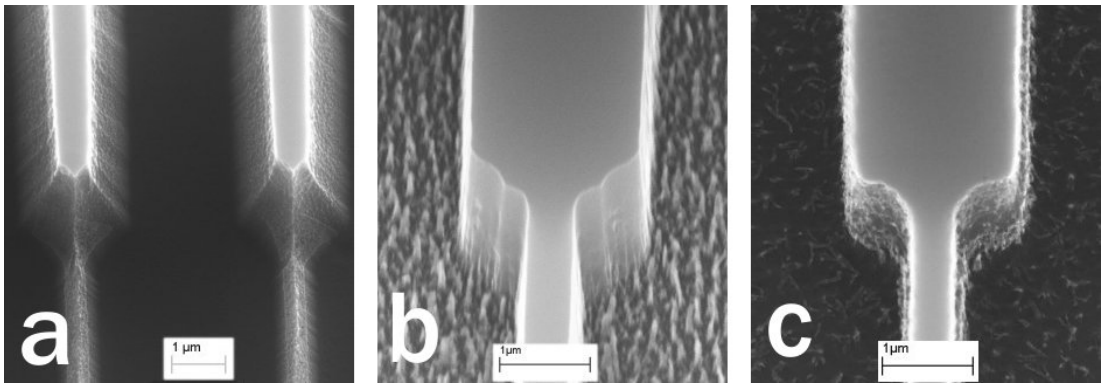

Figure 10.2: Etching processes. (a) Almost uniform etching in all directions. The channels are 2µm high, but due to the uniform etching they have a triangular shape. (b) Vertical etching. Creates very well distinguished rectangular cannels but also a very rough surface that causes problems with the PDMS. (c) Combination of both etching types. Vertical etching 2µm deep and then a brief uniform etching to smoothen the surface.

10.2 Device production

For the device production we follow the classic PDMS procedure under a clean hood to avoid dust as much as possible. The PDMS is mixed with the curing agent in a ratio of 10:1. Air bubbles, that occur frequently during the mixing, are removed by putting the mixture under low pressure until all bubbles are gone. The silicon mold is then put into a cup made out of aluminium foil and the PDMS is poured over it, so that the entire wafer is covered by a 1cm thick layer. Small bubbles that may arise during the pouring are pushed aside so that none remain above the device. The entire cup with the mold and the PDMS is then closed with a lid to avoid dust and baked at 65°C for at least 2h.

After the PDMS has hardened we come to the last step of the device production, during which we prepare the connection interfaces and bond the PDMS to a glass object holder. We begin by cleaning the object holder with hot water and soap. We then rinse all the soap with abundant water and remove the water with pure ethanol. Next we remove the PDMS from the mold and cut out the circuit, so that it fits on the object holder, but still has enough surface to bond to the glass. Now we poke the holes for the connector cable, through which we

will inject the medium later. This is done with special electro polished needle to create as clean as possible holes to avoid leaking under high pressure. The PDMS is then plasma bonded on the object holder and rebaked at 65°C for at least 2h. After cooling down, the devices are now ready for use in experiments.

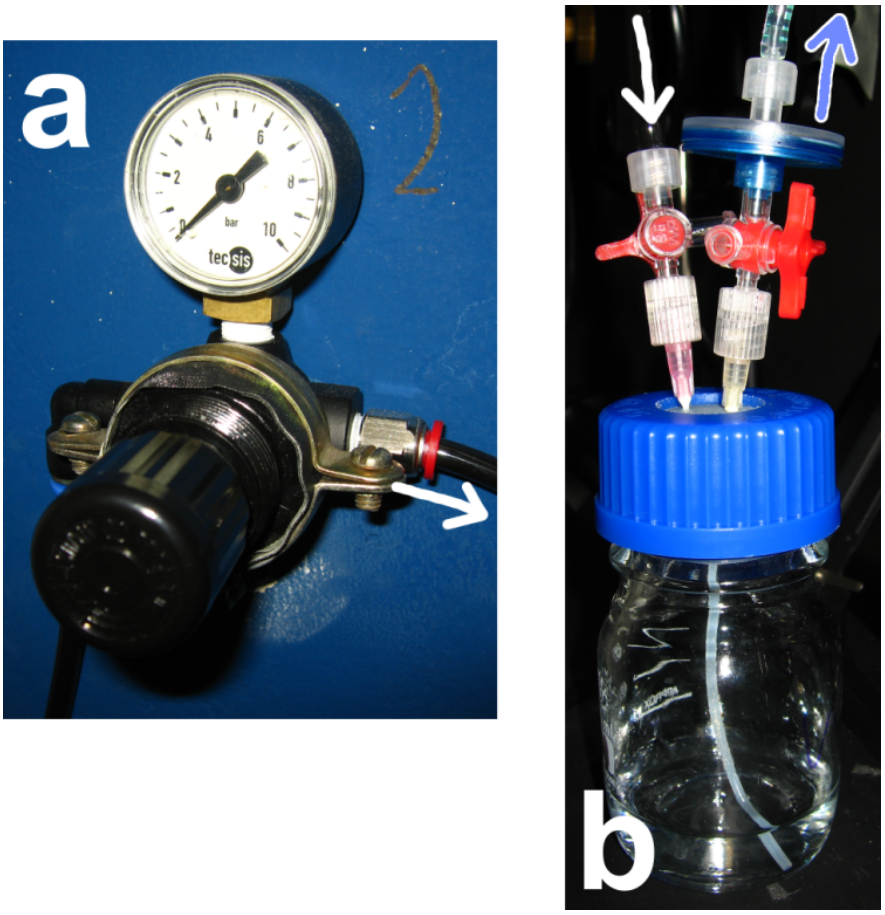

Figure 10.3: The pressure system to push the media and the bacteria into the devices. (a) Pressure valve with manometer. The compressed air flows out to the right (white arrow). (b) Pressure-sealed bottle. The compressed air enters (white arrow) and pushes the liquid out (blue arrow) into the device.

10.3 Experiment and observations

The devices have three connection points. One of them is used as entry from which the bacteria are flushed into the channels (fig. 10.4 A), the second one is used as reservoir where media and bacteria that did not go into a channel are collected (fig. 10.4 B) and the last one where the used media that went through the channels accumulates (fig. 10.4 C). When preparing an experiment we injected a small amount of bacteria in the connector hole A and then push

them trough the device. By independently adapting the pressure at A and B, the bacteria can be loaded into the channels and kept there during the experiment.

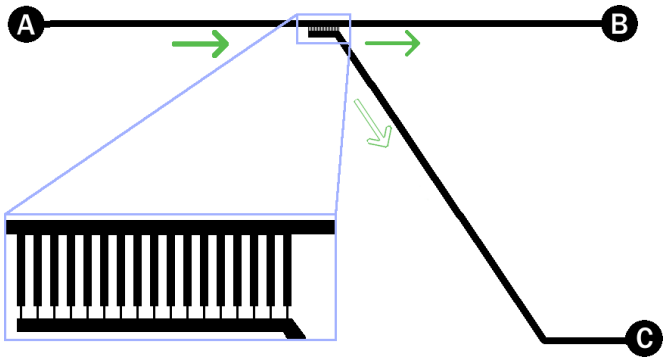

Figure 10.4: Device structure. The cyanobacteria are loaded into entry A and pushed with the media trough the device towards the exits B and C. By independently adapting, the applied pressure to A and B the bacteria enter the channels annd are trapped by the constrictions at their end.

Figure 10.6 shows a device in phase contrast and fluorescence microscopy with cyanobacteria in the channels. The channels are yet too narrow for some of the bacteria, so many bacteria do not enter the channel or get stuck before reaching the constriction. This also limits the flow of the medium and shortened our experiment duration. Figure 10.5 shows a cell division of a cyanobacterium inside one of the channels, proving that the bacteria are still alive when inside the device.

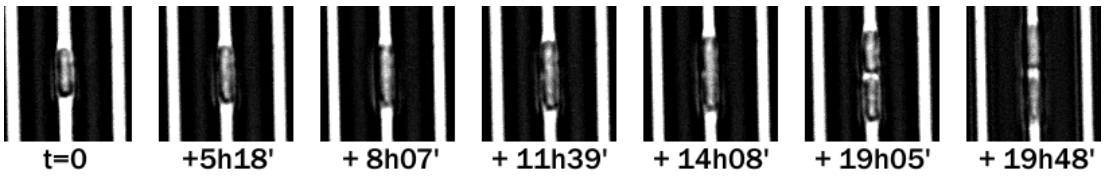

Figure 10.5: Cell division of a cyanobacterium inside a channel.

10.4 Further development

Principally, this bacteria trap can be used with any kind of bacteria, if adapting the different parameters (channel width and height and constriction design) to its requirements. For our cyanobacteria, the channels need to be widened and as they posses a rigid cell wall the constriction can be widened as well. The increase in flow rate should also simplify the entry into channels for the bacteria. To further improve the entry rate into the channels we imagine cone shaped entries into the channels and the supply lines (fig. 10.7a).

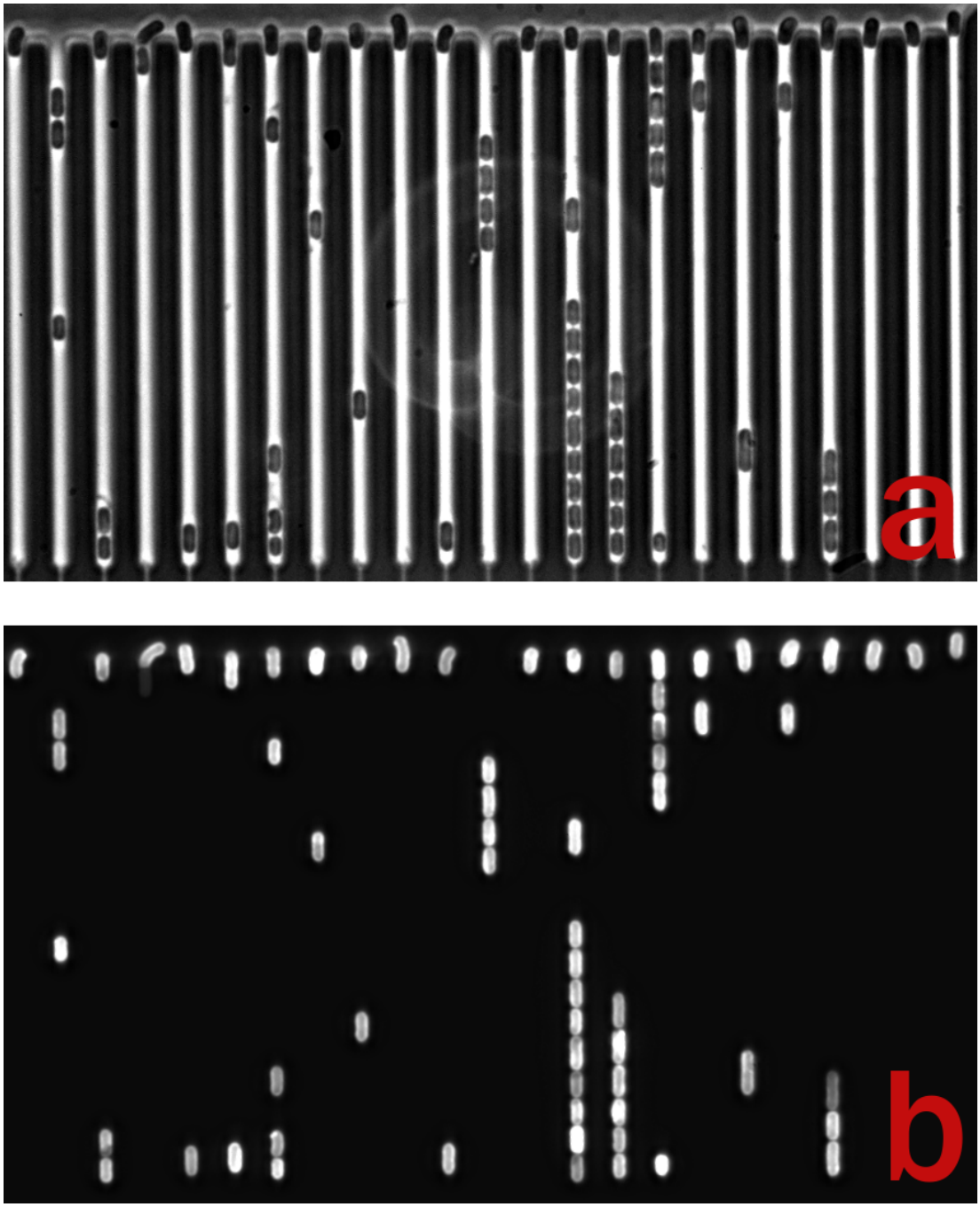

Figure 10.6: Bacteria inside a device. (a) Phase contrast image. (b) Fluorescence image.

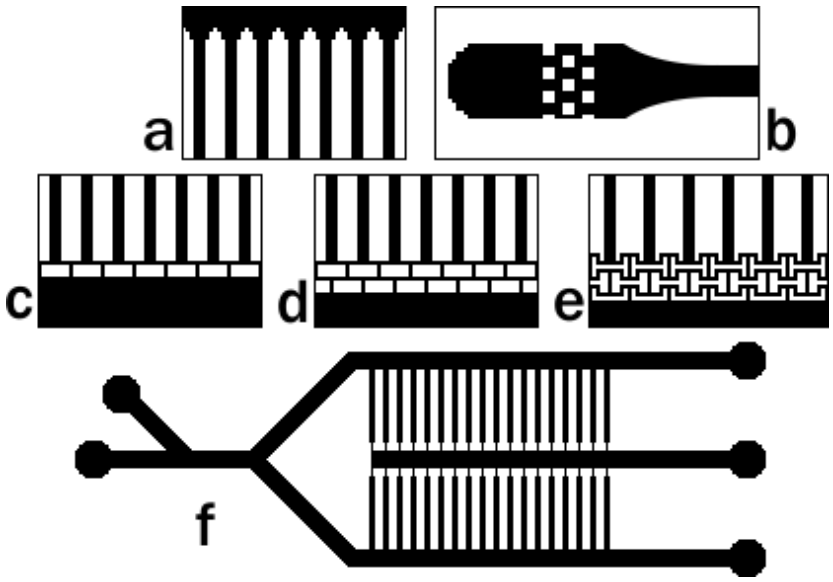

Figure 10.7: Ideas for further development of the microfluidic devices. (f) Additional entry for clean media and increased amount of channels to increase the number of bacteria per experiment. (c-e) Other types of constrictions based on right angles. This type of constriction was designed to trap the bacteria while allowing for a higher flowrate of the media. The high rigidity of the bacteria will not allow them to bend around the angle allowing for much wider constrictions then with the centered approach. (a) To easier get the bacteria into the channels, a cone shaped entry of the channels and supply lines would be helpful as well as a kind of rudimentary filter to prevent clogging of the device by larger accumulation of bacteria (b).

For long experiment duration, a separate entry connection for bacteria and medium will decrease the risk of clogging the device at the entry point by bacteria that did not enter the device, and also reduce the risk of contamination. To reduce the risk of clogging, the addition of PDMS pillars between the poking area and the entry into the circuit could help to trap accumulations of bacteria, allowing only individual bacteria to enter the device (fig. 10.7b).

As the cyanobacteria have a rigidity, they do not bend easily. This could be used by designing constrictions that trap the bacteria by sudden angles rather than a reduced channel size. By replacing the central constriction by a barrier we would also get the advantage of having two possible ways for the flowing of the media. In case a bacterium blocks one of them, the channel in question would still remain operational(fig. 10.7c-e). This type of constriction has the disadvantage to require more horizontal space than the central constrictions used. This reduces the number of bacteria that can be observed per experiment. We could compensate partly for this by adding a second of identical channels flipped upside down (fig. 10.7f).

Chapter 11

Outlook

Due to their simplicity and the possibility to follow the clock directly, cyanobacteria are a very good model organism for circadian research. Besides that they also offer the possibility to do experiments in vivo as well as in vitro and that their mechanisms creating the circadian oscillations have a high resistance towards stochastic noise. In this work we showed that the circadian clock of the cyanobacteria can be described by a simple phase oscillator model and that its phase evolution under external forcing can be described by the Adler equation taking the initial phase distribution under consideration.

We also developed a possibility to execute 2 independent zeitgeber signals, light and temperature, and underlined the need for single cell experiments to further investigate the role of noise on the system. For this we showed a proof of concept for a microfluidic device, that allows to trap bacteria, and with further development, should permit long term experiments on single cells.

This offers the perspectives for further studies:

- Investigate the behaviour under competing forcing by light and temperature to better understand the relation that might exist between them. The idea is to separate the different clusters with the light entrainment like we do actually for the temperature experiments (ch. 7.3). After the period under constant condition when the temperature oscillation begins one simply could add a light entrainment whose phases match the current clock phases of each respective entrainment condition. This allows to test different phase shifts between the light and temperature entrainment and different relative light amplitudes at once.

- Combine light and temperature entrainment to realise stronger entrainment conditions by synchronising the both entrainment types together. This

would allow to verify if the phase oscillator model in combination with the Adler equation is still appliable beyond the entrainment forces realised in this study.

- Further develop the single cell devices to be able to observe individual cells under external forcing and verify the results obtained from the population experiments. As shown here this is an essential step to better understand the role of the amplitude and to distinguish between a individual diffusion noise on the phase or a distribution of proper frequencies inside a population.

- Do the same experiments on existing mutated cyanobacteria that lack essential proteins of the clock mechanisms to understand the role of those proteins in the adaptation process by comparing their reaction to the external forcing. Possible candidates could be strains with modified period length like the clock mutants SP22, P30, and LP40 ([28]). Another possibility would be to use strains where proteins in the input pathways like Pex, LdpA or CikA were knocked out.

It seems surprising, that the circadian clock of an organism as simple as the cyanobacteria is as precise and apparently resistant to internal and external noise. These astonishing abilities, combined with the easiness of the organisms that allows to apply a wide variety of genetic tools, will allow for many different approaches in vivo and in vitro. The cyanobacteria and their circadian clock are thus a very good model organism for various studies and have surely not finished to surprise us.

Part IV

Appendices

Appendix A

Culture medium BG11

Component	Quantity
$NaNO_3$	150g
K_2HPO_4	40g
$MgSO_4 \cdot 7H_2O$	75g
$CaCl_2 \cdot 2H_2O$	36g
Citric acid width Ferric	6g
Ammonium citrate	6g
EDTA (disodium salt)	1g
Agar (for gel)	15g
Distilled water	1.0 l

Adjust pH to 7.5 before sterilization.

After sterilization (60 °C or below) add:

Component	Quantity
$NaCO_3$	20g
Trace metal solution A5 (see below)	1.0ml
Na_2S_2O(for gel)	0.2M
Proline (for gel)	20g

Trace metal mix solution A5:

Component	Quantity
H_3BO_3	2.857g
$MnCl_2 \cdot 4H_2O$	1.880g
$ZnSo_4 \cdot 7H_2O$	0.232g
$NaMoO_4 \cdot 2H_2O$	0.396g
$CuSO_4 \cdot 5H_2O$	0.085g
$Co(No_3)_2 \cdot 6H_2O$	0.0054g
Distilled water	1.0 l

Appendix B

TopCount reading sequence

To know when and how long the cyanobacteria get illuminated, we measured the time the different steps take during one reading cycle.

In total, plate **a** gets illuminated from step 5 till step 11 during 31' 39" (1899'') and remains in the dark (positioning, count delay, reading) from step 1 till step 5 during 9' 51" (591'').

Plate **b** gets illuminated from step 1 till step 6 and step 10 till step 11 during 30' 48" (1848'') and remains in the dark from step 6 till step 10 during 10' 42" (642").

a, **b** Plates

A, **B** Stacker Positions

Step	**t**	Δ
1. **a** leaving **A**	0'00"	-
	0"	-
2. begin count delay **a**	0' 54"	0' 54"
	54"	54"
3. start reading **a**	3' 54"	3' 00"
	234"	180"
4. end reading **a**	9' 39"	5' 45"
	579"	345"
5. **a** back on **A**	9' 51"	0' 12"
	591"	12"
6. **b** leaving **B**	29' 31"	19' 40"
	1771"	1180"
7. begin count delay **b**	29' 56"	0' 25"
	1796"	25"
8. start reading **b**	32' 57"	3' 01"
	1977"	181"
9. end reading **b**	38' 43"	5' 46"
	2323"	346"
10. **b** back on **B**	40' 13"	1' 30"
	2413"	90"
11. **a** leaving **A**	41' 30"	1' 17"
	2490"	77"

Two whole cycle takes 41' 30" for four microplates. Two of them carry bacteria and two intermediate plates are used to stretch out the cycle, as is was not possible to program a waiting time into the cycle. During each cycle, all four microplates are read by the TopCount NXT, each data acquisition taking thus approximately 10 minutes. This sums up to 1008 data acquisitions per week and 2016 plate handling operations.

Appendix C

Bioluminescence Light Intensity Compared to the External Illumination

In this section we evaluate the internal bioluminescence intensity for a well and then compare it with the growth light intensity. We show that a bacterium receives enormously more photons from the external lighting (at least 10^7 times more) than from the bioluminescence emitted either by itself or by the surrounding cells.

The light emitted by a bacterium with the luciferase reporter P_{kaiBC}::*luxAB* and P_{sbAI}::*luxCDE* is roughly $g_0 \cong 4$ photons/minute, ≈ 5 times less than the previously reported ([35]), stronger reporter P_{sbAI}::*luxAB* and P_{sbAI}::*luxCDE*. We neglect here the circadian periodic oscillation of the reporter activity and replace $\langle y(t) \rangle$ by its time average $\overline{\langle y(t) \rangle} = 1$. The external lighting intensity at the surface of the well is $L_0 = 900$ lux $\cong 10^{19}$photons$\cdot m^{-2}s^{-1}$ and decreases exponentially with depth in the absorbing well: $L_x = L_0 \cdot e^{\alpha \cdot (x-D)}$. As in the preceding section, we assume that the light emission of the bacterium will decrease proportionally to the external lighting. We therefore have to compare the emission of the bacterium situated only in top layers (g_0) with the maximum number of photons received from the external lighting: $l_0 = \sigma \cdot L_0$. Here σ is the absorption cross section estimated as $\sigma_{550\,nm} \cong 4 \cdot 10^{-9}\, cm$[21]. We obtain $l_0 = 4 \cdot 10^6$ photons/cell/s, which is $6 \cdot 10^7$ larger than g_0.

We next determine the overall emission of the bioluminescent cell in the well and compare it to the external lighting intensity. At each depth x, measured from

[1] For comparison the physical cross section of a cell is $S_{cell} \cong 1.5\,\mu m \cdot 5\,\mu m = 7.5 \cdot 10^{-8}\, cm^2$, this means that only 1/20 received photons are detected by the cell.

the bottom of the well (SI Fig. 9), the internal intensity of bioluminescence is a sum of two components. The first, $I_{\uparrow}(x)$, adds the contributions of the lower layers emitting upward, while the second, $I_{\downarrow}(x)$, sums the contributions of the upper layers emitting downward. In the preceding section, we showed that the intensity of the upwards-emitted bioluminescence is the solution of Eq. 5.4:

$$I_{\uparrow}(x) = \frac{g_0}{2\sigma} \cdot \frac{n_E}{n_T} \cdot e^{\alpha \cdot (x-D)} \cdot \left(1 - e^{-2\alpha x}\right)$$

with $I_{\uparrow}(x)$ instead of $I(x)$. Similarly, we deduce the equation for downwards emission

$$\frac{dI_{\downarrow}}{dx} = \alpha \cdot I_{\downarrow} - g_0 \cdot n_E \cdot e^{\alpha \cdot (x-D)}$$

and its solution:

$$I_{\downarrow}(x) = g_0 \cdot n_E \cdot e^{\alpha \cdot (x-D)} \cdot (D - x)\,.$$

Therefore, the internal intensity of bioluminescence at a given depth x is

$$I_{int}(x) = B_0 \cdot e^{\alpha \cdot (x-D)} \cdot \left(\frac{1 - e^{-2\alpha x}}{2} + \alpha\,(D - x)\right)$$

where, $B_0 = \frac{g_0}{\sigma} \cdot \frac{n_E}{n_T}$ is an upper limit for the internal bioluminescence. In our experiment, $B_0 \cong 8.3 \cdot 10^9$ photons$\cdot$m$^{-2}\cdot$s^{-1}, as $\frac{n_E}{n_T} = \frac{1}{20}$, $\sigma \cong 4 \cdot 10^{-9}$ cm^2 and $g_0 \cong 4$ photons/minute/cell.

The ratio between the internal bioluminescence intensity and the external lighting intensity at a depth x, has a maximum value at the bottom of the well

$$\left(\frac{I_{int}(x)}{L(x)}\right)_{x=0} = \frac{B_0}{L_0} \cdot \alpha D$$

and decreases continuously on going up toward the surface. In our experiments, the internal bioluminescence is $1.2 \cdot 10^9$ times smaller than the external lighting at the start (for an initial $\alpha D \cong 1$) and at least $1.2 \cdot 10^7$ times by the end of the experiments. The bioluminescence light (self produced by the cell, or received from the surrounding luminescent cells) is therefore insignificant, compared to the external lighting, being at least 10^7 times lower.

Appendix D

Parameters of the LED calibration

The measured values were fitted by a polynomial fit. Here we give the obtained parameters for each cluster.

Parameters for the lux to cps transformation.

Plate A

	Cluster A1	**Cluster A2**	**Cluster A3**	**Cluster A4**	**Cluster A5**	**Cluster A6**
n_1	4.62979	4.60029	4.5531	4.63455	4.58219	4.56976
n_2	0.09257	0.08388	0.10318	0.06937	0.11143	0.12785
n_3	-0.00622	-0.04296	-0.05933	-0.0201	-0.04651	-0.05049
n_4	0.02206	0.03408	0.04006	0.02897	0.03597	0.03471
n_5	-0.00232	-0.00375	-0.00455	-0.00328	-0.00403	-0.00377
n_6	7.86309E-5	1.3745E-4	1.74288E-4	1.23126E-4	1.51139E-4	1.39224E-4

Plate B

	Cluster B1	**Cluster B2**	**Cluster B3**	**Cluster B4**	**Cluster B5**	**Cluster B6**
n_1	4.63136	4.6323	4.63481	4.63182	4.63155	4.63036
n_2	0.09707	0.1131	0.07921	0.10003	0.11172	0.11252
n_3	-0.02695	-0.05547	-0.03656	-0.03904	-0.05219	-0.04002
n_4	0.02729	0.03786	0.03153	0.03585	0.03883	0.03428
n_5	-0.00283	-0.00424	-0.00342	-0.00417	-0.0045	-0.00399
n_6	9.55007E-5	1.61757E-4	1.2231E-4	1.62184E-4	1.75867E-4	1.56116E-4

Parameters for the cps to lux transformation.

Plate A

	Cluster A1	**Cluster A2**	**Cluster A3**	**Cluster A4**	**Cluster A5**	**Cluster A6**
n_1	-22787.4294	-36467.39245	-36808.01413	-40284.46379	-23393.16944	-11211.29476
n_2	26253.79919	42381.5109	43083.4034	46812.5193	27014.81682	12464.25421
n_3	-13153.69223	-21398.54294	-21902.19844	-23632.753	-13562.59952	-6027.17259
n_4	3742.12588	6129.95172	6315.49681	6768.97825	3865.39602	1655.20646
n_5	-661.04228	-1089.62912	-1129.68323	-1203.02572	-683.90503	-282.27897
n_6	74.24211	123.07127	128.36493	135.85586	76.91811	30.61027
n_7	-5.17705	-8.62621	-9.0492	-9.52058	-5.37032	-2.06125
n_8	0.20494	0.34308	0.36189	0.37858	0.21282	0.07881
n_9	-0.00353	-0.00593	-0.00629	-0.00654	-0.00367	-0.00131

Plate B

	Cluster B1	**Cluster B2**	**Cluster B3**	**Cluster B4**	**Cluster B5**	**Cluster B6**
n_1	-31424.55659	-34713.8479	-45250.33577	-34032.98983	-31650.52771	-25587.64446
n_2	36407.08947	40181.58914	52605.46292	39485.38401	36570.51127	29461.07065
n_3	-18334.22457	-20214.49013	-26567.35711	-19908.578	-18366.4879	-14748.39623
n_4	5240.67128	5771.91073	7612.21	5696.64811	5235.69736	4191.79208
n_5	-929.84285	-1022.97383	-1353.34987	-1011.67577	-926.49342	-739.70118
n_6	104.86084	115.23665	152.88244	114.18284	104.21343	82.98416
n_7	-7.34019	-8.05776	-10.71729	-7.99865	-7.27673	-5.77995
n_8	0.29161	0.31978	0.42631	0.31798	0.2884	0.22853
n_9	-0.00503	-0.00552	-0.00737	-0.00549	-0.00497	-0.00393

Bibliography

[1] URL http://www.ibvf.csic.es/Cultivos/Seccion_I.htm.

[2] URL http://www.youtube.com/watch?v=RMVxVbCIPjg.

[3] Juan A. Acebrón and Renato Spigler. The Remote Control and Beyond: The Legacy of Robert Adler. *SIAM News*, 40, 2007.

[4] Juan A. Acebrón, L. L. Bonilla, Conrad J. Pérez Vicente, Félix Ritort, and Renato Spigler. The Kuramoto model: A simple paradigm for synchronization phenomena. *Reviews of Modern Physics*, 77(1):137–185, Apr 2005. doi: 10.1103/RevModPhys.77.137. URL http://dx.doi.org/10.1103/RevModPhys.77.137.

[5] M. Amdaoud, M. Vallade, C. Weiss-Schaber, and I. Mihalcescu. Cyanobacterial clock, a stable phase oscillator with negligible intercellular coupling. *Proc Natl Acad Sci U S A*, 104(17):7051–7056, Apr 2007. doi: 10.1073/pnas.0609315104. URL http://dx.doi.org/10.1073/pnas.0609315104.

[6] Malika Amdaoud. *Stabilité du rythme circadien des cyanobactéries: Investigation d'un couplage entre oscillateurs.* PhD thesis, Université Joseph Fourier, Grenoble, 2007. URL http://www-lsp.ujf-grenoble.fr/pdf/theses/adma.pdf.

[7] Samuel Bernard, Didier Gonze, Branka Cajavec, Hanspeter Herzel, and Achim Kramer. Synchronization-induced rhythmicity of circadian oscillators in the suprachiasmatic nucleus. *PLoS Comput Biol*, 3(4):e68, Apr 2007. doi: 10.1371/journal.pcbi.0030068. URL http://dx.doi.org/10.1371/journal.pcbi.0030068.

[8] V. A. Boichenko. Photosynthetic units of phototrophic organisms. *Biochemistry (Mosc)*, 69(5):471–484, May 2004.

[9] Thomas Cavalier-Smith. Cell evolution and Earth history: stasis and revolution. *Philos Trans R Soc Lond B Biol Sci*, 361(1470):969–1006, Jun 2006. doi: 10.1098/rstb.2006.1842. URL http://dx.doi.org/10.1098/rstb.2006.1842.

[10] Jake Currie, Tadahiro Goda, and Herman Wijnen. Selective entrainment of the Drosophila circadian clock to daily gradients in environmental temperature. *BMC Biol*, 7:49, 2009. doi: 10.1186/1741-7007-7-49. URL http://dx.doi.org/10.1186/1741-7007-7-49.

[11] Guogang Dong and Susan S Golden. How a cyanobacterium tells time. *Curr Opin Microbiol*, 11(6):541–546, Dec 2008. doi: 10.1016/j.mib.2008.10.003. URL http://dx.doi.org/10.1016/j.mib.2008.10.003.

[12] Emery P Dubruille R. A plastic clock: how circadian rhythms respond to environmental cues in Drosophila. *Mol Neurobiol*, 38(2):129–145, Oct 2008. doi: 10.1007/s12035-008-8035-y. URL http://dx.doi.org/10.1007/s12035-008-8035-y.

[13] Jay C Dunlap and Jennifer J Loros. The neurospora circadian system. *J Biol Rhythms*, 19(5):414–424, Oct 2004. doi: 10.1177/0748730404269116. URL http://dx.doi.org/10.1177/0748730404269116.

[14] G. B. Ermentrout and N. Kopell. Multiple pulse interactions and averaging in coupled neural oscillators. *J. Math. Biol.*, 29:195–217, 1991.

[15] Paul E Hardin. The circadian timekeeping system of Drosophila. *Curr Biol*, 15(17):R714–R722, Sep 2005. doi: 10.1016/j.cub.2005.08.019. URL http://dx.doi.org/10.1016/j.cub.2005.08.019.

[16] Ken-Ichi Honma and Sato Honma. The SCN-independent clocks, methamphetamine and food restriction. *Eur J Neurosci*, Oct 2009. doi: 10.1111/j.1460-9568.2009.06976.x. URL http://dx.doi.org/10.1111/j.1460-9568.2009.06976.x.

[17] R Hubbard. *Boater's Bowditch: The Small Craft American Practical Navigator.* McGraw-Hill Professional, 1893.

[18] M. Ishiura, S. Kutsuna, S. Aoki, H. Iwasaki, C. R. Andersson, A. Tanabe, S. S. Golden, C. H. Johnson, and T. Kondo. Expression of a gene cluster kaiABC as a circadian feedback process in cyanobacteria. *Science*, 281(5382):1519–1523, Sep 1998.

[19] Hiroshi Ito, Hakuto Kageyama, Michinori Mutsuda, Masato Nakajima, Tokitaka Oyama, and Takao Kondo. Autonomous synchronization of the circadian KaiC phosphorylation rhythm. *Nat Struct Mol Biol*, 14(11):1084–1088, Nov 2007. doi: 10.1038/nsmb1312. URL http://dx.doi.org/10.1038/nsmb1312.

[20] Natalia B Ivleva, Matthew R Bramlett, Paul A Lindahl, and Susan S Golden. LdpA: a component of the circadian clock senses redox state of the cell. *EMBO J*, 24(6):1202–1210, Mar 2005. doi: 10.1038/sj.emboj.7600606. URL http://dx.doi.org/10.1038/sj.emboj.7600606.

[21] Carl Hirschie Johnson. Global orchestration of gene expression by the biological clock of cyanobacteria. *Genome Biol*, 5(4):217, 2004. doi: 10.1186/gb-2004-5-4-217. URL http://dx.doi.org/10.1186/gb-2004-5-4-217.

[22] I. M. P. Joseph and R. J. Butera. A simple model of dynamic interactions between respiratory centers. In *Proc. 27th Annual International Conference of the Engineering in Medicine and Biology Society IEEE-EMBS 2005*, pages 5840–5842, 17–18 Jan. 2006. doi: 10.1109/IEMBS.2005.1615817.

[23] Roenneberg T. Kantermann T. Is light-at-night a health risk factor or a health risk predictor? *Chronobiol Int*, 26(6):1069–1074, Aug 2009. doi: 10.1080/07420520903223984. URL http://dx.doi.org/10.1080/07420520903223984.

[24] M. Katayama, N. F. Tsinoremas, T. Kondo, and S. S. Golden. cpmA, a gene involved in an output pathway of the cyanobacterial circadian system. *J Bacteriol*, 181(11):3516–3524, Jun 1999.

[25] Mitsunori Katayama, Takao Kondo, Jin Xiong, and Susan S Golden. ldpA encodes an iron-sulfur protein involved in light-dependent modulation of the circadian period in the cyanobacterium Synechococcus elongatus PCC 7942. *J Bacteriol*, 185(4):1415–1422, Feb 2003.

[26] Yota B Kiyohara, Mitsunori Katayama, and Takao Kondo. A novel mutation in kaiC affects resetting of the cyanobacterial circadian clock. *J Bacteriol*, 187(8):2559–2564, Apr 2005. doi: 10.1128/JB.187.8.2559-2564.2005. URL http://dx.doi.org/10.1128/JB.187.8.2559-2564.2005.

[27] T. Kondo, C. A. Strayer, R. D. Kulkarni, W. Taylor, M. Ishiura, S. S. Golden, and C. H. Johnson. Circadian rhythms in prokaryotes: luciferase as a re-

porter of circadian gene expression in cyanobacteria. *Proc Natl Acad Sci U S A*, 90(12):5672–5676, Jun 1993.

[28] T. Kondo, N. F. Tsinoremas, S. S. Golden, C. H. Johnson, S. Kutsuna, and M. Ishiura. Circadian clock mutants of cyanobacteria. *Science*, 266(5188): 1233–1236, Nov 1994.

[29] T. Kondo, T. Mori, N. V. Lebedeva, S. Aoki, M. Ishiura, and S. S. Golden. Circadian rhythms in rapidly dividing cyanobacteria. *Science*, 275(5297): 224–227, Jan 1997.

[30] S. Kutsuna, T. Kondo, S. Aoki, and M. Ishiura. A period-extender gene, pex, that extends the period of the circadian clock in the cyanobacterium Synechococcus sp. strain PCC 7942. *J Bacteriol*, 180(8):2167–2174, Apr 1998.

[31] Shinsuke Kutsuna, Takao Kondo, Haruki Ikegami, Tatsuya Uzumaki, Mitsunori Katayama, and Masahiro Ishiura. The circadian clock-related gene pex regulates a negative cis element in the kaiA promoter region. *J Bacteriol*, 189(21):7690–7696, Nov 2007. doi: 10.1128/JB.00835-07. URL http://dx.doi.org/10.1128/JB.00835-07.

[32] Chentao Lin and Takeshi Todo. The cryptochromes. *Genome Biol*, 6(5):220, 2005. doi: 10.1186/gb-2005-6-5-220. URL http://dx.doi.org/10.1186/gb-2005-6-5-220.

[33] De Mairan. Observation Botanique, Histoire de l'Academie Royale des Sciences. *J.J.O.*, page 35, 1729.

[34] Reppert SM Merlin C, Gegear RJ. Antennal circadian clocks coordinate sun compass orientation in migratory monarch butterflies. *Science*, 325(5948): 1700–1704, Sep 2009. doi: 10.1126/science.1176221. URL http://dx.doi.org/10.1126/science.1176221.

[35] Irina Mihalcescu, Weihong Hsing, and Stanislas Leibler. Resilient circadian oscillator revealed in individual cyanobacteria. *Nature*, 430(6995):81–85, Jul 2004. doi: 10.1038/nature02533. URL http://dx.doi.org/10.1038/nature02533.

[36] R. E. Mistlberger, E. G. Marchant, and T. E. Kippin. Food-entrained circadian rhythms in rats are insensitive to deuterium oxide. *Brain Res*, 919(2): 283–291, Nov 2001.

[37] Ralph E Mistlberger. Food-anticipatory circadian rhythms: concepts and methods. *Eur J Neurosci*, Oct 2009. doi: 10.1111/j.1460-9568.2009.06965.x. URL http://dx.doi.org/10.1111/j.1460-9568.2009.06965.x.

[38] Takahashi A. Ikemoto H. Cao S. Arai T. Mitsui A., Kumazawa S. Strategy by which nitrogen-fixing unicellular cyanobacteria grow photoautotrophically. *Nature*, 323:720–722, 1986.

[39] N. Mrosovsky. Phase response curves for social entrainment. *J Comp Physiol A*, 162(1):35–46, Jan 1988.

[40] Paloma Más. Circadian clock function in Arabidopsis thaliana: time beyond transcription. *Trends Cell Biol*, 18(6):273–281, Jun 2008. doi: 10.1016/j.tcb.2008.03.005. URL http://dx.doi.org/10.1016/j.tcb.2008.03.005.

[41] H.Y. Lin T.J. Chow N. Grobbelaar, T.C. Huang. Dinitrogen-fixing endogenous rhythm in Synechococcus RF-1. *FEMS Microbiology Letters*, 37:137–177, 1986.

[42] Masato Nakajima, Keiko Imai, Hiroshi Ito, Taeko Nishiwaki, Yoriko Murayama, Hideo Iwasaki, Tokitaka Oyama, and Takao Kondo. Reconstitution of circadian oscillation of cyanobacterial KaiC phosphorylation in vitro. *Science*, 308(5720):414–415, Apr 2005. doi: 10.1126/science.1108451. URL http://dx.doi.org/10.1126/science.1108451.

[43] Taeko Nishiwaki, Yoshinori Satomi, Masato Nakajima, Cheolju Lee, Reiko Kiyohara, Hakuto Kageyama, Yohko Kitayama, Mioko Temamoto, Akihiro Yamaguchi, Atsushi Hijikata, Mitiko Go, Hideo Iwasaki, Toshifumi Takao, and Takao Kondo. Role of KaiC phosphorylation in the circadian clock system of Synechococcus elongatus PCC 7942. *Proc Natl Acad Sci U S A*, 101(38):13927–13932, Sep 2004. doi: 10.1073/pnas.0403906101. URL http://dx.doi.org/10.1073/pnas.0403906101.

[44] Taeko Nishiwaki, Yoshinori Satomi, Yohko Kitayama, Kazuki Terauchi, Reiko Kiyohara, Toshifumi Takao, and Takao Kondo. A sequential program of dual phosphorylation of KaiC as a basis for circadian rhythm in cyanobacteria. *EMBO J*, 26(17):4029–4037, Sep 2007. doi: 10.1038/sj.emboj.7601832. URL http://dx.doi.org/10.1038/sj.emboj.7601832.

[45] D. A. Paley, N. E. Leonard, R. Sepulchre, D. Grunbaum, and J. K. Parrish. Oscillator Models and Collective Motion. 27(4):89–105, Aug. 2007. doi: 10.1109/MCS.2007.384123.

[46] Kurths J Pikovsky A, Rosenblum M. *Synchronization: A Universal Concept in Nonlinear Science*. Cambridge University Press, 2002.

[47] T. Roenneberg and R. G. Foster. Twilight times: light and the circadian system. *Photochem Photobiol*, 66(5):549–561, Nov 1997.

[48] T. Roenneberg and M. Merrow. Circadian systems: different levels of complexity. *Philos Trans R Soc Lond B Biol Sci*, 356(1415):1687–1696, Nov 2001. doi: 10.1098/rstb.2001.0969. URL http://dx.doi.org/10.1098/rstb.2001.0969.

[49] H. J. Rolf and K. Fischer. Serum testosterone, 5-alpha-dihydrotestosterone and different sex characteristics in male fallow deer (Cervus dama): a long-term experiment with accelerated photoperiods. *Comp Biochem Physiol A Physiol*, 115(3):207–221, Nov 1996.

[50] Michael J Rust, Joseph S Markson, William S Lane, Daniel S Fisher, and Erin K O'Shea. Ordered phosphorylation governs oscillation of a three-protein circadian clock. *Science*, 318(5851):809–812, Nov 2007. doi: 10.1126/science.1148596. URL http://dx.doi.org/10.1126/science.1148596.

[51] O. Schmitz, M. Katayama, S. B. Williams, T. Kondo, and S. S. Golden. CikA, a bacteriophytochrome that resets the cyanobacterial circadian clock. *Science*, 289(5480):765–768, Aug 2000.

[52] Naoki Takai, Shingo Ikeuchi, Katsushi Manabe, and Shinsuke Kutsuna. Expression of the circadian clock-related gene pex in cyanobacteria increases in darkness and is required to delay the clock. *J Biol Rhythms*, 21(4):235–244, Aug 2006. doi: 10.1177/0748730406289400. URL http://dx.doi.org/10.1177/0748730406289400.

[53] Naoki Takai, Masato Nakajima, Tokitaka Oyama, Ryotaku Kito, Chieko Sugita, Mamoru Sugita, Takao Kondo, and Hideo Iwasaki. A KaiC-associating SasA-RpaA two-component regulatory system as a major circadian timing mediator in cyanobacteria. *Proc Natl Acad Sci U S A*, 103(32):12109–12114, Aug 2006. doi: 10.1073/pnas.0602955103. URL http://dx.doi.org/10.1073/pnas.0602955103.

[54] T. K. Tamai, A. J. Carr, and D. Whitmore. Zebrafish circadian clocks: cells that see light. *Biochem Soc Trans*, 33(Pt 5):962–966, Nov 2005. doi: 10.1042/BST20050962. URL http://dx.doi.org/10.1042/BST20050962.

[55] S. Usui. Gradual changes in environmental light intensity and entrainment of circadian rhythms. *Brain Dev*, 22 Suppl 1:S61–S64, Sep 2000.

[56] S. Usui, T. Okazaki, and Y. Takahashi. The lower entrainable limit of rat circadian rhythm to sinusoidal light intensity cycles: a preliminary study. *Psychiatry Clin Neurosci*, 53(2):215–217, Apr 1999.

[57] B. P. van der Pol and J. M. van der Mark. The Heartbeat Considered as a Relaxation Oscillation, and an Electrical Model of the Heart. *Phil. Mag.*, 6: 763–775, 1928.

[58] RR Ward. *The Living Clocks*. Alfred A. Knopf, New York, 1971.

[59] Yao Xu, Tetsuya Mori, Rekha Pattanayek, Sabuj Pattanayek, Martin Egli, and Carl Hirschie Johnson. Identification of key phosphorylation sites in the circadian clock protein KaiC by crystallographic and mutagenetic analyses. *Proc Natl Acad Sci U S A*, 101(38):13933–13938, Sep 2004. doi: 10.1073/pnas.0404768101. URL http://dx.doi.org/10.1073/pnas.0404768101.

[60] Takuya Yoshida, Yoriko Murayama, Hiroshi Ito, Hakuto Kageyama, and Takao Kondo. Nonparametric entrainment of the in vitro circadian phosphorylation rhythm of cyanobacterial KaiC by temperature cycle. *Proc Natl Acad Sci U S A*, 106(5):1648–1653, Feb 2009. doi: 10.1073/pnas.0806741106. URL http://dx.doi.org/10.1073/pnas.0806741106.

[61] Xiaofan Zhang, Guogang Dong, and Susan S Golden. The pseudo-receiver domain of CikA regulates the cyanobacterial circadian input pathway. *Mol Microbiol*, 60(3):658–668, May 2006. doi: 10.1111/j.1365-2958.2006.05138.x. URL http://dx.doi.org/10.1111/j.1365-2958.2006.05138.x.

[62] W. F. Zimmerman, C. S. Pittendrigh, and T. Pavlidis. Temperature compensation of the circadian oscillation in drosophila pseudoobscura and its entrainment by temperature cycles. *J Insect Physiol*, 14(5):669–684, May 1968.